5-3-2021

Automation and Advancement of Non-Invasive Continuous Blood Glucose Measurements

Andrew deVries
ard6268@rit.edu

Automation and Advancement of Non-Invasive Continuous Blood Glucose Measurements

By

Andrew deVries

Thesis

Submitted in Partial Fulfillment of the Requirements for the Degree of

MASTER OF SCIENCE IN ELECTRICAL ENGINEERING

Department of Electrical and Microelectronic Engineering

Kate Gleason College of Engineering

Rochester Institute of Technology, Rochester, NY

Supervised by:

Dr. Jayanti Venkataraman

May 3rd, 2021

Automation and Advancement of Non-Invasive Continuous Blood Glucose Measurements

Approved by:

Dr. Jayanti Venkataraman 5/5/2021

Thesis Primary Advisor: Professor, Department of Electrical and Microelectronic Engineering Kate Gleason College of Engineering

---

Dr. Gill Tsouri 5/5/2021

Committee Member: Professor, Department of Electrical and Microelectronic Engineering Kate Gleason College of Engineering

---

Dr. Panos Markopoulos 5/7/2021

Committee Member: Assistant Professor, Department of Electrical and Microelectronic Engineering, Kate Gleason College of Engineering

---

Dr. Ferat Sahin 5/9/2021

Department Head: Professor, Department of Electrical and Microelectronic Engineering Kate Gleason College of Engineering

Acknowledgements

Thank you to all of my professors and peers for making RIT a community where I was able to grow as a person and as an engineer. The connections that I have made on this campus will have a lasting impact on my career. I am especially grateful for Dr. Venkataraman, who worked with me on this research through a pandemic. Despite only meeting in person three times during the ten-month duration of this project we were able to maintain steady progress. I am also thankful for all of the other professors, like Dr. Rabbani, who challenged me and motivated me during my time at RIT. I am inspired by you.

Thank you to all of the students who contributed to this project in years past. It was a privilege to be able to do my part amongst a very talented group of individuals. I have great respect for the work that I was able to build upon and I hope that what I've done will be just as valuable for future students.

Thank you to Alex Budwey, Mike Kobasa and the rest of the employees at TTM Syracuse. The opportunity to work with you for my first co-op had a profound impact on my life. The encouragement, direction and instruction that I was afforded in Syracuse were invaluable and that internship kick-started my graduate career at RIT.

Thank you to Matt Edlich. I enjoyed getting to work with you on this project and I can't wait to see what you are able to do next. I am also grateful for Connor Devitt and Sofia Quinones who joined us in the lab.

Thank you to Herrick Technology Laboratories and Craig Lewis. I had a great time working with you in Maryland for the summer.

Thank you to my committee members, Dr. Tsouri and Dr. Markopoulos. I am glad that I get to share the work that I have done with you.

Thank you to my friends and my family for continuous support.

Thank you to the LASSO team. It was an amazing experience to go through that project together.

Abstract

Researching the RF application of noninvasive continuous, real time, blood glucose monitoring has been a persistent topic of interest for the research group at the electromagnetic theory and application (ETA) lab at RIT. The technique is based on the effects of glucose on the dielectric properties of blood. When the dielectric permittivity of the tissue changes due to glucose, the resonant frequency and input impedance of an antenna sensor can be related to the change in glucose level, as shown in [1] and [2]. The feasibility of this technique has been demonstrated successfully with one diabetic and one non-diabetic patient in [3].

The goal of this work is to utilize the existing developments to create a robust automated system to be used in clinical trial in a hospital setting. The system has been designed to make real time measurements of blood glucose and remotely monitor the data through a cell phone app. The clinical trial will consist of on-body antenna sensor measurements, and dielectric permittivity measurements of in-vitro blood samples contaminated by glucose. Four different phases are mapped out focusing on consistency, correlation, data collection and accuracy verification. The clinical trial will consist of on-body antenna sensor measurements, dialectic permittivity measurements of blood and traditionally measured blood glucose values. Developing a relationship between these measurements will lead to an algorithm for determining the blood glucose level of a patient.

Utilizing existing designs, the antenna sensor is a planar monopole antenna with an artificial magnetic conductor design from [5]. The sensor assembly is a more robust antenna than that which was previously constructed with an AMC layer. The sensor is designed to be insensitive to patient movement because the stability of the sensor is critical for performance in the clinical trial. Simulations have also been performed with a human body model in HFSS to ensure that the Specific Absorption Rate (SAR) levels conform to FDA regulations for biomedical applications. Antenna sensors of each design were fabricated and tested to show an agreement with simulation results for both the resonant frequencies and radiation patterns.

An automated measurement system has been developed using MATLAB App Designer to be compatible with bench top Agilent network analyzers as well as the small and portable R140

network analyzer from Copper Mountain Technologies. The application is capable of recording S-parameter measurements and doing real time analysis, as well as uploading the data to an RIT server. Once the processed data is on the server, it can be accessed immediately over the internet by a different computer or a smartphone application. A MATLAB app was designed for monitoring the data remotely and a smart phone application was also developed for the same purpose.

The clinical trial will also include an in-vitro study where permittivity measurements will be collected of blood samples containing glucose. In order to support the antenna sensor measurements, a correlation will be obtained from the in-vitro samples between the dielectric permittivity and the concentration of glucose. The dielectric probe has been automated in preparation for the trial.

In order to prepare the system for use in clinical trials, extensive testing using an experimental test setup was carried out. The test setup incorporated both the antenna sensor and the dielectric probe to make measurements of water and glucose. With the antenna close enough to the dish and the dielectric probe in the water, both the antenna sensor response and the relative permittivity of the water are observed to change when the concentration of glucose in the dish changes. This combined testing will be imitated in the clinical trial when the antenna sensor is used on a patient's body and permittivity measurements are made of in-vitro blood samples.

Table of Contents

List of Figures

List of Tables

List of Abbreviations, Symbols and Terms

CGM – Continuous blood glucose monitoring

SAR – Specific Absorption Rate

HFSS – ANSYS Program for High Frequency Structure Simulation

Inflection Impedance – Real impedance value of an antenna response at the frequency where the imaginary impedance value is closest to zero and the magnitude of reflection is minimized

Resonant Frequency – The frequency in which the minimum energy excitation into an antenna is reflected back to the source and a maximum is radiated

Inflection Frequency – The frequency at which the imaginary part of the input impedance value of an antenna is closest to zero and the magnitude of reflection is minimized

VNA – Voltage Network Analyzer

MUT – Medium Under Test

SMA Connector – Subminiature Version A RF connector (3.5mm)

AMC – Artificial Magnetic Conductor

ISM band – Frequency spectrum allocated for industrial, scientific and medical use

SSH – Secure shell protocol, used to access the server

SCP – A secure copy paster operation, through an SSH connection

1. Introduction: Motivation & Summary of Prior Research

Innovations in blood glucose monitoring are driven by technological developments and a consistently increasing demand for simple, convenient and comfortable blood glucose measurement systems. One of the companies making advances is Dexcom [4], which advertised a new continuous blood glucose monitoring (CGM) system during the 2021 Super Bowl. Their system features a wearable patch with a sensor wire that uses interstitial fluid to make measurements as frequently as every 5 minutes. This system is an improvement upon traditional blood glucose monitoring systems which are based on discrete and blood samples extracted from the body. This system uses a small wire to measure an interstitial glucose concentration and the error in such a system was characterized in [5]. The data and analysis are shown to the user on a smartphone application in real-time throughout the day. There is work being done to add insulin distribution to this kind of device in [6]. The prevalence of this technology demonstrates the high interest in continuous blood glucose monitoring systems, even if they are invasive. Along with continuous measurements, there is a strong interest in advancing a system further to be non-invasive.

Figure 1.1. Dexcom System [4]

The goal of this research is to improve upon the existing efforts made towards continuous non-invasive blood glucose measurement. More specifically, the work that was done with microwave sensors at the RIT Electromagnetic Theory and Application (ETA) laboratory will be the basis for this study. This work aims to prepare a potential glucose monitoring system for a clinical trial

in cooperation with physicians. There are many different possible solutions to this problem. Even within the field of electromagnetics, various antenna and resonator sensors have been tested. [7] Some of the issues that still need to be overcome are discussed in [8]. Recent advances to address the challenges are being made, such as the multi-sensor system proposed in [9]. Work was done in [10] to implement an artificial magnetic conductor layer to help minimize an antenna sensor and shield it from interference. The most recent attention to this topic has been from local physicians looking to utilize this technology as an automated system that can provide continuous real time blood glucose measurements for patients with abnormal blood sugar levels. In order to expand upon previous research, all relevant contributions are considered when developing the system for the trial.

1.1. Dielectrics of blood and tissue

The electrical properties of biological substances have been of interest for a multitude of useful applications relating to healthcare. MRI, X-ray and EEG are a few examples of technologies that use electromagnetics to gather information about the human body.

In order to develop an antenna sensor to be used for continuous blood glucose monitoring, the electrical properties of the space around the antenna must be considered. The dielectric permittivity and conductivity of different biological tissues have been modeled in order to better design on-body sensors. [11] When an antenna is on the skin, the human body will function as a lossy medium for the electromagnetic waves to propagate. The combination of everything within range of the antenna will create an effective dielectric permittivity that will impact the radiation of the antenna. For the purposes of CGM, the blood within the body around the site of the antenna will be the most critical contributor.

The mathematical model for the complex permittivity of blood as a function of frequency developed in [11] is given as:

$$1.\quad \hat{\varepsilon}(\omega) = \varepsilon_\infty + \sum_n \frac{\Delta\varepsilon_n}{1+(j\omega\tau_n)^{(1-\alpha n)}} + \frac{\sigma_i}{j\omega\ _0}$$

This model is known as the Cole-Cole equation and it is a broadened version of the Debye equation for multiple dispersions based on an empirical distribution parameter α. The equation is parametric where the parameters for each tissue were determined with experimental data. The parameters for blood are: $\varepsilon_\infty = 4.0$, $\Delta\varepsilon_1 = 56$, $\tau_1 = 8.38$ps, $\alpha_1 = 0.10$, $\Delta\varepsilon_2 = 5200$, $\tau_2 = 132.63$ps, $\alpha_2 = 0.10$, $\Delta\varepsilon_3 = 0.0$, $\Delta\varepsilon_4 = 0.0$ and $\sigma = 0.7$ where $\varepsilon_0 = 8.854 * 10^{-1}$ F/m. The empirical measurements for this data were taken at 37°C.

The model shows that within the range of 1-10 GHz, the permittivity changes linearly with frequency. Blood will also have a higher permittivity and conductivity than other tissues present. The electrical properties of blood based on the equation are shown in figure 1.2 as well as a comparison with other tissues.

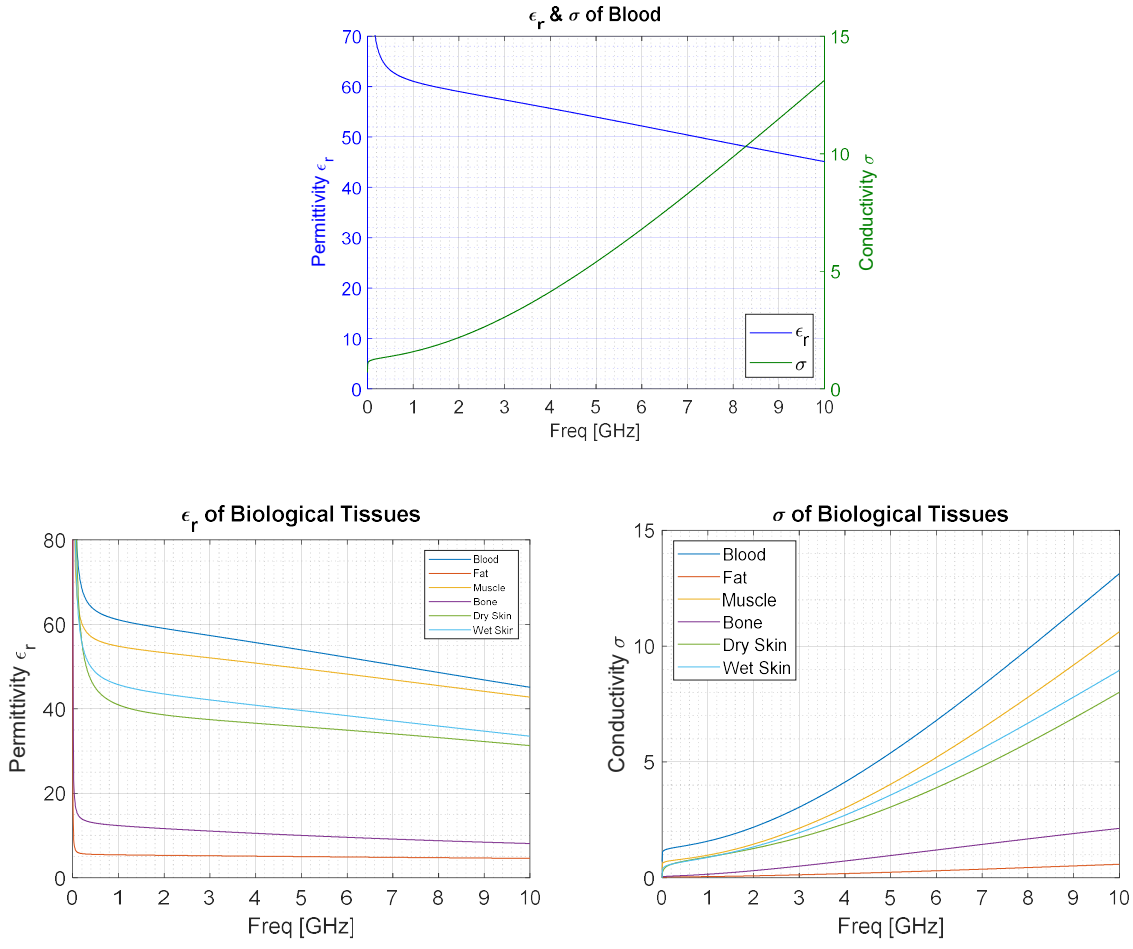

Figure 1.2. Cole-Cole Model for Biological Tissues

When the Cole-Cole model was developed, the amount of glucose in the blood was not being considered. Research has been done more recently to study the impact of the blood glucose level on the permittivity and conductivity. A study of in-vitro blood samples with different blood glucose levels was done and referenced in [3]. A glucose dependent adjustment factor for the real part of the Cole-Cole model was developed to account for different levels of glucose. In general, the permittivity decreased as the glucose concentration increased, but the data was inconsistent because each sample was from a different person. The modified model from [3] compared to the collected data at 1 GHz is shown in Figure 1.3.

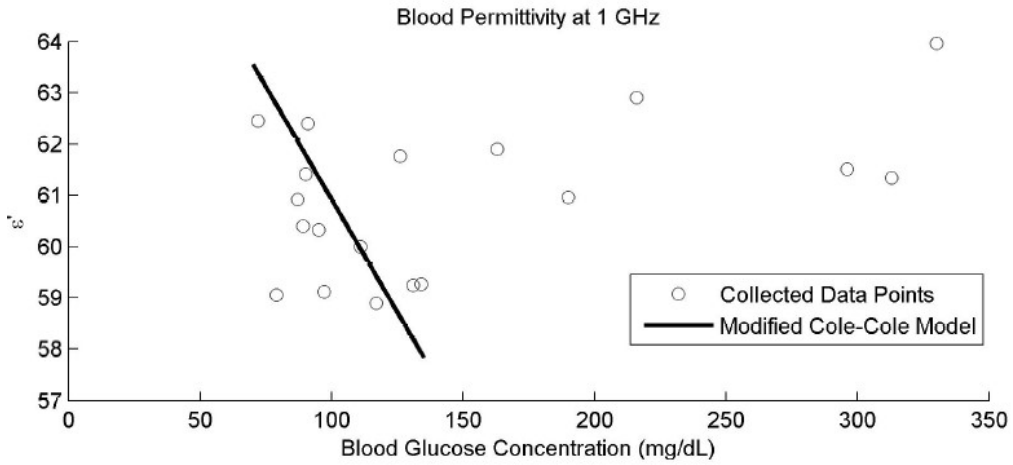

Figure 1.3. Modified Cole-Cole Model from [3]

A subsequent study in [12] also aimed to develop a modified Cole-Cole model for the permittivity of blood with a dependence on glucose levels. Instead of an additional factor, this research developed a glucose dependent model for each of the Cole-Cole model parameters ε_∞, $\Delta\varepsilon_1$, τ_1, and σ where the model only has one pole. These four parameters were each fit to a second order polynomial based on the glucose level. The same trend was observed, where the permittivity decreased as the glucose concentration increased and figure 1.4 shows the comparison of the model with the measurements from [12].

This second study had more consistent data but there is still an issue with directly measuring the permittivity as discussed in [8]. There are other molecules in blood that must remain constant in order to isolate glucose as the singular factor driving the change in permittivity. Each molecule

can have a complex effect on the permittivity through different relaxation mechanisms. [8] This is why phantom substances used as substitutes for blood such as water can give results that differ significantly from how actual blood would perform. It is still clear that the conductivity will not change as much as the relative permittivity with glucose level and therefore utilizing this change in permittivity will be the focus for the on-body sensor.

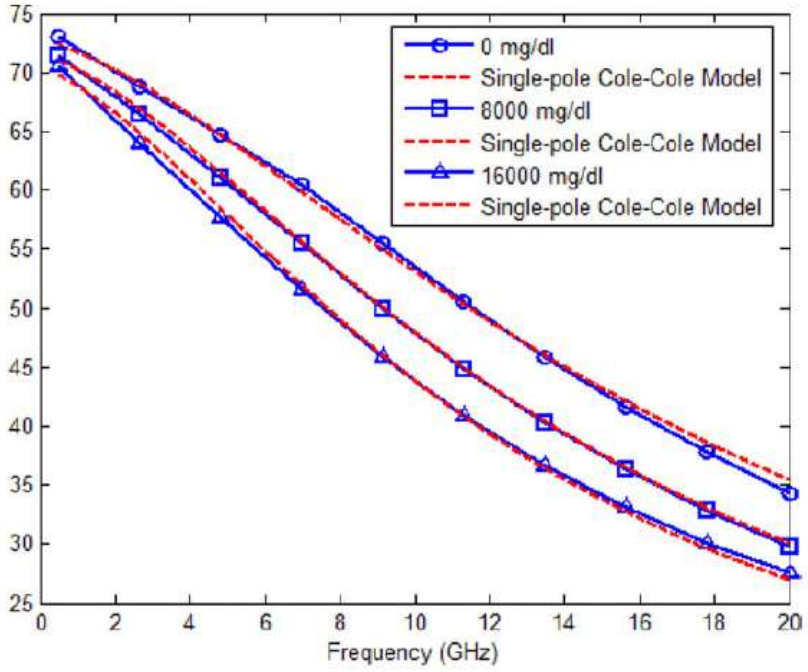

Figure 1.4. Modified Cole-Cole Model from [12]

For the development of the testing system described in this work water was used as a substitute for blood. The trend held that increasing the glucose concentration will decrease the permittivity of water. However, in order to get an accurate picture of how the permittivity of the blood changes with glucose, the clinical trial features in-vitro measurements of blood samples corresponding to real-time measurements using an on-body continuous blood glucose sensor which will both be compared to traditional blood glucose measurements. This combination of measurements will yield more information in determining a model for blood glucose level based on the sensor.

1.2. Non-invasive real time blood glucose monitoring

In order to capture the changing permittivity in blood that is within the body, an antenna sensor was designed in [3] to be placed against the skin. Figure 1.5 shows the detection sensor that was proposed.

The radiation from the antenna in the near field is impacted by the permittivity of the blood as well as all other tissue within a certain range. The range of propagation is frequency dependent and will be determined by the penetration depth of each tissue. Looking at the penetration depth of blood, which is the distance where the energy is deteriorated to 37% of the incidence, a possible frequency range of 300 MHz to 4 GHz was chosen for the sensor. This will give the electromagnetic waves a penetration depth of at least 1cm.

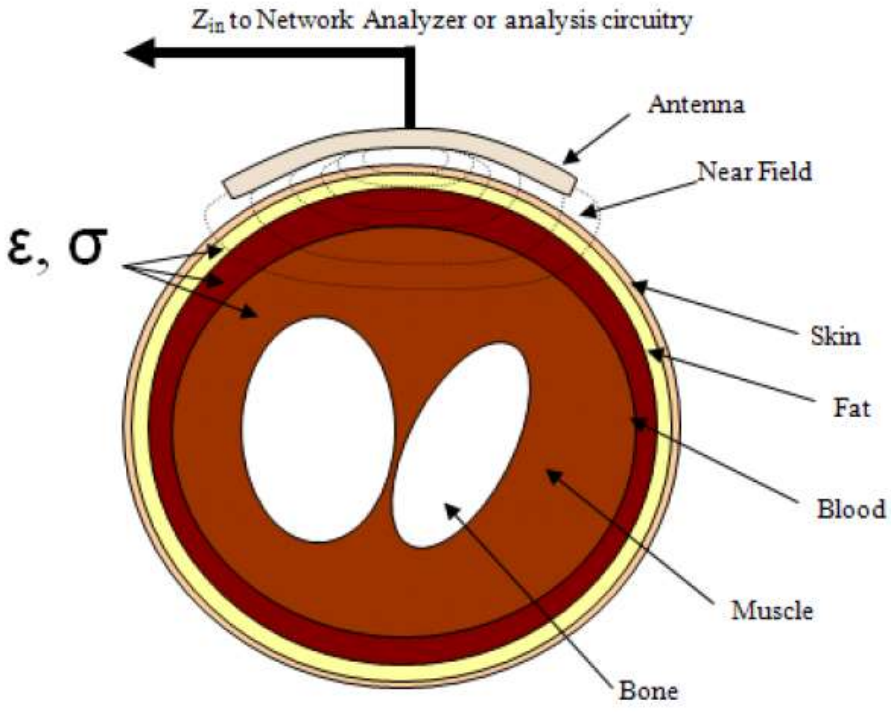

Figure 1.5. Antenna Sensor from [3]

The proportion of incident energy that is radiated by the antenna can be measured a network analyzer looking at the input impedance or the reflection coefficient. When the incident energy is at a frequency such that minimal energy is reflected back to the source by the antenna, a maximum of energy being radiated is reached and this frequency is a resonant frequency for the antenna. A monopole antenna sensor was designed in [3] with an on-body resonance around 2 GHz based on a simulated change in the resonant frequency as the permittivity of blood in a simplified human body model changed, shown in figure 1.6.

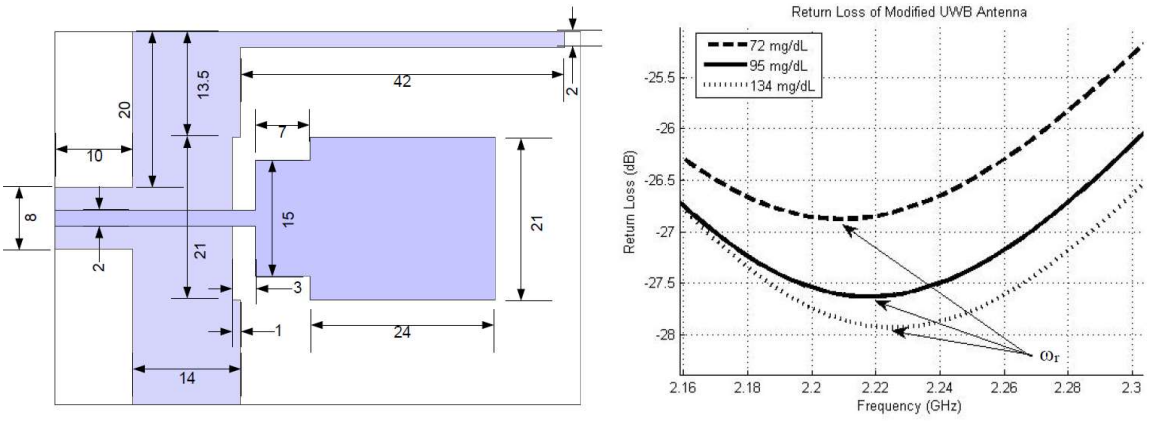

Figure 1.6. Simulated Antenna Sensor from [3]

The simulation results showed an increase in resonant frequency as the concentration of glucose increased. The permittivity decrease driving an increase in resonant frequency agrees with electromagnetic theory based in impedance spectroscopy.

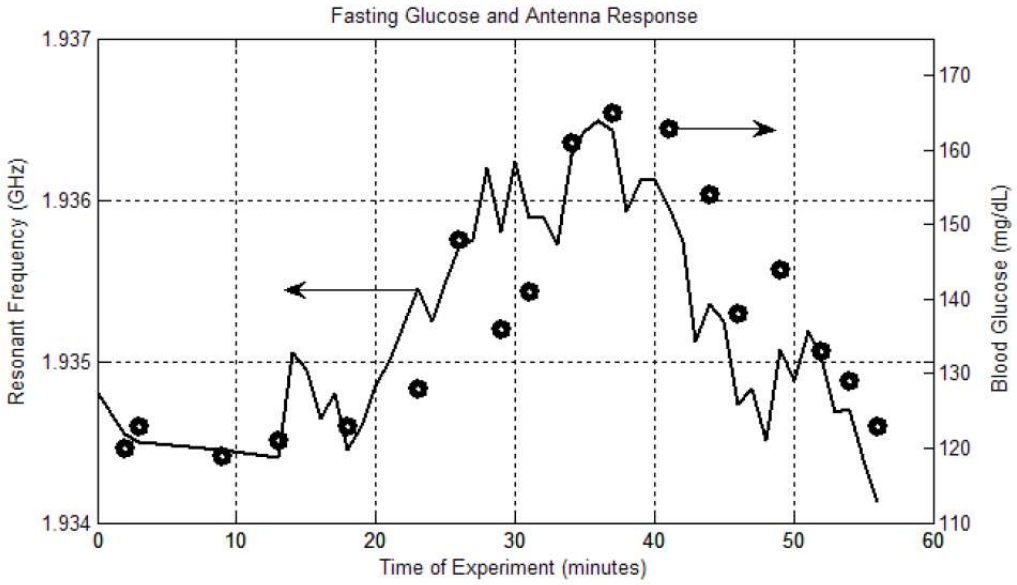

Figure 1.7. Glucose Level Monitoring Test from [3]

The sensor from was manufactured and tested on the leg of a person while their blood glucose level was being recorded using a traditional method. The test lasted 60 minutes, starting after glucose was ingested, and the resonant frequency over time was recorded for the duration of the test. The results of this test are shown in figure 1.7.

The test results showed that as the blood glucose level increased and therefore the permittivity of the blood inside the leg decreased, the resonant frequency of the antenna increased. The same relationship held for the subsequent decrease in blood glucose level of the subject.

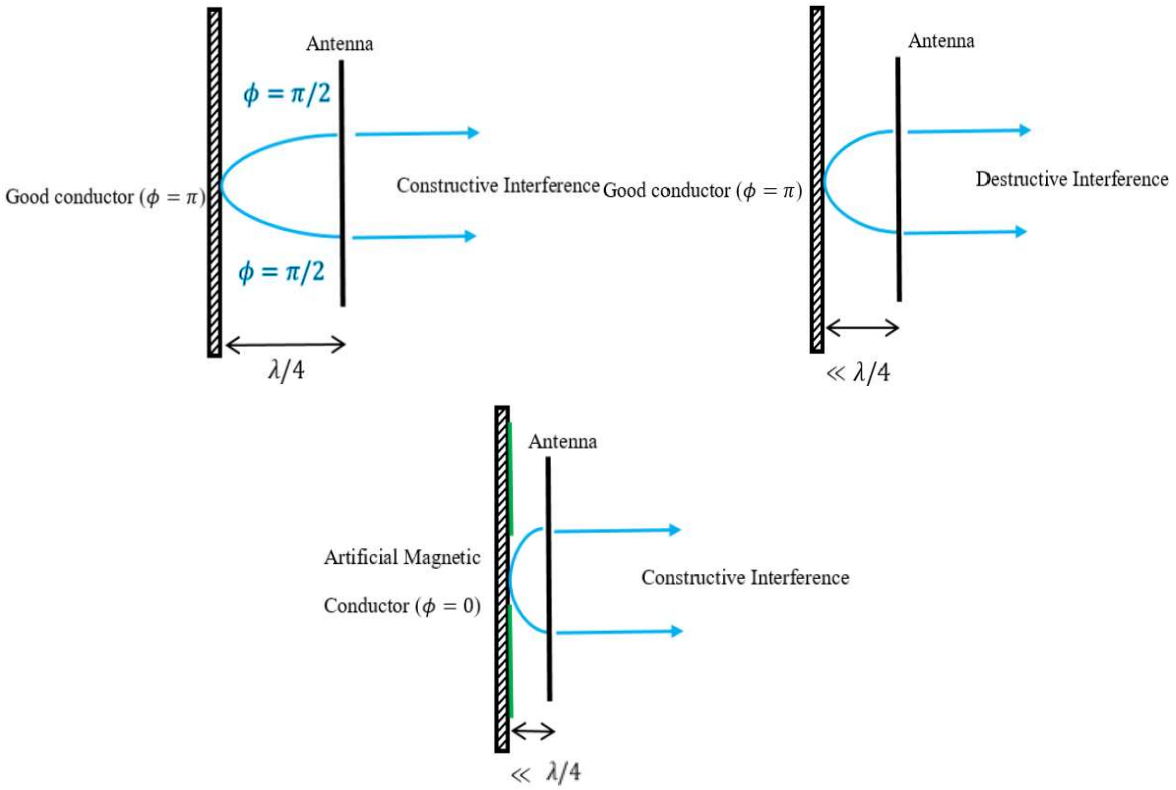

Figure 1.8. Good Conductor vs. AMC Response from [10]

One of the issues with the antenna sensor from [3] was the omnidirectional radiation pattern of the monopole antenna. Ideally, the antenna will only radiate into the body, and the antenna resonance will be unaffected by interferences in the environment such as patient movement. In order to improve the sensor design, work was done in [10] to develop an artificial magnetic conductor layer. This layer is designed to reflect electromagnetic waves in-phase for a specific frequency. A regular conduction layer placed very close to the source will function as a short and will reflect waves 180 degrees out of phase. The reflected wave will only be in-phase when there is a phase difference of π/2 between the short and the source. In contrast, the in-phase reflection of the AMC allows for constructive interference when the layer is very close to the source. This property from [10] is demonstrated in figure 1.8.

The addition of the AMC layer on the outside of the antenna will effectively shield the antenna from interferences and focus the radiation pattern towards the body. In order to achieve a plane with a phase reflection of 0 degrees, several unit cells were designed and then repeated four

times to cover the outside of the antenna in a pattern. The most favorable AMC pattern has the smallest area, as this will allow for the most compact sensor to be employed.

The AMC unit cell designed in [10] is based on an "I" shape and the reflected wave will have 0 degrees of phase at 2.5 GHz. The design was dictated by equations derived from an equivalent circuit model of a series inductor and capacitor, both with a shunt inductor. Figure 1.9 shows the AMC design simulated in HFSS compared with an equivalent circuit model simulation from [10].

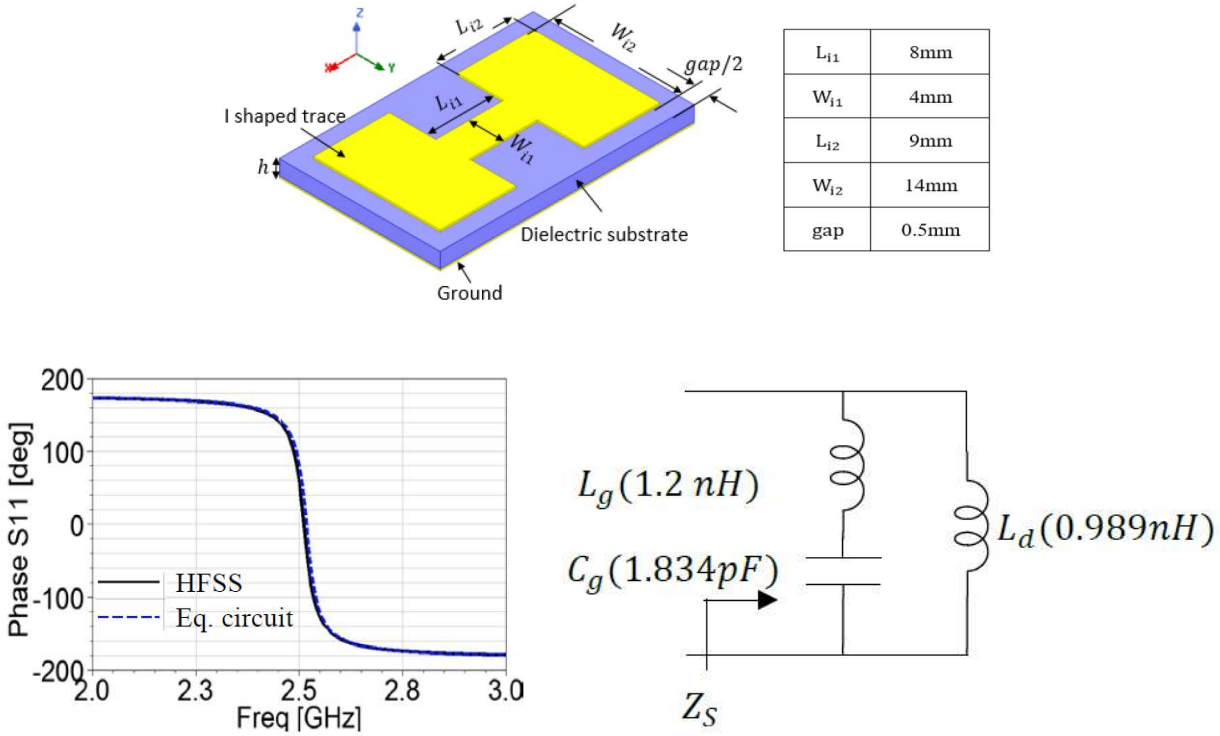

L_{i1}	8mm
W_{i1}	4mm
L_{i2}	9mm
W_{i2}	14mm
gap	0.5mm

Figure 1.9. I Shaped AMC Design from [10]

The AMC layer was manufactured and tested for an impact on the antenna performance. Two new, smaller monopole antennas were designed to work with the AMC layer. The sensor was taped onto the arm and the AMC was placed on the outside. It was shown that the antenna performance was steadier than the previous design when environmental interference was tested.

The addition of the AMC led to a more stable sensor, but more work to improve the structure is necessary. The effectiveness of the AMC layer is very sensitive to its placement relative to the

antenna which led to some practical implementation issues because they were individual parts. Establishing a singular and consistent sensor structure is one of the focuses of this research.

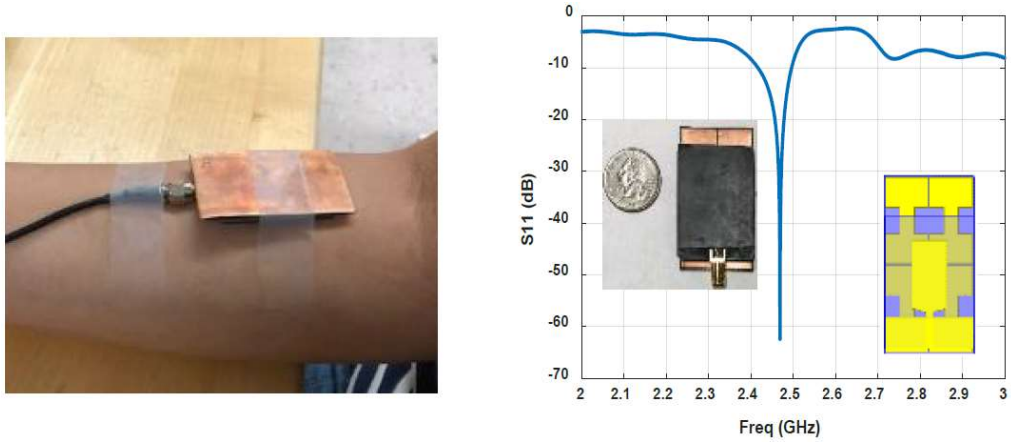

Figure 1.10. Sensor with AMC On Arm Resonance from [10]

In addition to testing sensors for on-body resonance, resonating antenna sensors have also been tested using a phantom substance for tissue. As with the permittivity measurements, water has been used in place of the human body in order to directly control the glucose level of the MUT. In [13] a compact microwave sensor was designed at 4.5 GHz to have high capacitance and maximize the radiated electric field. This sensor, shown in figure 1.11, was tested with a sample water and glucose and an increase in resonant frequency was observed as the concentration of glucose increased. However, when realistic concentrations of glucose used, very small changes in permittivity were observed and no useful change in the sensor response was observed.

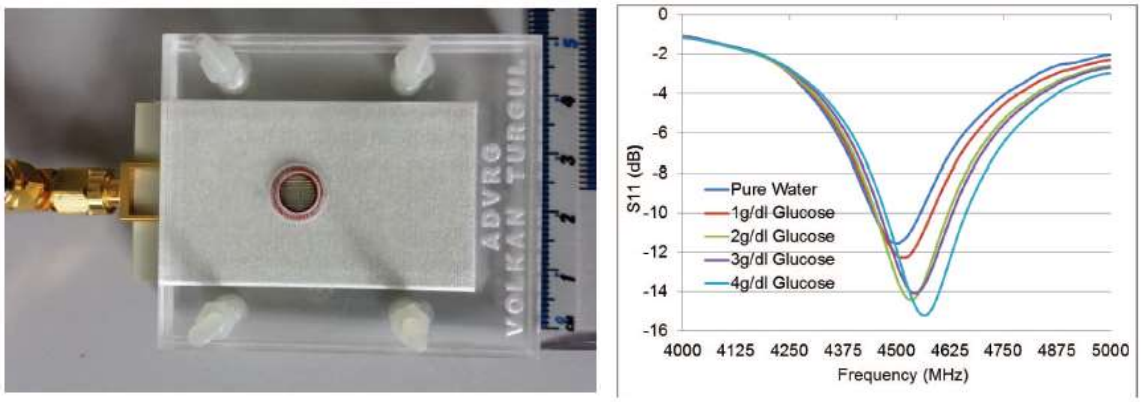

Figure 1.11. Sensor Tested with Glucose Water from [13]

Sensor sensitivity is an issue that will be focused on for the sensors developed in this research. Phantom and test scenarios are useful for predicting the performance of the sensor but ultimately the behavior in a clinical trial will be the most informative.

The resonant frequency of the sensor has been the main metric of the response for tracking changes in blood glucose level, but it may be useful to look at the real and imaginary parts of the input impedance separately. In [14], the sensor from [3] simulated over an aqueous solution and the real and imaginary parts of the impedance were observed as the permittivity of the aqueous solution was changed. Figure 1.12 shows the simulation and the results.

Instead of looking at the resonant frequency, based on this simulation result it was determined that the frequency at which the imaginary input impedance is zero is a good metric for tracking the change in permittivity of the MUT. This frequency is defined as the inflection frequency for the purposes of this research. This alternative metric can be quite different from the resonant frequency and is critically dependent on the imaginary input impedance curve.

When designing the antenna sensors to be placed on the body, the creeping wave radiation is a factor that needs to be considered. Investigations into permittivity measurements through parameter extraction when multiple antennas are used need could offer a more direct metric for determining blood glucose levels. This method is similar to other spectroscopy methods that have been tested for doing non-invasive blood glucose monitoring.

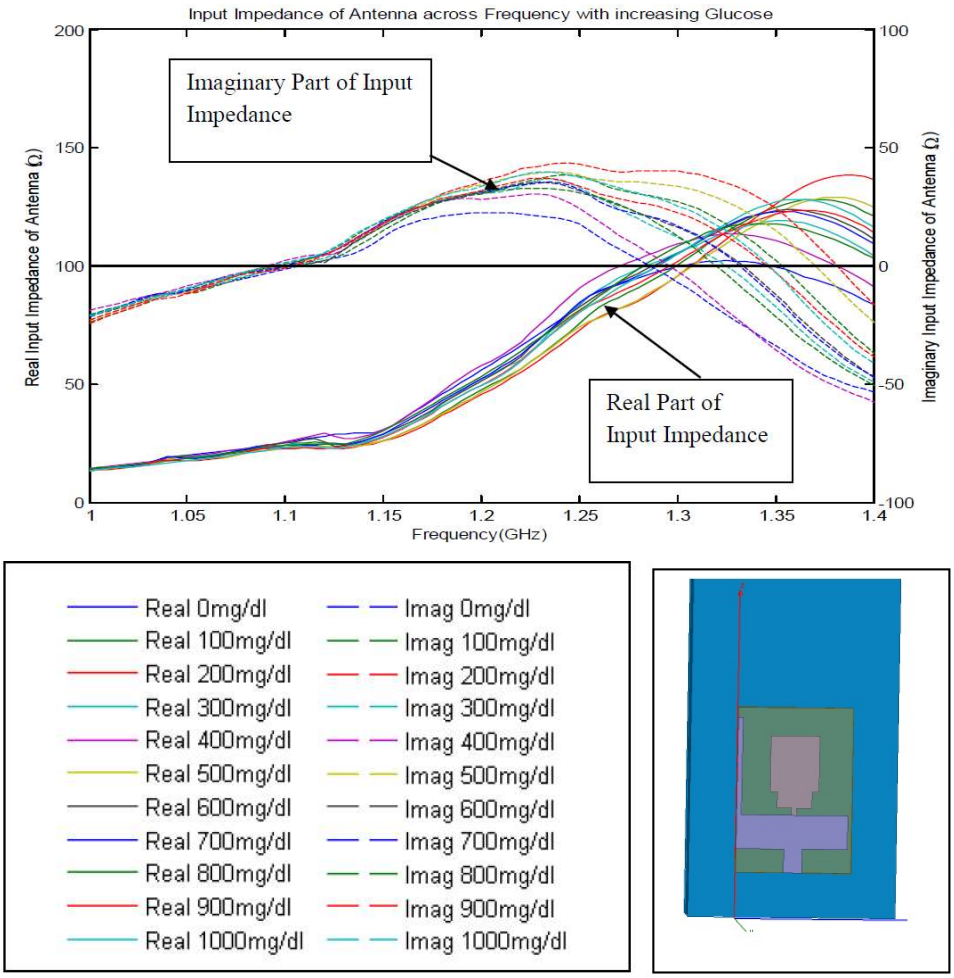

Figure 1.12. Sensor Simulation with Glucose Water from [14]

1.3. Clinical Trials

In order to verify the effectiveness of a non-invasive blood glucose monitoring system, clinical trials are used. A clinical trial was done in [9] to test an antenna sensor for monitoring blood glucose. This clinical trial was testing a novel system for continuous non-invasive blood glucose monitoring that employed both an antenna sensor and a filter to be placed on the body, shown in figures 1.13 and 1.14.

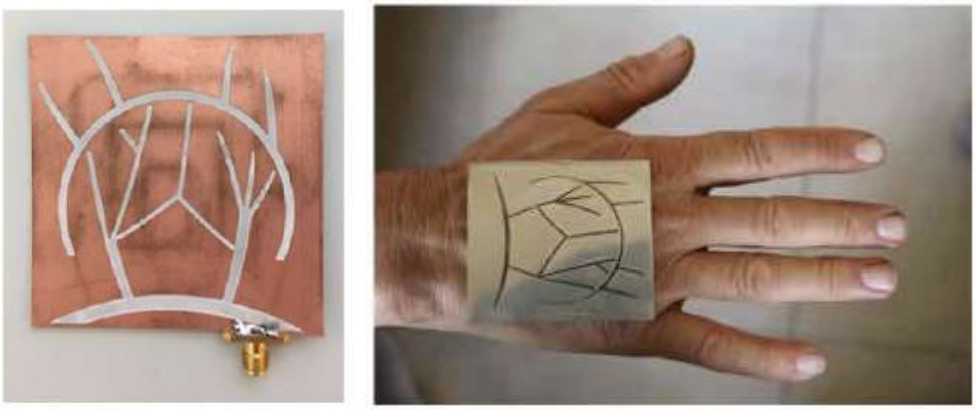

Figure 1.13. Antenna Sensor from [9]

Figure 1.14 Filter Sensor from [9]

The analysis on measurement data is carried out by a machine learning algorithm and training data from traditionally measured blood glucose levels. This approach, differs from analysis based purely on electromagnetic theory because it passes the s-parameters directly over as features into the classification algorithm using a non-linear gaussian process kernel. The kernel helps reduce the impact of noise and non-ideal factors that would generate a distribution in the measurement. The testing was done with a fetal bovine solution as a phantom for blood, lab rats and human subjects. The data from the two sensors is combined to look for maximum correlation with measured glucose concentrations. The clinical trial setup is shown in figure 1.15.

The scope of the research presented in [9] is greater than the ultimate goal of this work, but a similar model for the clinical trial will be employed. The focus of this research remains the

clinical trial implementation of an improved version of the single-sensor system first developed in [3]. It will also be useful to consider similar machine learning approaches when developing an analytical model based on the measurement data.

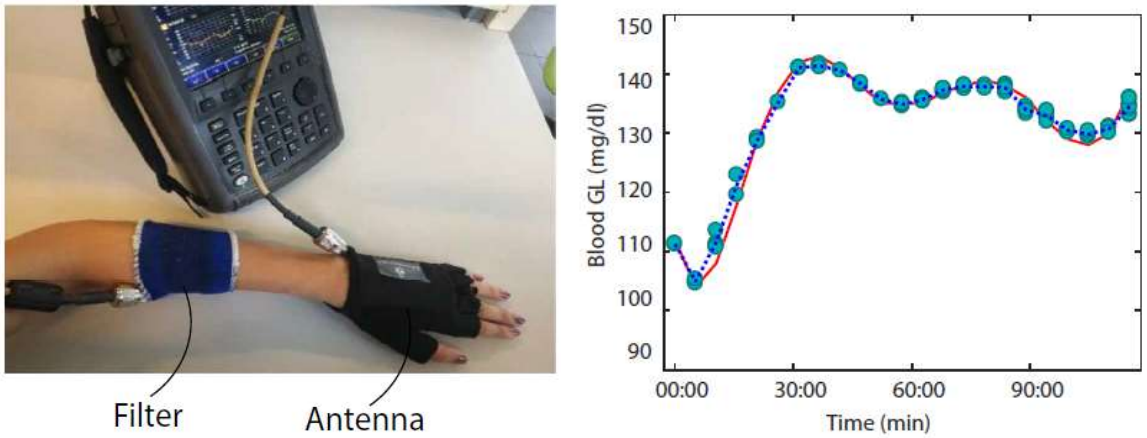

Figure 1.15. Clinical Trial Results from [9]

1.4. Goal of present work

As stated in [8], it is proven that RF sensors can measure changes in permittivity. The challenge remaining is a sensor that can accurately and repeatable detect the changes in realistic blood glucose levels. The aim of the present work is to prepare to implement a feasible sensor and measurement system in a clinical trial.

SAR (100 kHz – 6 GHz)	**Whole Body**	**Partial Body**	**Hands, Wrists, Feet & Ankles**
Occupational/Controlled Exposure Limits (W/kg)	0.4	8.0	20.0
General Population/Uncontrolled Exposure Limits (W/kg)	0.08	1.6	4.0

Table 1.1. FCC Limits on SAR from [15]

An investigation is done into the implementation of a multiple antenna sensor system with both a transmit and receive antenna. The two-port system would yield more information about the MUT via the transmission coefficient, which is not available when there is only one radiating antenna sensor. Simulations with ANSYS HFSS (high frequency structure simulation) are used to predict the performance of such a system. Ultimately it is decided to continue to pursue the single antenna sensor approach due to inconsistencies in transmitting through the human body. Using multiple sensors, as presented in [9], remains a viable avenue for future work as an improvement to this system.

When considering a single antenna sensor system, several factors are critical for the design of the sensor. The stable antenna sensor designs need to be small and compact while still demonstrating consistent performance. Multiple antennas are fabricated with AMC layers and tested in the present work. A solid multi-layered assembly is used in order to ensure the physical antenna aligns with the simulated stackup. The sensors will be used in the clinical trial, so the safety of the sensors needs to be assessed. In order to test the SAR (specific absorption rate), a human body model will be used in ANSYS HFSS. The SAR is described in [16] as the time derivative of the incremental energy absorbed by an incremental mass in a volume. In this case, the volume absorbing the energy is a portion of the human body and this is bound by a maximum set by governmental organizations. These antennas are tested against human tissue and in an experimental test setup. Table 1.1 shows the FCC imposed limits on SAR for devices. The results from previous studies will be replicated with the sensors for validation.

In parallel to the antenna sensor based clinical trial, in-vitro blood samples will also be gathered from the patients. A coaxial probe will be used to measure the permittivity of the samples and the actual glucose level will be recorded. Collecting the permittivity data directly from the patients who are in the antenna sensor trial will yield a more complete test data set for better improving the sensor. The permittivity measurements can also be used to improve upon the Cole-Cole model modifications for glucose level.

A system for real-time monitoring of the antenna response is also developed. The data will be constantly uploaded to a server and processed so that the change over time can be read from a Smartphone app. The users of the system will be healthcare professionals and the system should

be able to help them monitor patients. The analysis on the data for determining changes in glucose level should also occur in real time, with the results being fed to the physicians.

With both the permittivity measurements and the antenna response measurements to compare to traditional blood glucose measurements through the clinical trial an analytical model based on the Cole-Cole equation will be considered. This model will differ from the model of the lab test setup used and may require different parameters for each patient. Developing and refining this model for a working sensor with clinical trial data is the ultimate goal for advancing the technology of non-invasive continuous blood glucose monitoring. Machine learning, looking at all of the statistically significant and correlating features from the data can be utilized in order to develop an optimal algorithm. A machine learning process is utilized in [9] with training data from a clinical trial.

In order to gather data for either an analytical model or a machine learning algorithm that will relate the antenna sensor response to the measured glucose level, a four-phase clinical trial is designed. This clinical study will focus on verification of the antenna sensor using both in-vitro permittivity measurements of blood samples and traditionally measured blood glucose values. Once the sensor is shown to be consistent and a correlation is observed, training data can be collected to map the sensor response to an absolute glucose level measurement. The final phase of the clinical trial is used to validate the accuracy of the system against test data.

1.5. Major Contributions

- Optimized robust antenna with consistent and stable performance, insensitive to patient movement. The antenna sensors presented in this work are designed with an AMC backing to have a steady resonance when placed on the body. A clinical trial will test the antenna sensors in a realistic hospital setting with actual patients.
- Study of the correlation of antenna response with glucose permittivity. A phantom substance is used and permittivity measurements are made as the concentration of glucose is changed. The response of the antenna sensor also changes as the concentration of glucose is changed. The relationship between the glucose concentration of the phantom, the permittivity of the phantom and the antenna sensor response is investigated.

- Automated measurements of glucose. A MATLAB application, in conjunction with VNA software, is designed to automatically record the antenna sensor response. An algorithm for tracking the glucose concentration of a MUT near the sensor based on changes in the response and the correlation with permittivity is presented. The system uses an RIT server to store and transfer data along with another MATLAB application for remote monitoring of the continuous measurements in real time. A clinical trial will utilize the system for monitoring patients.
- Automated measurements of dielectric permittivity. A dielectric probe kit is tested with a phantom substance of glucose and water for taking permittivity measurements. The software package enables measurement automation and this is tested on an MUT as the glucose concentration changes. The dielectric probe will be used in the clinical trial to measure the permittivity of in-vitro blood samples from patients.
- Creation of a Smartphone App. An Android application was developed to work in step with the MATLAB applications for getting the real time measurement data and plots onto a smartphone. The application uses an internet connection to access the latest data from the RIT server.
- Final optimized automated system. In order to improve the system for use in a clinical setting, a clinical trial is designed that will test out the functionality and efficacy of the proposed antenna sensors. Each phase of the trial will result in a more optimized system.

2. Antenna Sensor Design and Fabrication

There are several different trade-offs to consider when designing an antenna sensor. Both [7] and [8] summarize the challenges sensor design that exist in the literature. One trade-off that ties directly into selecting the frequency range of operation is sensitivity versus penetration depth. The higher frequency radiation will be more sensitive to smaller changes in permittivity but the energy will dissipate faster and therefore the sensor will have less range. The penetration depth of blood is shown in figure 2.1.

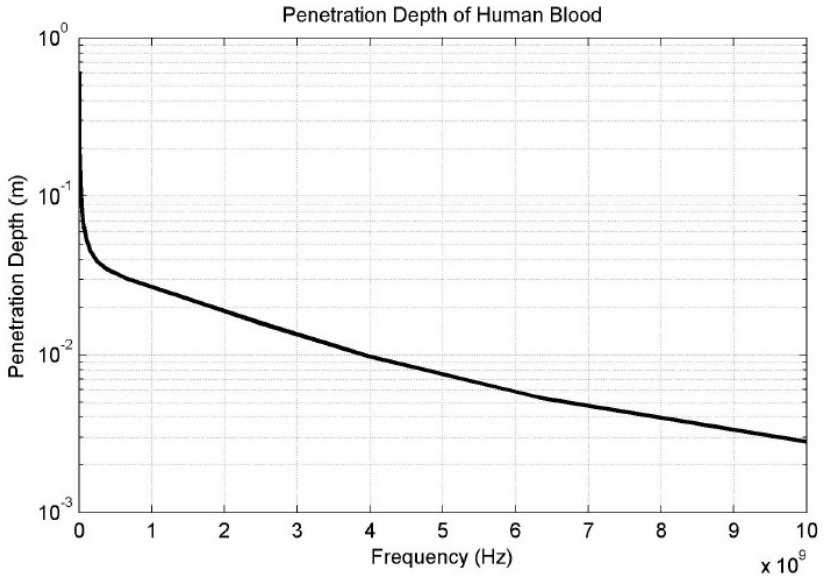

Figure 2.1. Penetration Depth of Human Blood from [3]

The antennas designed in [10] corresponded to the frequency range of 2.4 - 2.5 GHz, which is an unlicensed ISM band. This frequency range was chosen in order to have effective radiation into the body while still maintaining a small size for the antennas in an unlicensed medical band. The same frequency range will be used for the sensors proposed in this work.

2.1. Investigation into transmit and receive antennas

Several different antenna miniaturization techniques are discussed in [10] including the use of high-permittivity dielectric materials, lengthening the current flow path on the antenna surface,

adding shorting pins and patch stacking. Both monopoles and dipoles have been the focus of designs due to the inherently small size.

The implementation of multiple sensors was seen in [9] for the purpose of collecting more data and helping the system overcome inconsistencies and interferences. That system used an antenna and a filter, both having responses impacted by the permittivity of the MUT. Single antenna sensor systems rely purely on the response of one antenna, seen at the network analyzer as S11. When a two-port device, such as the filter, is added the transmission calculated from S21 is very useful for parameter extraction, specifically the permittivity and conductivity. The procedure for determining permittivity from both reflection and transmission coefficients is described in [17]. An investigation into using multiple antenna sensors for transmission was carried out with antennas from [10] and [15]. For the simulation, the human body model within HFSS was used. Figure 2.2 shows the simulation results for a concave single dipole antenna with in free space from [15].

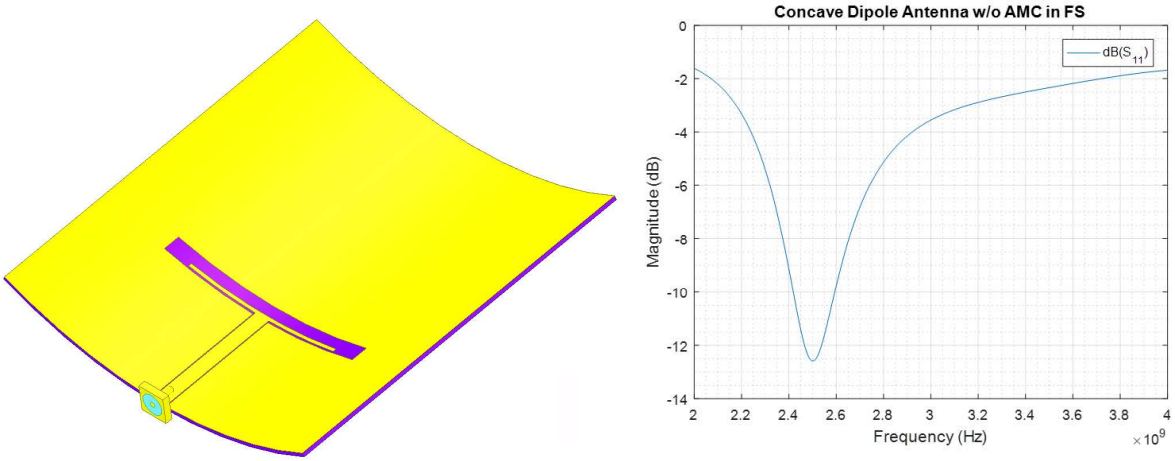

Figure 2.2. Dipole Antenna with AMC in Free Space from [15]

The dipole antennas lend themselves better to establishing a successful transmission due to the naturally omnidirectional radiation pattern. The dipole antenna is radiating at 2.5 GHz and the concave nature of the sensor will be used to fit two different dipoles to a model of a human arm. It is possible to use AMC with this antenna but in the interest of getting effective transmission established, the AMC layers were left out. This way the antennas will function as true dipoles for transmission.

The setup for the dual antenna simulation is shown in figure 2.3. Other orientations of the antennas were tested but this was the most successful at transmission. The antennas are on opposing sides of the arm but they are aligned in the same direction.

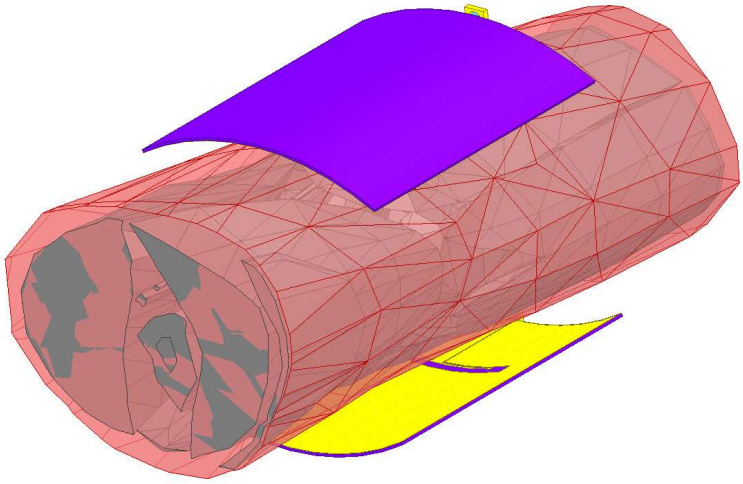

Figure 2.3. Human Body Model Setup for Dipole Antennas from [15]

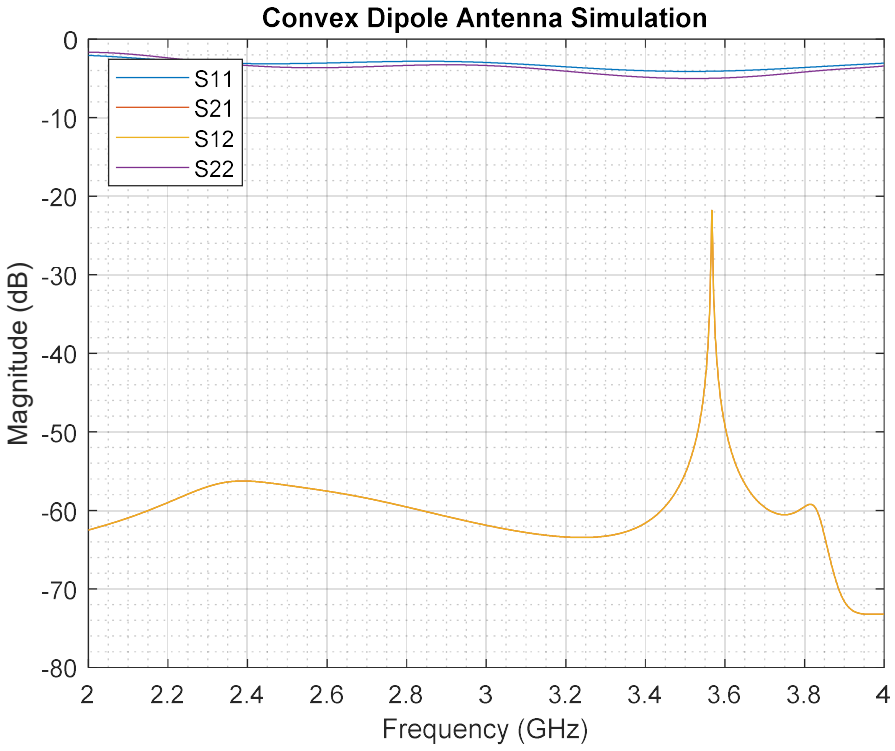

Figure 2.4. Simulation Results for Multiple Dipole Antenna Setup

The results in figure 2.4 show a very narrow band and weak transmission for the antennas. This makes sense due to the limited penetration depth of the electromagnetic waves through the arm. The electric field intensity in the arm was plotted in figure 2.5 to show the propagation into the body.

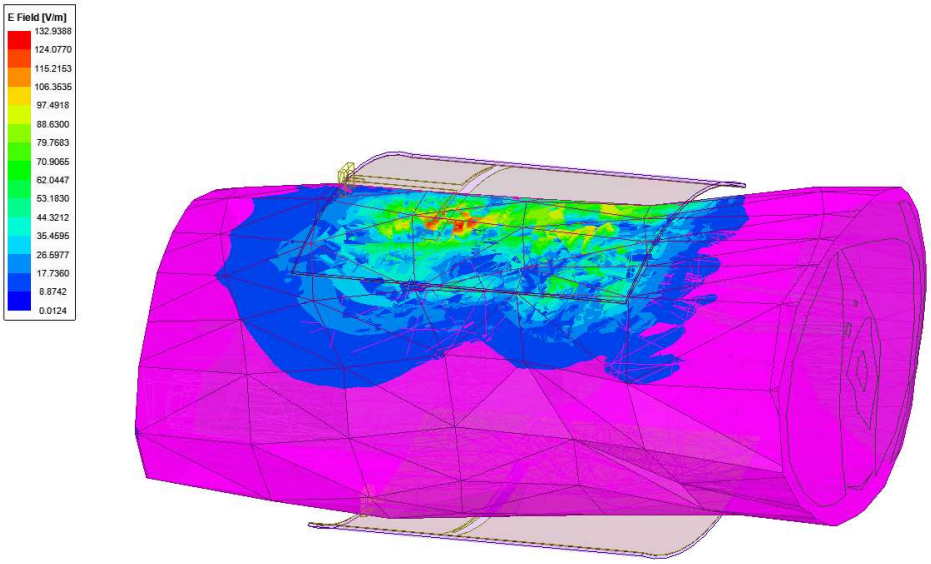

Figure 2.5. Electric Field in Arm from Multiple Dipole Setup

In addition to the dipole antennas, simulations were also done with the beveled rectangular monopole antenna with square shaped AMC from [10]. The antenna simulation in free space is shown in figure 2.6.

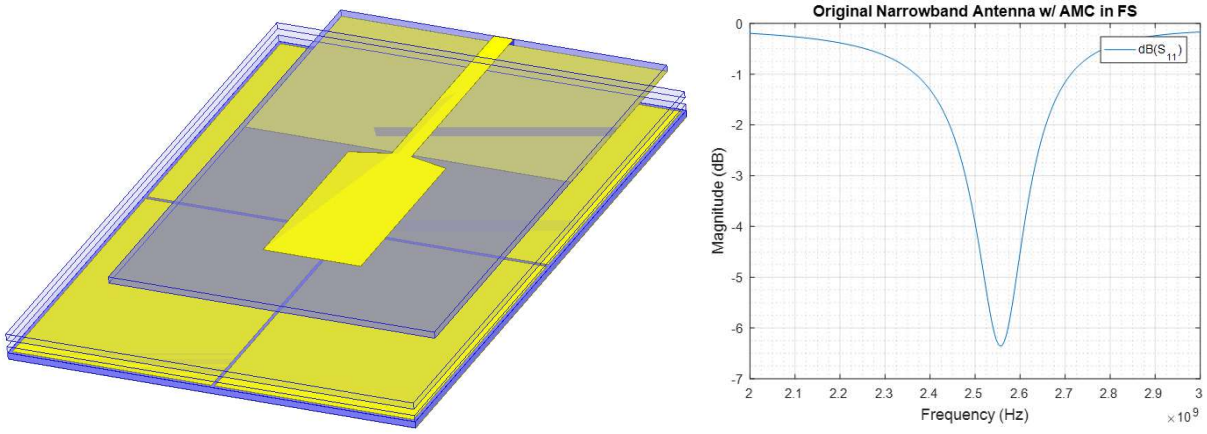

Figure 2.6. Free Space Simulation of Monopole with AMC from [10]

This antenna was then simulated on the arm of the human body model in HFSS. The results from the single antenna simulation are shown in figure 2.7.

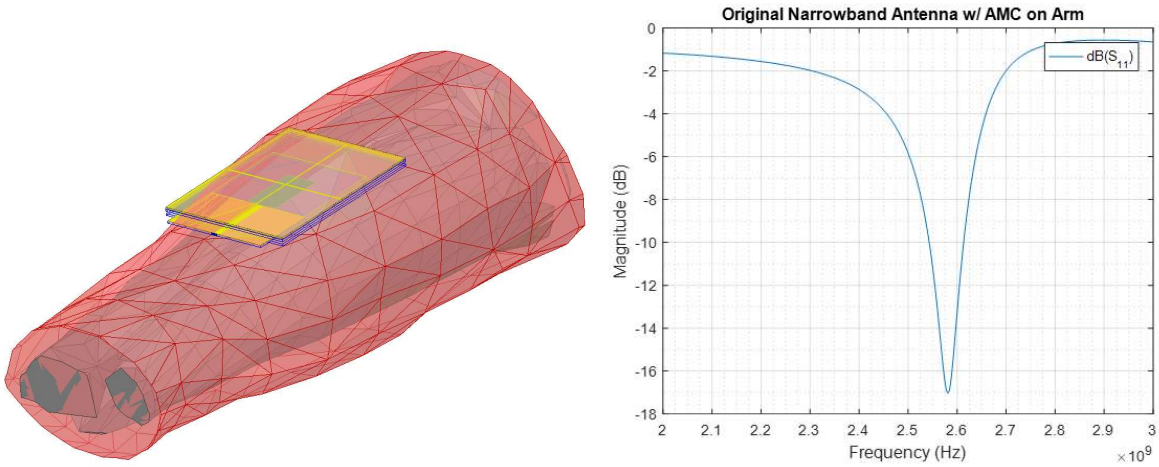

Figure 2.7. On Arm Simulation of Monopole with AMC from [10]

The antenna was designed for on arm use so the simulated resonance is stronger than the free space result. A second antenna was added to the opposing side of the arm to test for transmission. Figure 2.8 shows the setup for the simulation with two antennas.

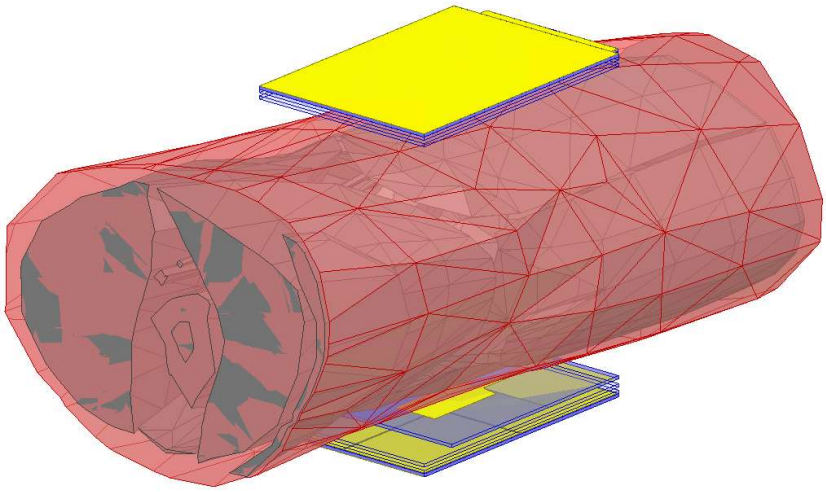

Figure 2.8. Human Body Model Setup for Monopole Antennas from [10]

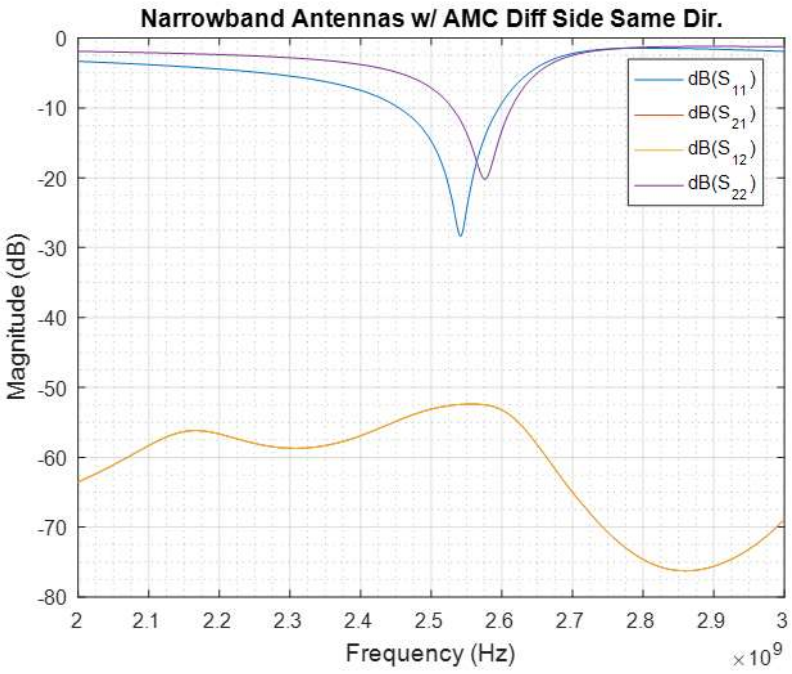

Figure 2.9. Simulation Results for Multiple Monopole Antenna Setup

The simulation results are shown in figure 2.9. For this simulation, the strength of the electric field was also plotted to investigate the nature of the radiation and propagation of the electromagnetic wave in figures 2.10 and 2.11.

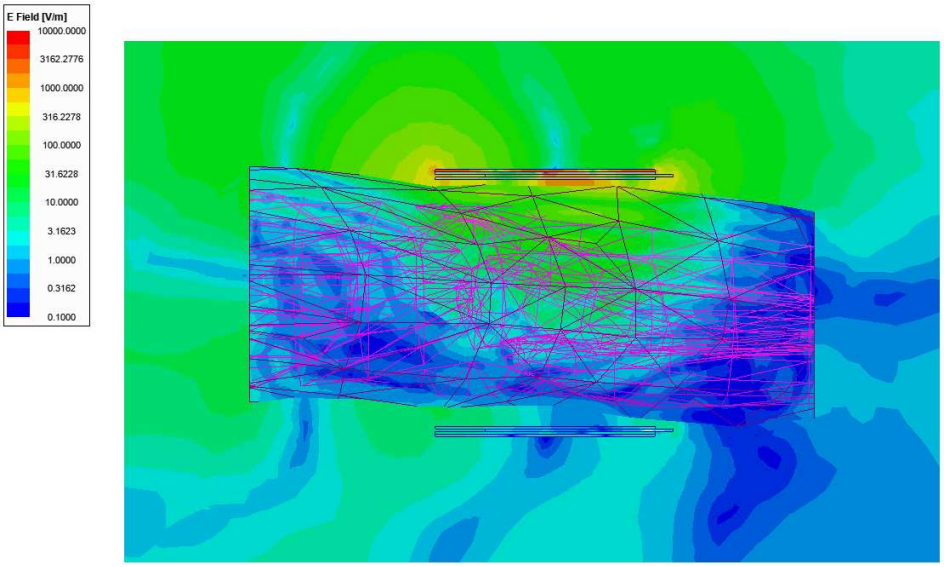

Figure 2.10. Electric Field in Arm from Monopole Antenna Side View

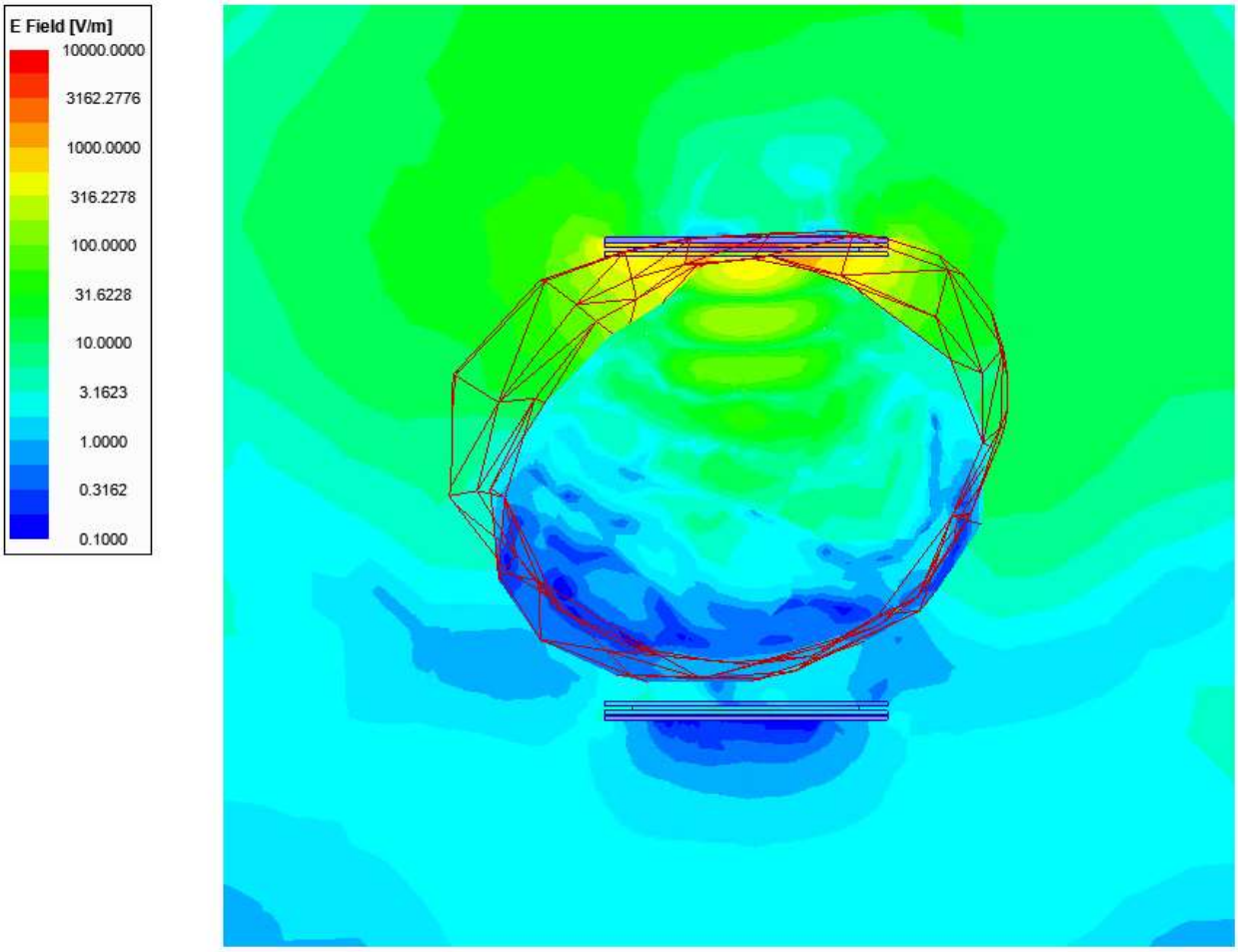

Figure 2.11. Electric Field in Arm from Monopole Antenna Front View

Based on the simulations with multiple antennas, it was decided to move forward improving on previous single sensor designs. The simulated transmission could not be established reliably enough in order to develop a metric for measuring changes in permittivity. A simplified cylindrical alternative to the human body model was tested with similar results.

2.2. Summary of antenna designs

The best approach for a single sensor system is established as a linear monopole in [10]. Linear monopole antenna designs are decided on in this work in order to have a small printed antenna design. The wide-band monopole antenna design from [3] is also used in this work for developing the antenna sensor. Overall, three different monopole antenna designs are utilized as sensors. Multiple of each are manufactured for testing across assembly tolerances. The planar

design is favorable for the application of the antennas, which will be placed on the skin. Flexible substrates were considered in [15] and the sensor from [9] actually did utilize a flexible substrate for printing the sensor. The flexibility of the substrate allows the sensor to wrap directly to the curved surface of the body. For the sensors proposed in this work, the form factor was considered small enough to find a flat enough surface on the body to be effective.

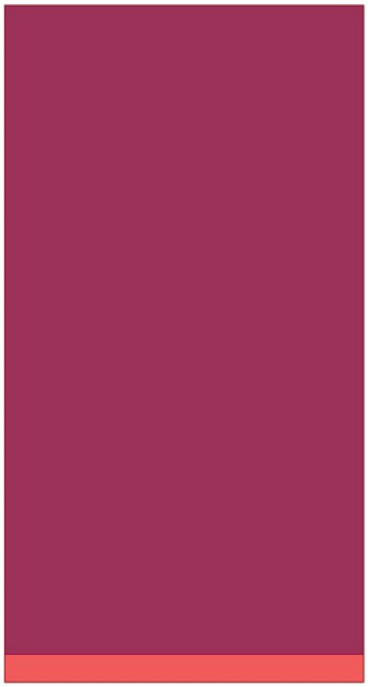

Figure 2.12. Sensor Substrate Form Factor

Each of the sensors were designed to be printed on the same rectangular substrate base size. This will help with their interchangeability during testing. The substrate layer used for design was Rogers 5880 Duroid with $\varepsilon_r = 2.2$. This is the same substrate that was used to manufacture the antenna from [10] shown in figure 1.10. This substrate is used to make each layer of a three-layer stackup. The top layer, which has the monopole antenna and the microstrip feedline, is slightly longer so that the SMA connector can access both sides of the dielectric. The dimensions of the stackup are shown in figure 2.12. The connector assembly is shown in figure 2.13.

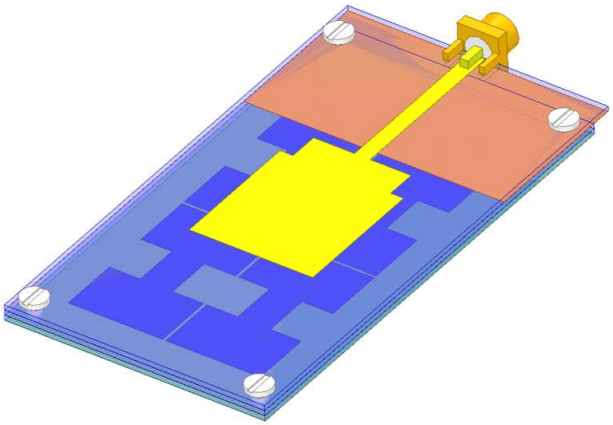

Figure 2.13. SMA Connector Assembly to Antenna Sensor

Each of these antennas are fed by a microstrip feedline that will connect with a SMA connector fitted for the boards. The first antenna designed, antenna A, is a linear monopole with two rectangular sections. The design for this antenna comes from [3] and is shown in figure 2.14.

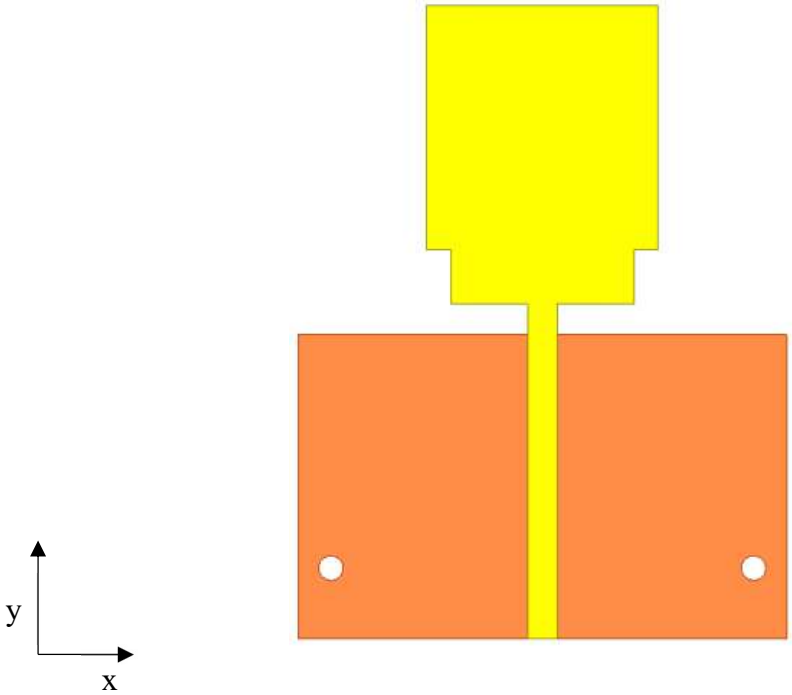

Figure 2.14. Dual Rectangular Monopole Antenna Design (A)

The ground plane for the microstrip feedline is shown in orange. The circular holes in the ground plane will be used later on as a reference for the complete screw assembly.

The second antenna designed is from [10]. This antenna, antenna B, is a beveled rectangular monopole. The design for this antenna is shown in figure 2.15.

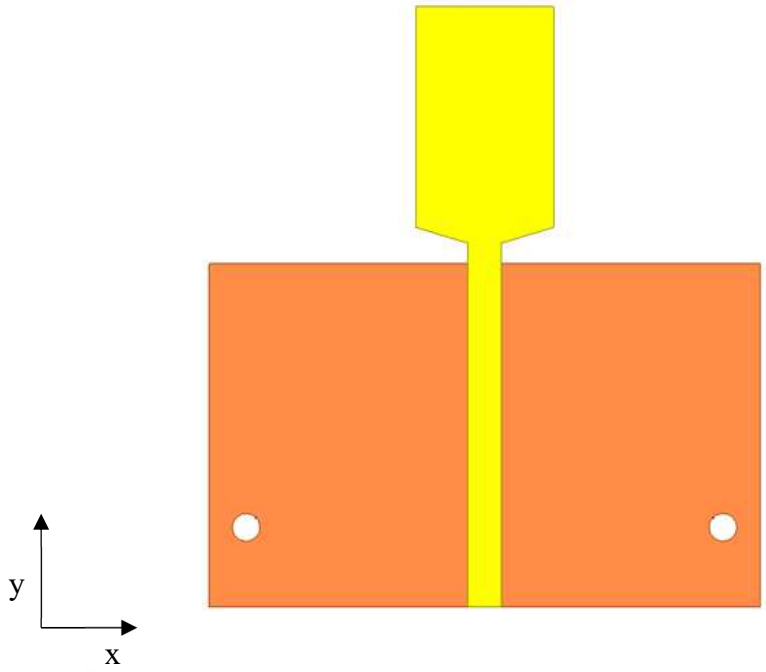

Figure 2.15. Beveled Rectangular Monopole Antenna Design (B)

The third antenna is also designed from [10]. Antenna C is a square monopole design. The dimensions for antenna C are shown in figure 2.16.

2.3. Artificial Magnetic Conductor (AMC)

When printed onto the substrate, each of the monopole antennas will radiate outward from the board on both the top and bottom. This will create an issue when the antenna is used as a blood glucose sensor on the body. As shown in figure 1.5, the ideal sensor will only radiate into the body. All of the environmental factors around the sensor will come into play if the sensor is also radiating outwards from the body into the air. This was an issue with the sensors developed in [3] and was improved upon in [10]. The AMC was shown to change the gain of the antenna to be improved in the direction towards the body and reduced in the direction away from the body.

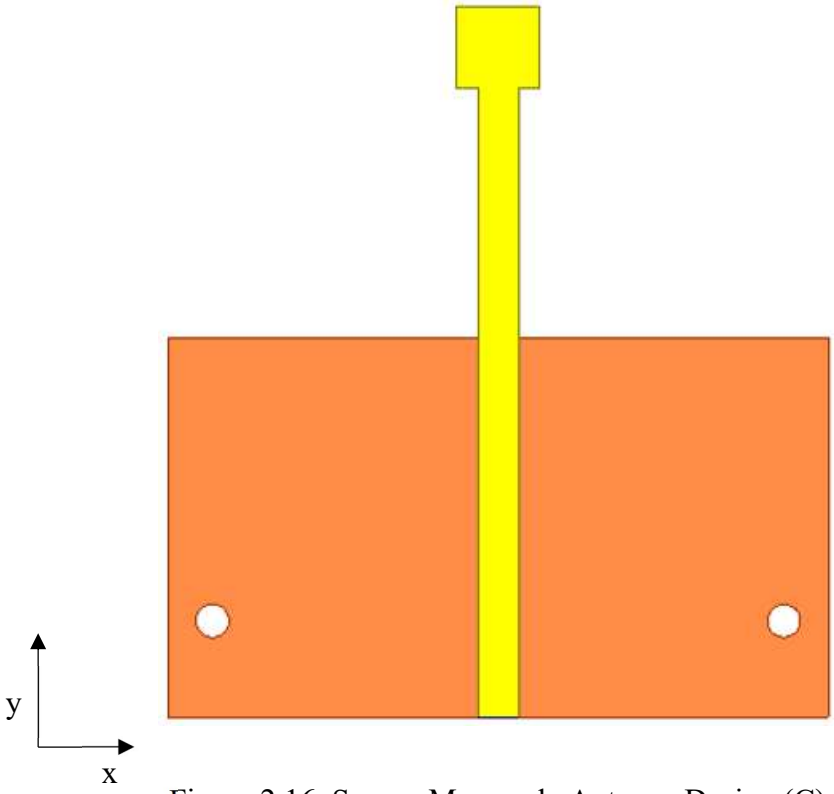

Figure 2.16. Square Monopole Antenna Design (C)

The unit cell from figure 1.9 was selected for these monopole antenna designs because it was the smallest unit cell developed in [10]. A pattern of four of the I-shaped unit cells is necessary to cover the entire backside of the antenna. The AMC should also not contact the ground plane of the microstrip feedline, so another layer of dielectric is necessary. This maintains the distance requirement shown in figure 1.8. Therefore, the sensors will each be in the same three-layer stackup, shown in figure 2.17.

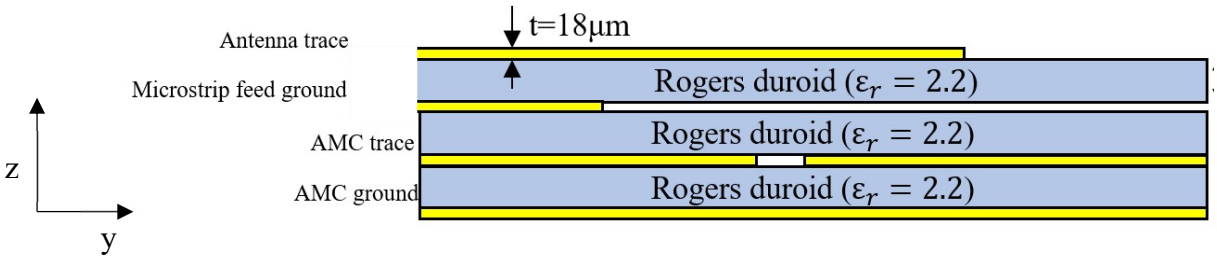

Figure 2.17. Antenna Sensor Stackup

The combined effects of the antennas and the AMC were studied in [10] through simulation. The antenna sensor response was shown to be very sensitive to the placement of the AMC unit cells, shown in figure 2.18, as they move parallel to the plane of the antenna in the y-direction.

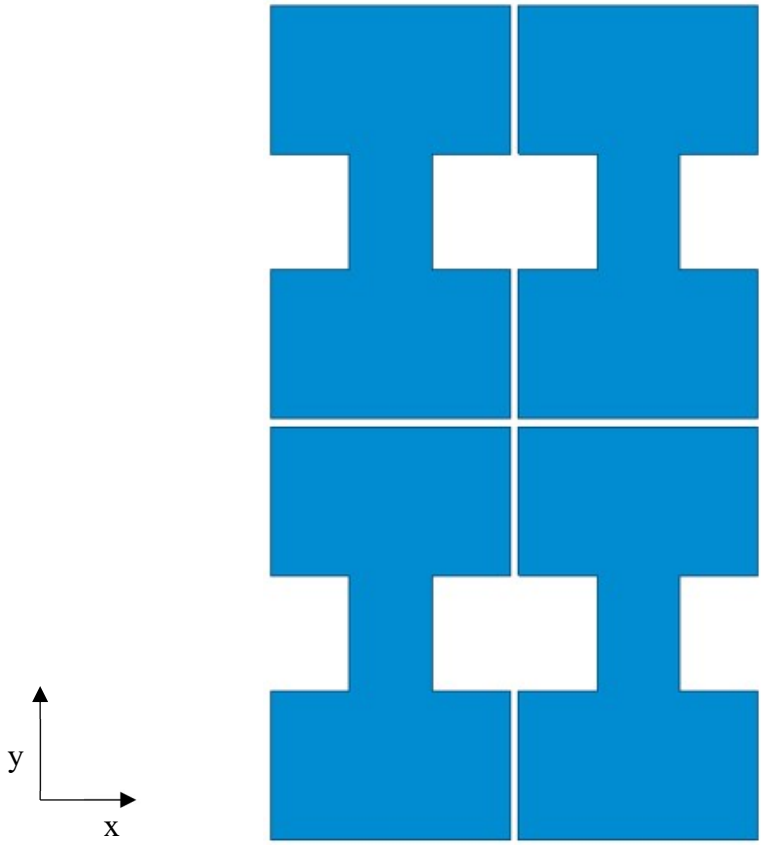

Figure 2.18. AMC Unit Cell Arrangement

Each monopole requires a different relative placement of the AMC in the y-direction. HFSS simulation parametric tuning was used to find the best possible placement of the AMC for the different monopoles. The resonance of the antenna in free space was used as a metric, looking for which AMC placement gave the antenna a resonance with the lowest return loss. The AMC placement is shown in figure 2.19.

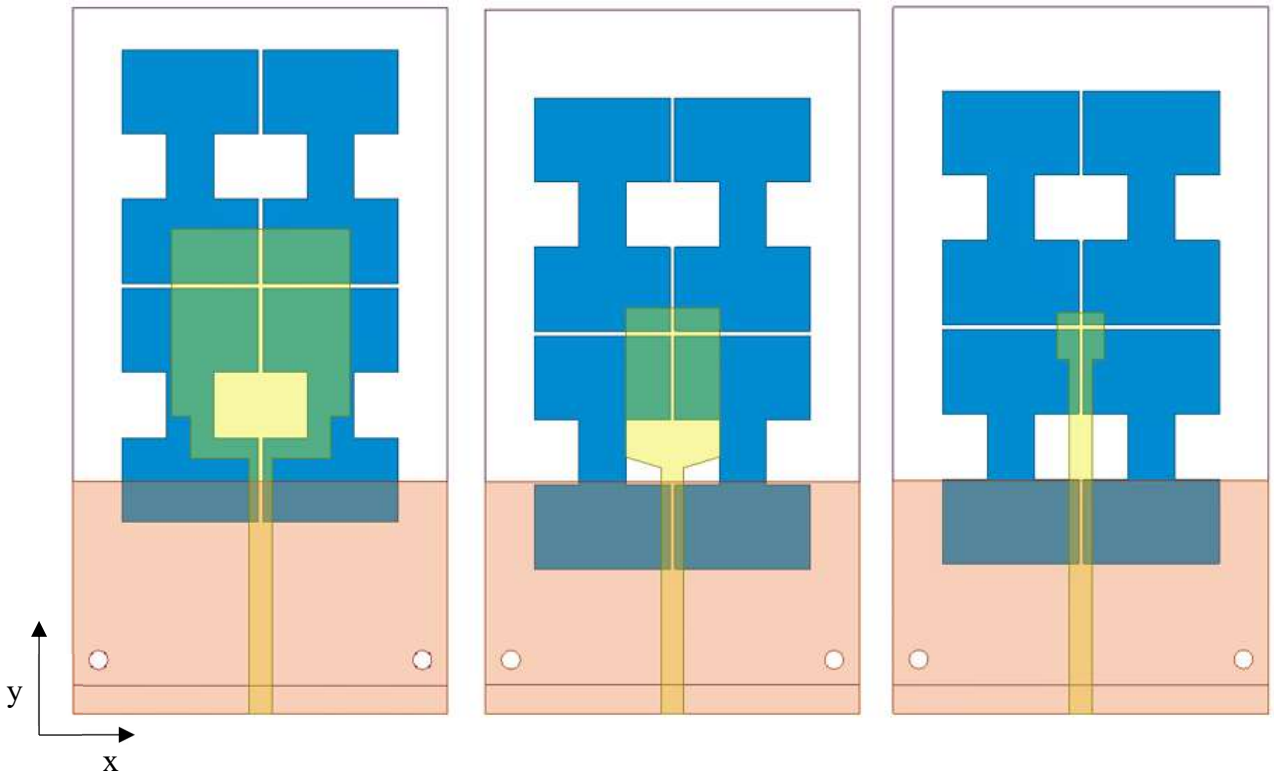

Figure 2.19. AMC Placement for Each Antenna Sensor

2.4. Rigid design

One issue from [10] was maintaining a consistent AMC placement once it was found. In order to maintain the same position for each of the layers in the stackup, four nylon dielectric screws are added. These screws are 1/4” long and are threaded as 2-56. Nylon nuts were also used to hold the crews in place. The parts were ordered form McMaster-Carr and had the part numbers of 93135A013 and 94812A100 for the nuts and screws respectively. The dimensions are shown in figure 2.20.

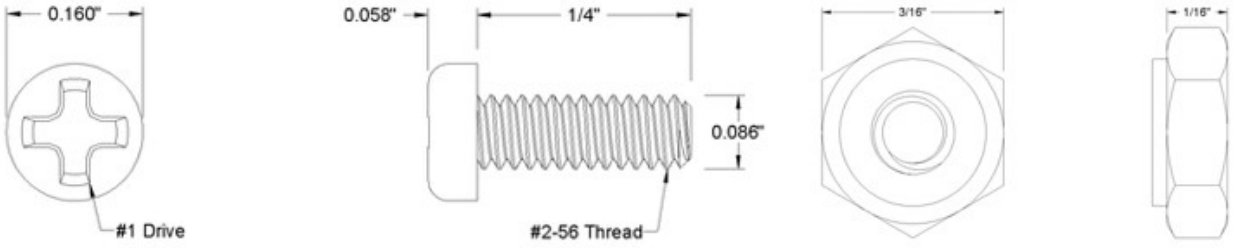

Figure 2.20. Nylon Screw and Nut Dimensions

A drill with a 5/64” bit was used to drill holes in the dielectric for the screws. In order to mark the drill spots relative to the antenna and AMC, copper trace was used and there were holes cut out of the ground planes in the gerber file. The center of the circle was drilled to be 2.7mm from each edge of the lower dielectrics.

2.5. Simulations for the monopoles

In order to predict the antenna’s performance, the full assembly was simulated in HFSS. The full assembly for antenna A, the dual rectangular monopole antenna is shown in figure 2.21. The antennas were designed for a free space resonance frequency significantly higher than the 2.4 – 2.5 GHz target frequency range. This is because when then antenna is places on the arm the resonant frequency will shift down from where it was in free space. An existing fabricated antenna was used to estimate that the shift would be about 200 MHz and the antennas were designed accordingly.

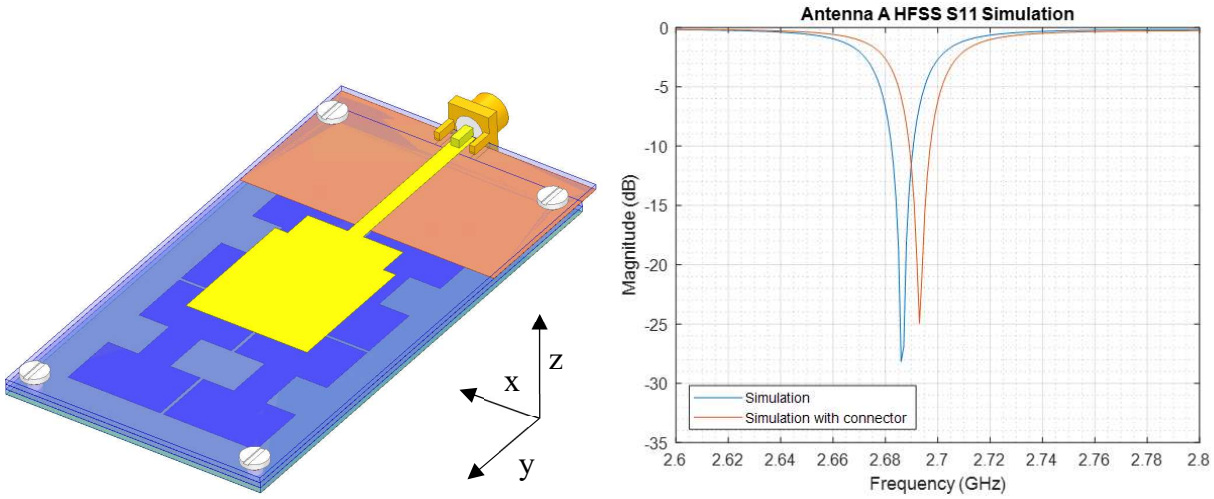

Figure 2.21. Dual Rectangular Monopole Antenna Assembly Simulation (HFSS)

The SMA connector was modeled with a simple circular conductor and nylon cylinder for the dielectric. This model is not very accurate and ultimately across the three designs the fabricated antennas were not impacted too strongly by the connector.

The 3-D radiation pattern for antenna A is shown in figure 2.22. This radiation pattern shows most of the gain in the +z-direction, which is away from the AMC layer.

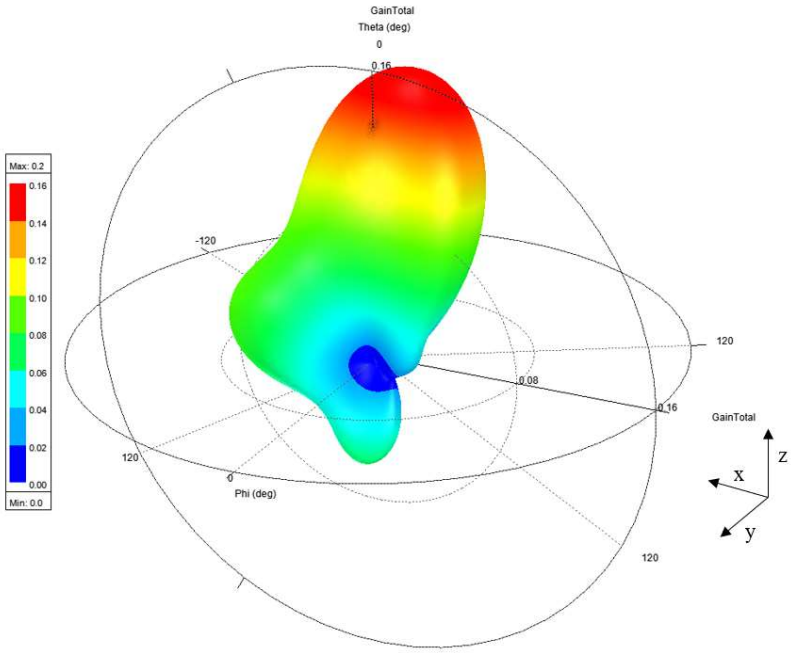

Figure 2.22. Dual Rectangular Monopole Antenna Radiation Pattern

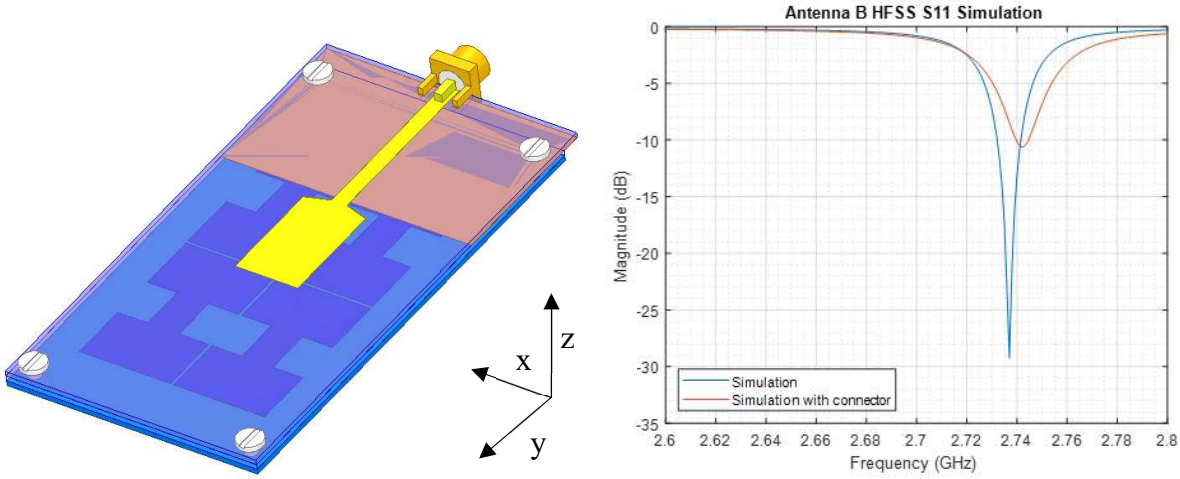

Figure 2.23. Beveled Rectangular Monopole Antenna Assembly Simulation

Antenna B is at a slightly higher frequency than antenna A. The simulation with the connector shows a significant degradation in performance but this was attributed to an insufficient model for the connector.

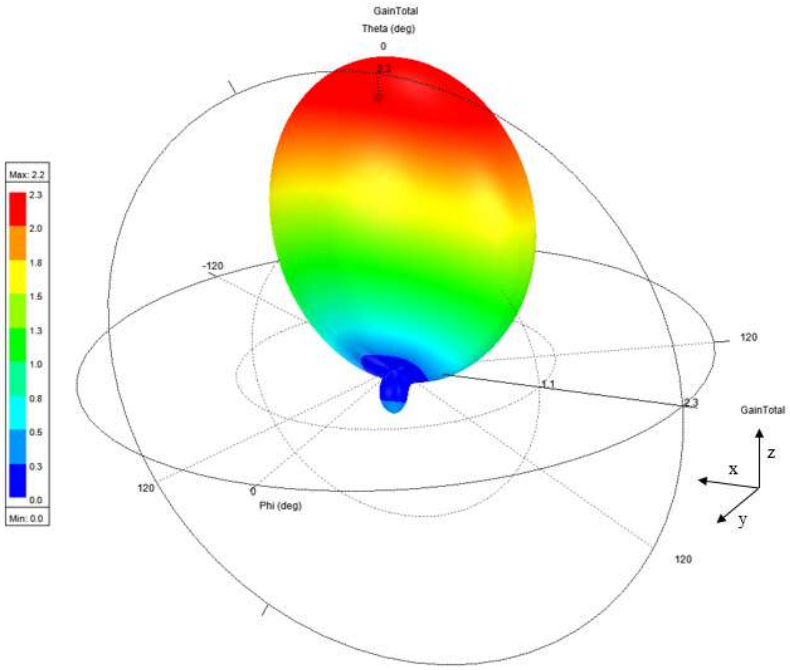

Figure 2.24. Beveled Rectangular Monopole Antenna Radiation Pattern

A similar radiation pattern is observed between the antennas for free space simulation.

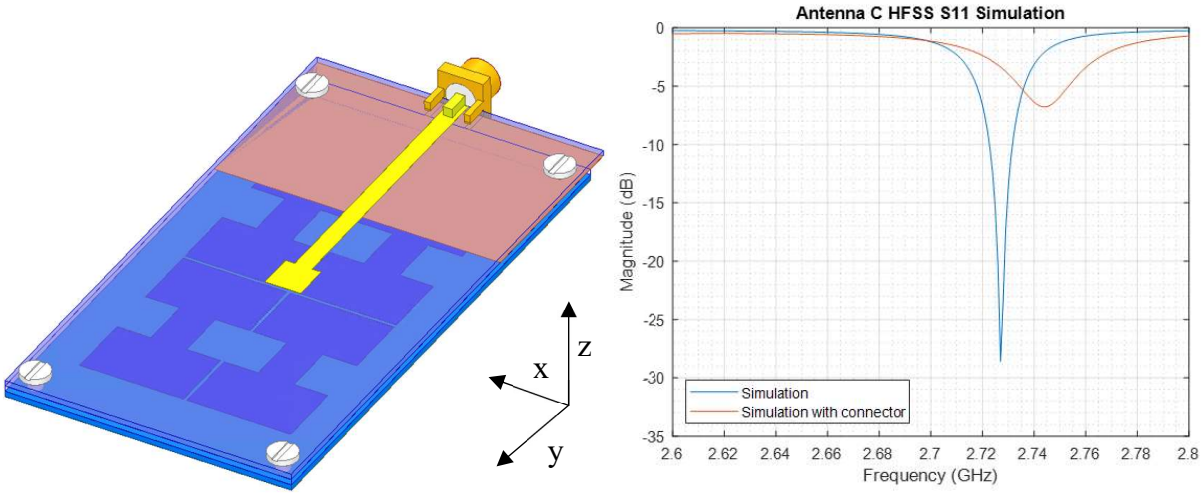

Figure 2.25. Square Monopole Antenna Assembly Simulation

Antenna C has a resonant frequency that is between the resonant frequency of antennas A and B. The connector performance is the worst with this antenna but that is again attributed to an inaccurate model being used.

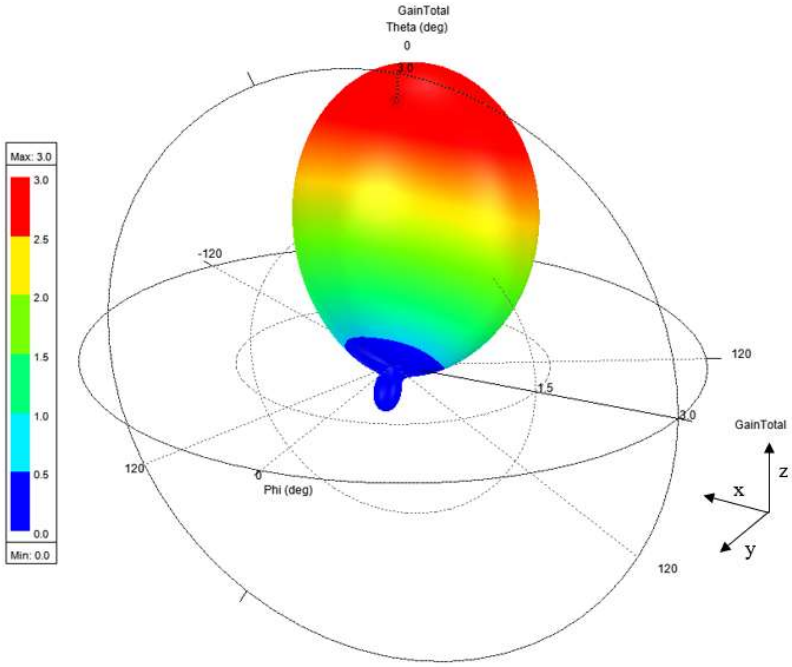

Figure 2.26. Square Monopole Antenna Radiation Pattern

2.6. SAR Simulation

Each of the antenna simulations showed a radiation pattern in free space that would make for viable blood glucose sensor along with a strong resonance that will shift to within the frequency band of interest.

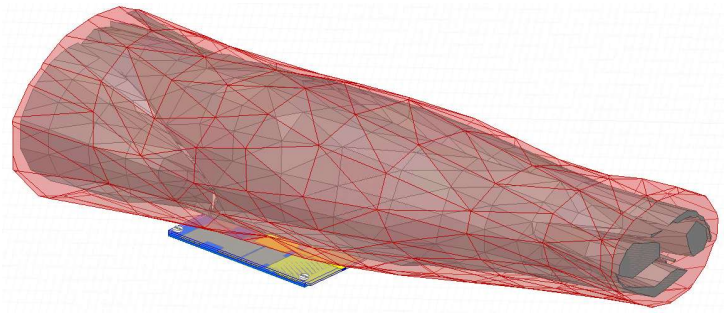

Figure 2.27. SAR Simulation Setup for Antenna B

As shown in table 1, the FCC limit for SAR is 1.6 W/kg [18]. The HFSS human body model was used to calculate the average SAR for antenna B when it is placed near the arm. The merits of this technique are discussed in [19]. The peak value was 1.0953 W/kg using the default input

power of 10mW, and the setup for this simulation is shown in figure 2.27. The calculated electric field itself is in figure 2.28. This value was deemed acceptable to move forward with the antenna designs. The primary VNA used with this antenna will be the R140 from Copper Mountain Technologies. In high power mode, the excitation power is 0 dBm or 1 mW, as stated in [20]. Therefore, this antenna is considered low power and similar to other radiating devices in the same frequency range, as discussed in [21]. The SAR values of several modern smartphones were characterized by a report in [22] and are present in table 2 for comparison.

FCC ID	BCG-E3161A	A3LSMG960U	IHDT56XC4	N/A
Manufacturer	Apple	Samsung	Motorola	RIT
Description	iPhone XS Portable Handset	Galaxy S9 Portable Handset	Moto e5 Play Portable Handset	Antenna Sensor for Blood Glucose Level
Wireless Tech Tested	GPRS	CDMA	WCDMA	N/A
Test Distance (mm)	5	15	5	2
Frequency (GHz)	2.404-2.478	2.305-2.315	2.3075-2.3125	2.3-2.5
FCC Lab Maximum Measured SAR Value (W/kg)	1.350	0.538	1.020	1.0953 (From HFSS)
Output Power (mW)	74	156	72.3	1 (From R140)

Table 2.1. Comparable On-Body Electromagnetic Devices from [22] and [21]

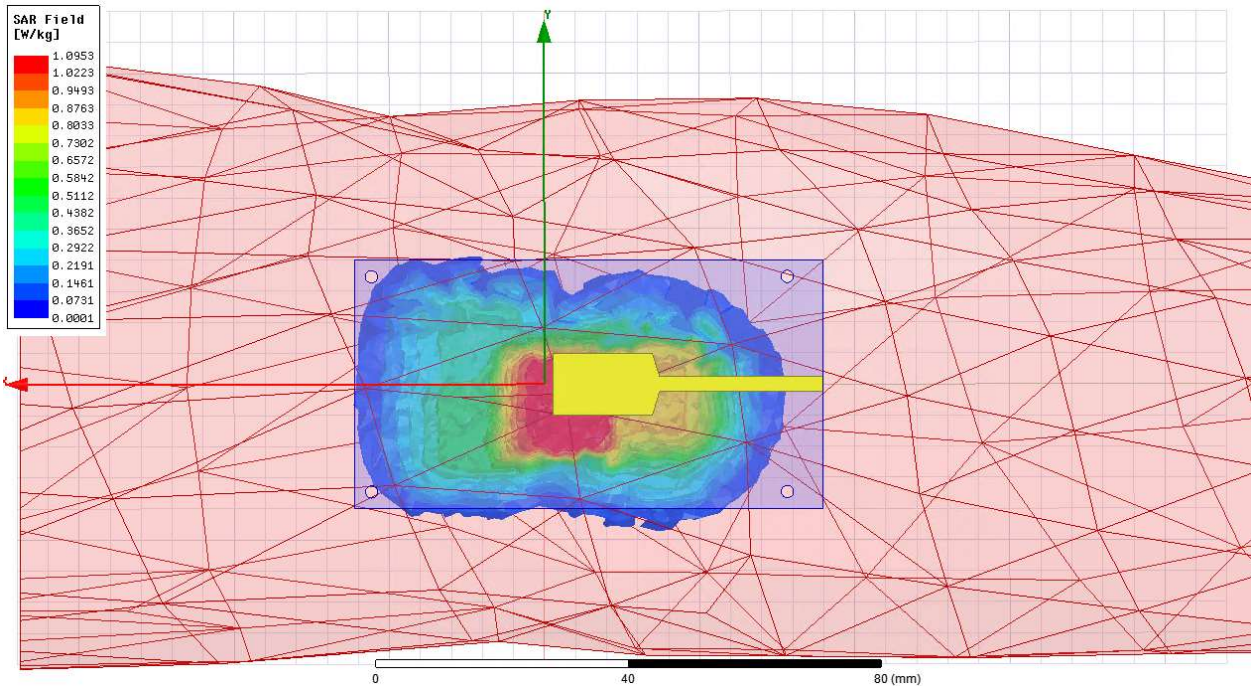

Figure 2.28. SAR Simulation Results for Antenna B

Overall, the antenna designs from [3] and [10] were improved and incorporated into a robust three-layer stackup. Three different sensors are brought to fabrication in order to verify the performance of different types of monopoles. Verification of the designs in HFSS using the human body model is difficult because of the simplifications present. Different approximations for the human body have been tried throughout the literature but there is no accurate and consistent way to simulate the antenna being on an arm for analyzing the response. In order to have confidence in the designs, they were compared with a similar two-layer stackup with just a loose dual rectangular monopole and an I-shaped AMC layer. This prototype was already manufactured and left over from [10]. As a result of testing this prototype on the human body in the lab, the on-arm performance of the new antenna designs could be estimated from the simulated free space resonances.

2.7. Fabrication and experimental validation

In order to have enough antenna sensors to test, a board with enough space for 17 full stackups was filled. There were six dual rectangular monopoles, six beveled rectangular monopoles and five square monopoles. A portion of the gerber file for the board is shown in figure 2.29.

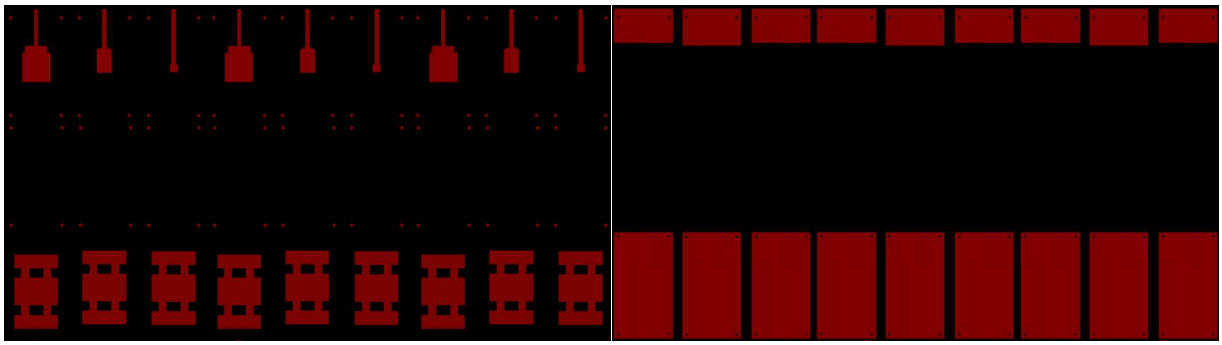

Figure 2.29. Sensor Board Gerber File (Top and Bottom)

The antennas were assembled in order to maintain the alignment of the AMC and the antenna sensor. Each antenna was tested for free space resonance after the stackup had been assembled. Each S11 was measured and compared with the simulation results from HFSS.

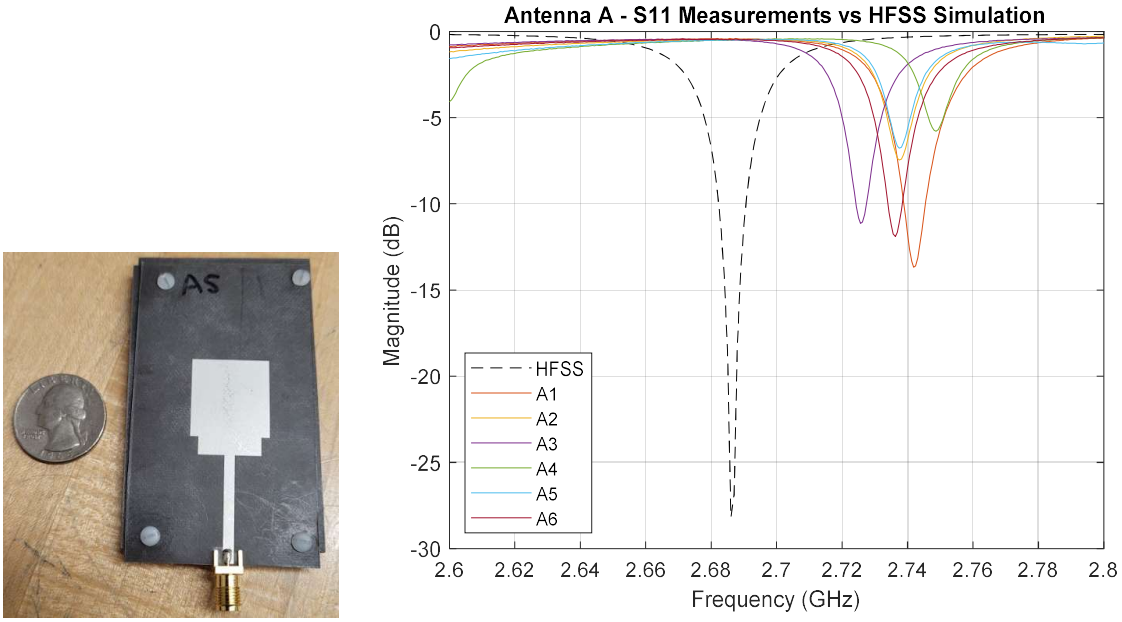

Figure 2.30. Dual Rectangular Monopole Antenna Free Space Response

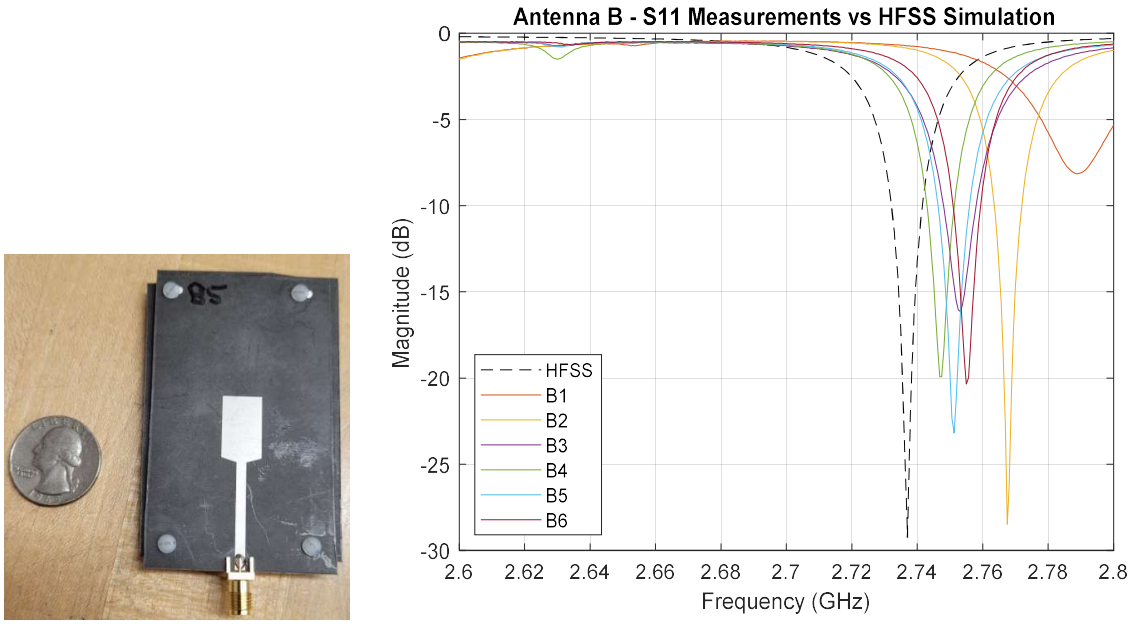

Figure 2.31. Beveled Rectangular Monopole Antenna Free Space Response

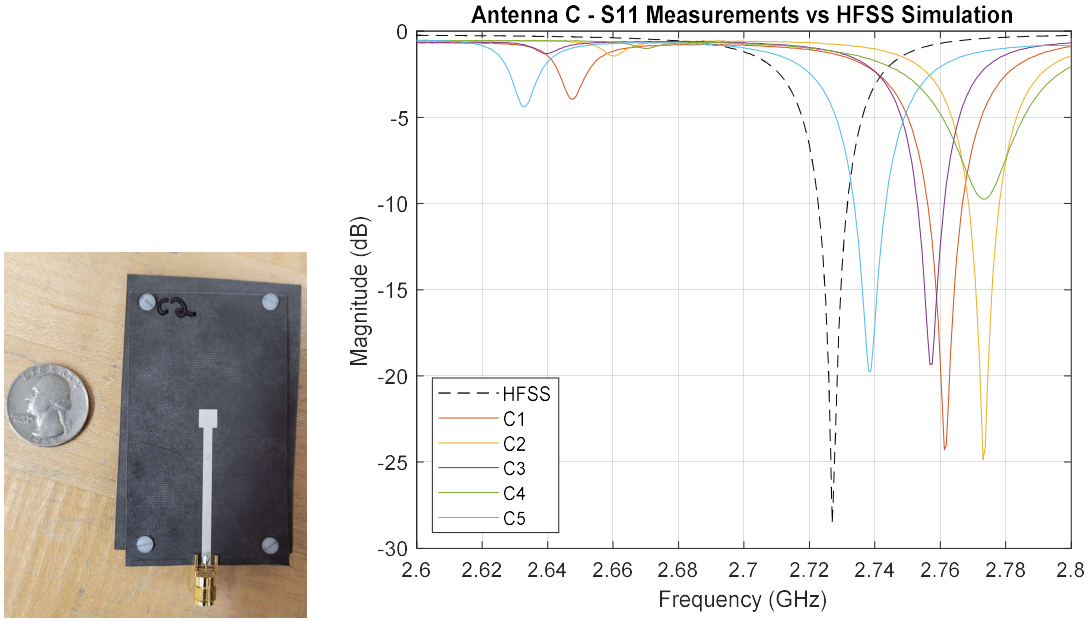

Figure 2.32. Square Monopole Antenna Free Space Response

Figures 2.30, 2.31 and 2.32 show the measured responses of each of the manufactured antennas. As expected, there was a slight shift upward in frequency from where the simulation results had calculated the resonance to be. The on-body resonance of the antennas was also measured. It was

necessary to leave a small air gap between the surface of the antenna and the skin. Both the dual rectangular monopole antennas and the beveled rectangular monopole antennas were effective at resonating on the body. The setup for an on-body resonance test is shown in figure 2.33.

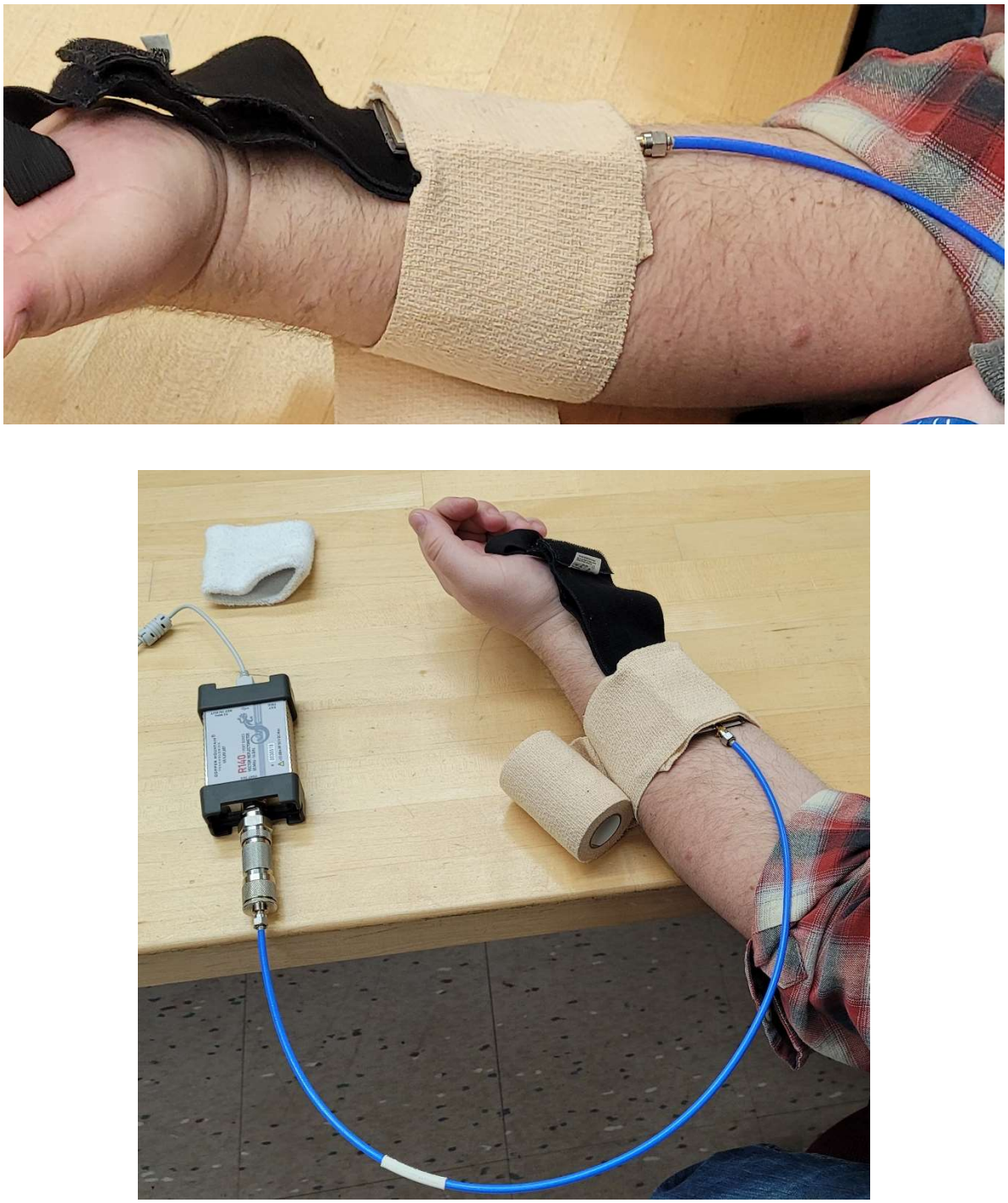

Figure 2.33. On-Body Resonance Test Setup

As shown in figure 2.33, the antenna is secured to the arm with a compression wrap bandage. The wrap needed to be adjusted in order to hold the antenna securely without putting too much pressure on the sensor. A separate back strap was placed between the non-connector end of the sensor and the arm in order to lift the sensor slightly off of the skin. The measured response for this setup over a 3-minute stable period is shown in figure 2.34.

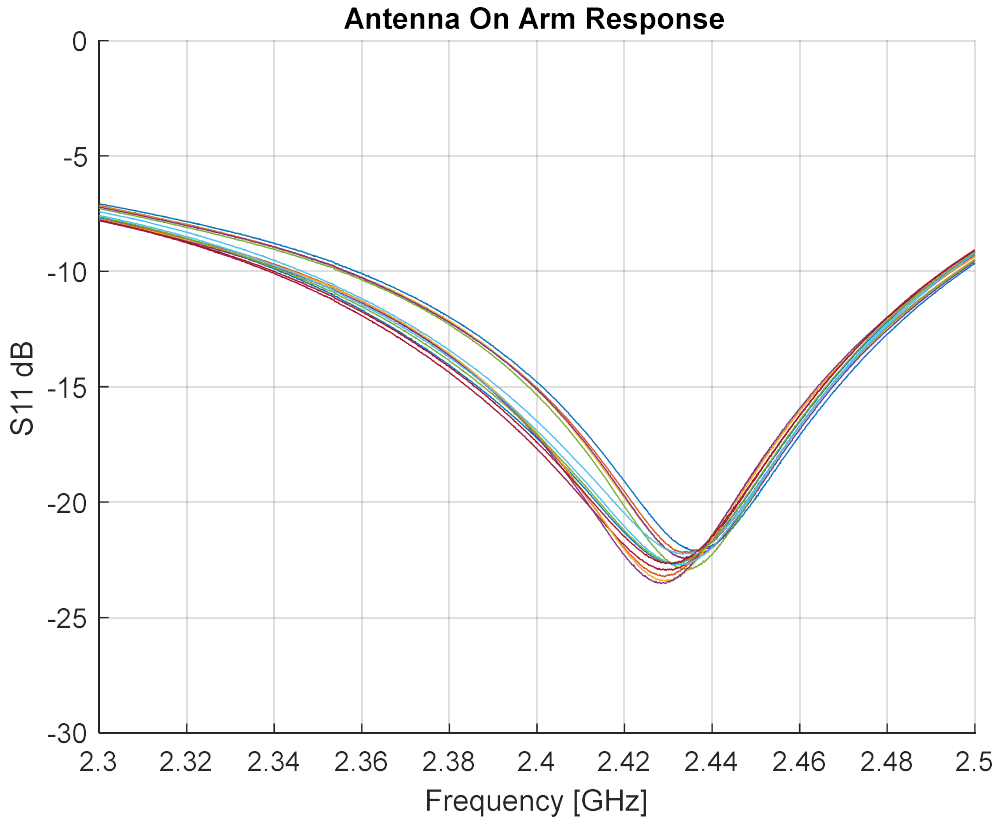

Figure 2.34. On-Body Antenna Sensor Response Over 3 Minutes

Showing a strong resonance while on the body is critical for the sensor to be able to detect changes in permittivity. In order to verify the radiation of the sensor, an anechoic chamber was used to measure the normalized radiation pattern perpendicular to the antenna. Each type of antenna was powered by an electromagnetic source that matched its free space resonating frequency. Measurements were taken as the antenna was rotated, varying theta with phi equal to zero. Theta was only swept from 0 to 180 degrees, so the side of the antenna blocked by AMC

was not measured. Figures 2.35, 2.36 and 2.37 show the measured normalized free space radiation patterns for each type of sensor.

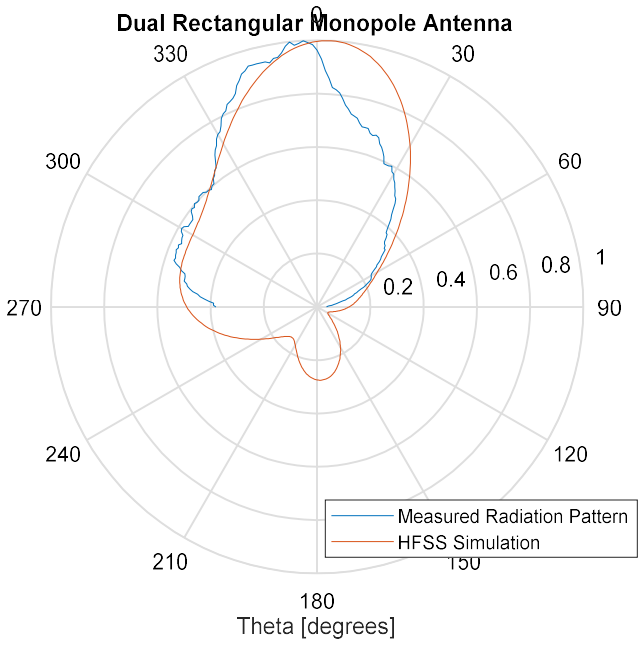

Figure 2.35. Dual Rectangular Monopole Antenna Radiation Pattern (φ=0)

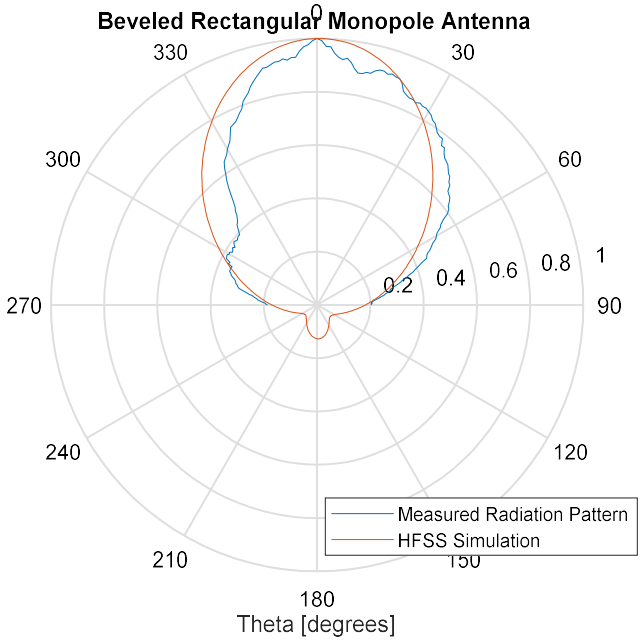

Figure 2.36. Beveled Rectangular Monopole Antenna Radiation Pattern (φ=0)

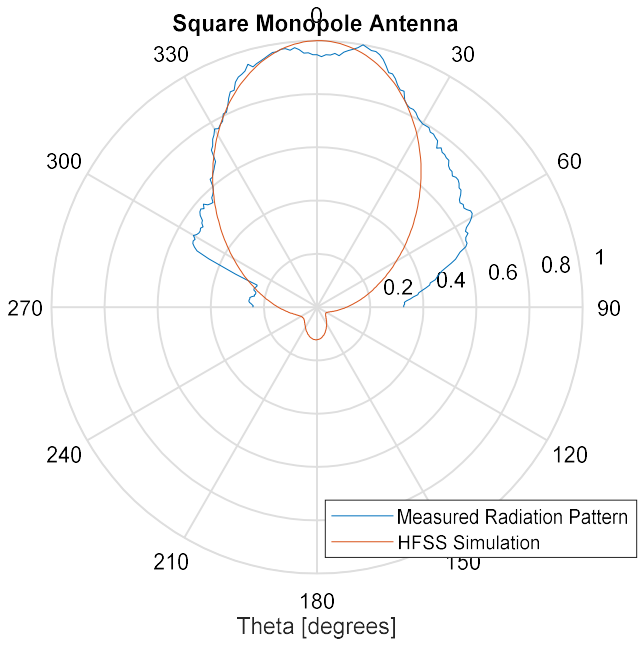

Figure 2.37. Square Monopole Antenna Radiation Pattern (φ=0)

The measured radiation plots shown agreement with the simulation results from figures 2.22, 2.24 and 2.26. The manufactured sensors show consistent performance with prior designs with the added improvements of being compact and stable assemblies. Having multiple sensors is also necessary for testing in the clinical trial. Chapter 4 details how these sensors will be integrated into a continuous measurement system. The R140, shown in figure 2.33, VNA was used to record the antenna responses in free space and on the arm. This will be the main VNA implemented in the continuous measurement system.

3. Automated Measurement of Dielectric Permittivity of Blood

The Cole-Cole model shown in equation 1 is a generalized description of biological tissue. The equation approximates the complex permittivity as a function of frequency and parameters specific to the type of tissue. As stated in chapter 1, there has been work done in order to add a glucose dependency into this equation. In [3] a linear factor was added to the equation itself and in [12] each of the parameters of the Cole-Cole model were given their own glucose dependence. The conclusions in [8] describe the challenges that can impact a permittivity measurement due to the complex concoction of molecules that are present in human blood. The basis for the non-invasive antenna sensors proposed in chapter 2 is the change in permittivity of the blood within the body, and therefore a measurable change in the permittivity of the body tissue as a whole. In order to support and validate the measurements made from a non-invasive antenna sensor, the permittivity of the blood needs to be measured accurately in-vitro and the impact of glucose needs to be characterized.

Figure 3.1 Coaxial Dielectric Probe - 85070E Dielectric Probe Kit

3.1. Automated permittivity measurements

A dielectric permittivity probe is a coaxial instrument useful for measuring the permittivity of liquid substances. Such a probe will be used to make permittivity measurements of in-vitro blood samples. More specifically, the 85070E Dielectric Probe Kit from Keysight will be employed. This probe is shown in figure 3.1. The end of the probe has a small metal coaxial tip that must be submerged in the substance being measured. The end of the coaxial probe is shown in figure 3.2.

Figure 3.2. Tip of Coaxial Dielectric Probe

In order to use the probe with a network analyzer, a Keysight Materials Measurement Suite Software package was used. This software required the probe to be calibrated in free space, while connected to a shorting block and while submerged in distilled water. Each of these calibration steps are shown in figure 3.3.

Figure 3.3. Free Space, Short and Water Calibration Steps

Once the probe was calibrated, the software could be set to make automated measurements at regular intervals. These measurements saved both the permittivity measurement and conductivity measurement over frequency for the set frequency range. A MATLAB script was written to automatically plot the data as it was generated by the Keysight program. This automation will be utilized in the combination tests described in chapter 5.

3.2. Impact of glucose on dielectric permittivity

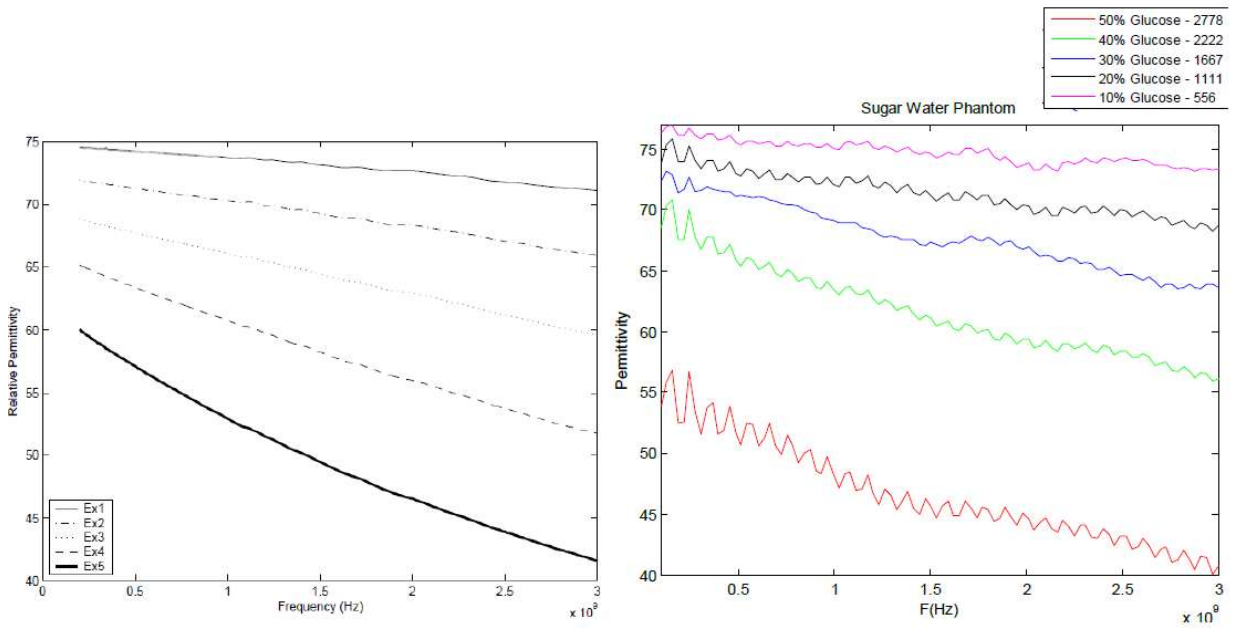

Figure 3.4. Permittivity Measurements of Sugar Water Phantom from [23]

Before the clinical trial can begin with in-vitro blood samples, a phantom substance was used in the place of blood to verify the measurements. A simple mixture of substances was suggested for this kind of research in [23]. The researchers in [9] used fetal bovine serum. A close approximation to blood is useful in predicting results, but for verification of these in-vitro measurements simply substituting water in for blood is sufficient. The work in [8] describes the challenges of phantom models due to the complexity of blood, which emphasizes the value in the actual blood samples made available in the clinical trial. The phantom of water cannot be used to validate the measurements of a non-invasive system, only predict the performance.

Permittivity measurements of a phantom with varying glucose levels from [23] are shown in figure 3.4. These results will be replicated in this work in order to verify the permittivity measurements. The conductivity measurements are also analyzed, but the conductivity was shown to change less than the permittivity with glucose. The same methodology was followed for this work as was demonstrated in [23].

In order to make an accurate measurement with the probe in a petri dish, only about 1 mL of liquid substance is necessary, depending on the viscosity. The probe was cleaned in between measurements. Cleaning the probe is important because glucose can attach to the end of the probe while it is in the water. It will also be important to clean and sterilize the probe in between measurements with blood samples in the clinical trial. The probe must be sterilized in order to avoid cross-contamination of the in-vitro blood samples. The measurement setup for 1 mL of fluid is shown in figure 3.5.

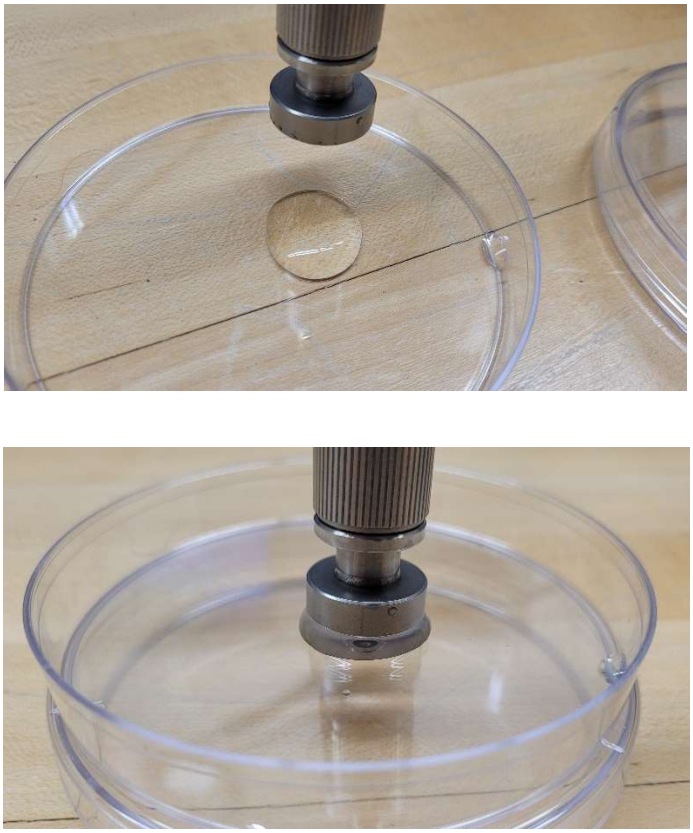

Figure 3.5. Phantom Measurement Setup with Dielectric Probe

After the phantom measurement setup was established, different amounts of glucose were added to the phantom solution. The amount of glucose was added to 300 mL of water, incrementing by one tablespoon. The results for the permittivity measurement within the frequency range of interest from 2-3 GHz, for each concentration of glucose are shown in figure 3.6.

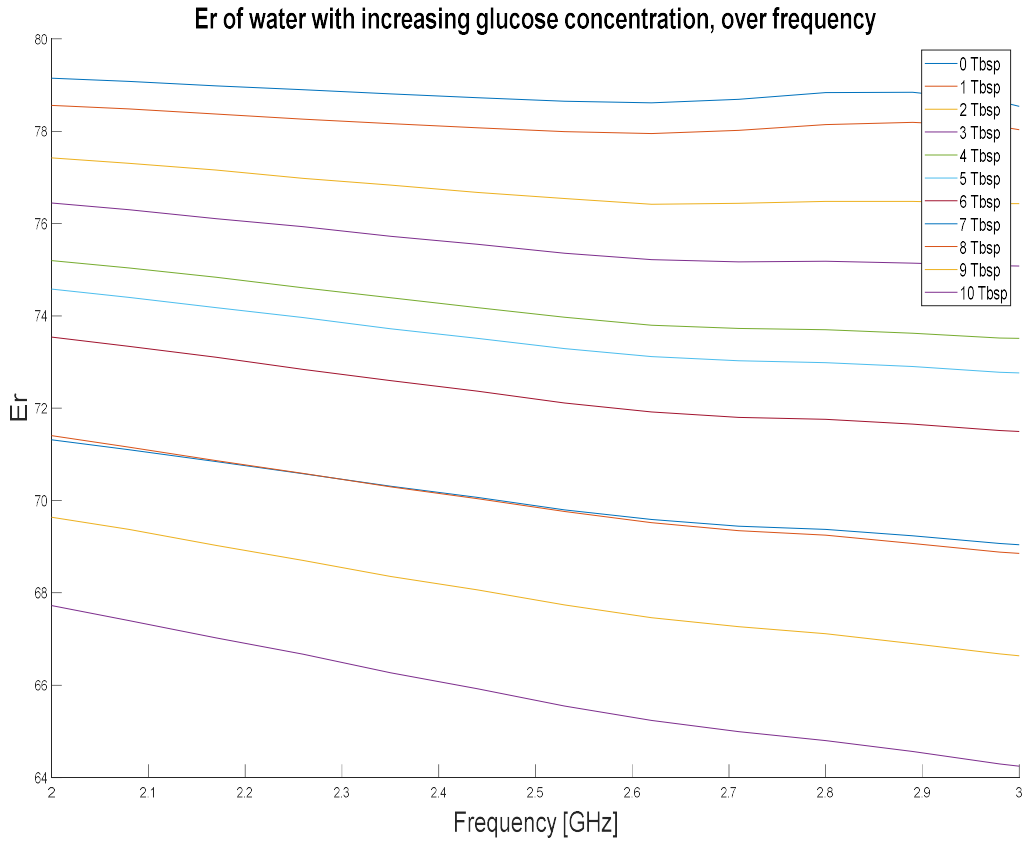

Figure 3.6. Phantom Measurement Results with Increasing Glucose

As observed from the phantom measurements, increasing the glucose concentration causes a decrease in permittivity. This is in agreement with the other studies that have made similar measurements, such as [12]. These results predict that increasing the concentration of glucose in blood and therefore the body tissue will decrease the dielectric permittivity. The critical factor becomes the amount of glucose and the amount of change in permittivity. The concentrations of glucose used to demonstrate the phantom measurements are much greater than concentrations of glucose that will be typically found within the human body. The range of glucose values will correspond to a range of permittivity levels. During the clinical trial, the range of permittivity change in blood can be established with in-vitro measurements in a setup parallel to the phantom measurements. This range of permittivity change, once defined, will inform the non-invasive sensor and further phantom testing. Figure 3.7 shows the measured permittivity change localized

to three distinct frequencies. It will be important to consider the permittivity change at each frequency point when analyzing data from the non-invasive sensor.

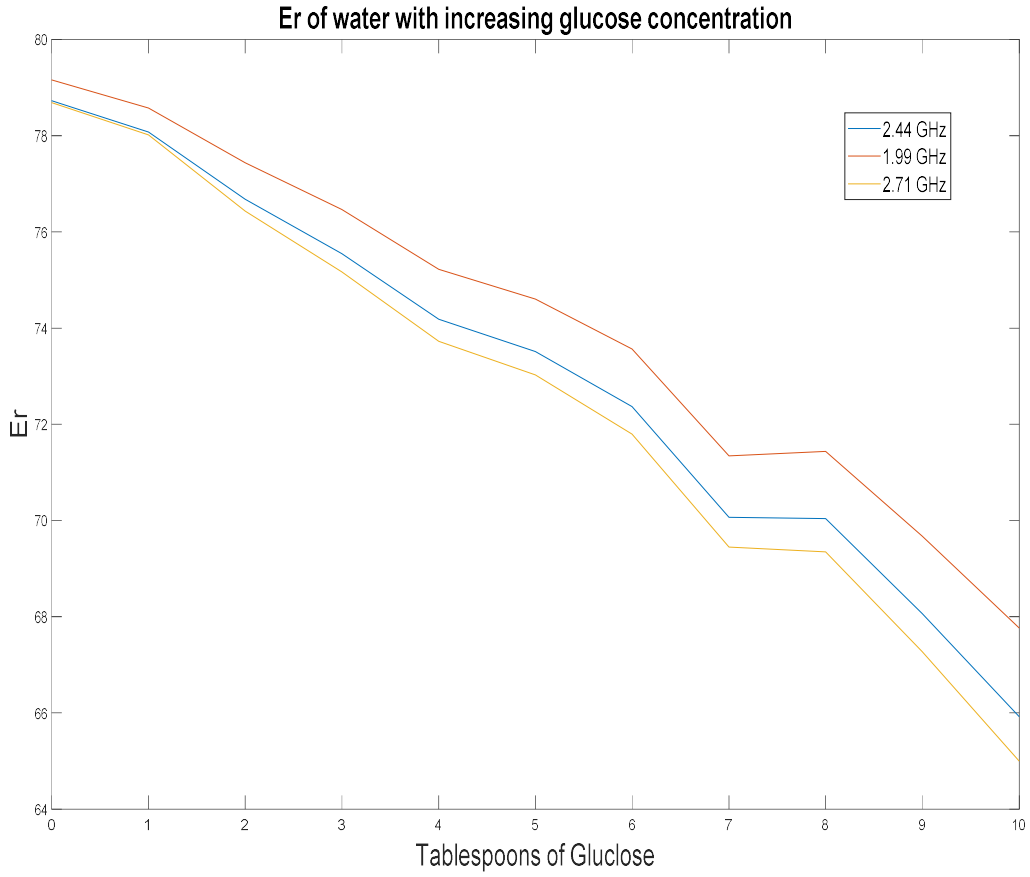

Figure 3.7. Phantom Measurement Results Localized in Frequency

3.3. Modified Cole-Cole model

The Cole-Cole model can be modified based on the probe measurements. With a large number of in-vitro permittivity measurements of blood samples, the analytical change to the Cole-Cole model to add a glucose dependency can be investigated. Depending on the data, a linear factor could be added, each parameter could be made dependent or a machine learning approach could be employed. The Cole-Cole model was not changed based on the phantom measurements. In order to have the most accuracy, the blood samples in-vitro permittivity measurements will be compared directly against the traditional in-vitro blood glucose measurements to derive a

relationship. This will also force the glucose concentrations being considered to be within the realistic range for the human body. The research in [9] included clinical trials that looked at differences in blood samples across different patients. The patient consistency will also be considered when developing a glucose dependency for the Cole-Cole model.

4. Automated Measurement, Analysis and Network Transmission of Antenna Response

Prior work had proposed a system solution for automating the measurement collection of an antenna sensor. The system would need to be compatible with a wide range of available network analyzers. The proposed system is compatible with all network analyzers present in the ETA lab, but the main focus was the R-140 network analyzer due to its compact size. Figure 4.1 shows a high-level flow diagram of the proposed system.

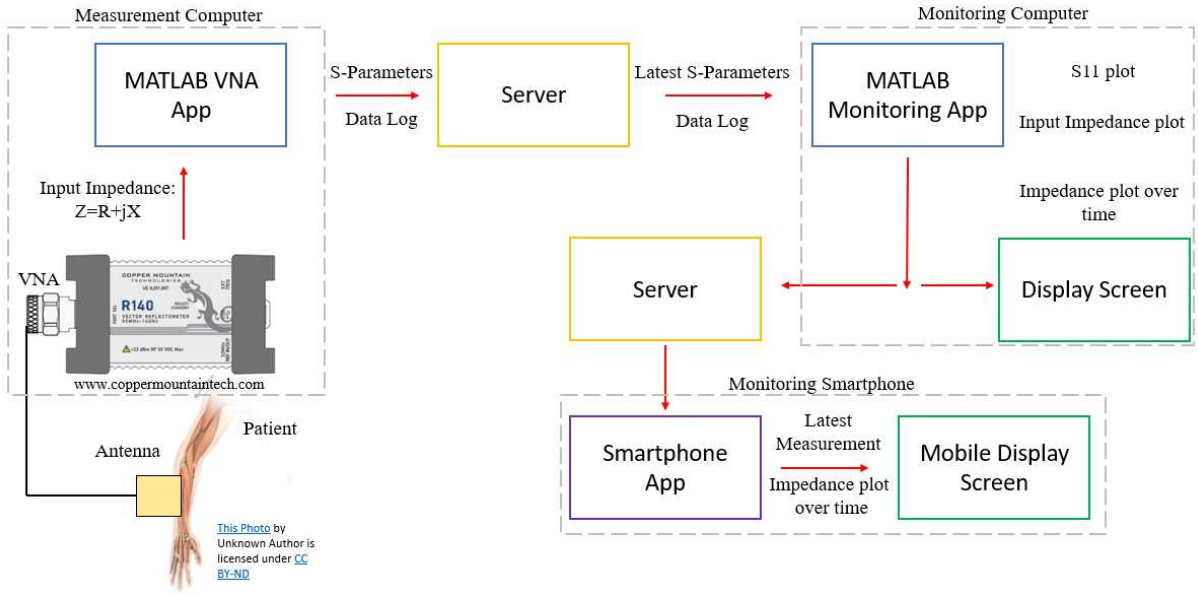

Figure 4.1. System Block Diagram

4.1. Measurement collection

An automated system was necessary in order to carry out the systematic testing and ultimately prototype a clinical-use application. In order to utilize both the lab bench VNA's and the R140 VNA by Copper Mountain Technology, MATLAB applications were developed. The new MATLAB Application Designer suite was utilized.

The VNA's are controlled by a computer and the measurements are automated. For the R140, which is more portable and easier to use than the lab bench VNA's, the application can load in a

pre-saved calibration file. This ‘state’ file will store the full configuration of the VNA, including frequency range, calibration coefficients, electrical delay, number of points and display format. In contrast, the lab bench VNA’s need to be calibrated manually on the device before the MATLAB program is launched. This can be done by loading in a pre-save as well. For most VNA’s the application will be able to save a ‘connection’ record to easily reconnect with the same VNA, but the calibration and setup of the VNA will need to be complete before the application communicates with the VNA.

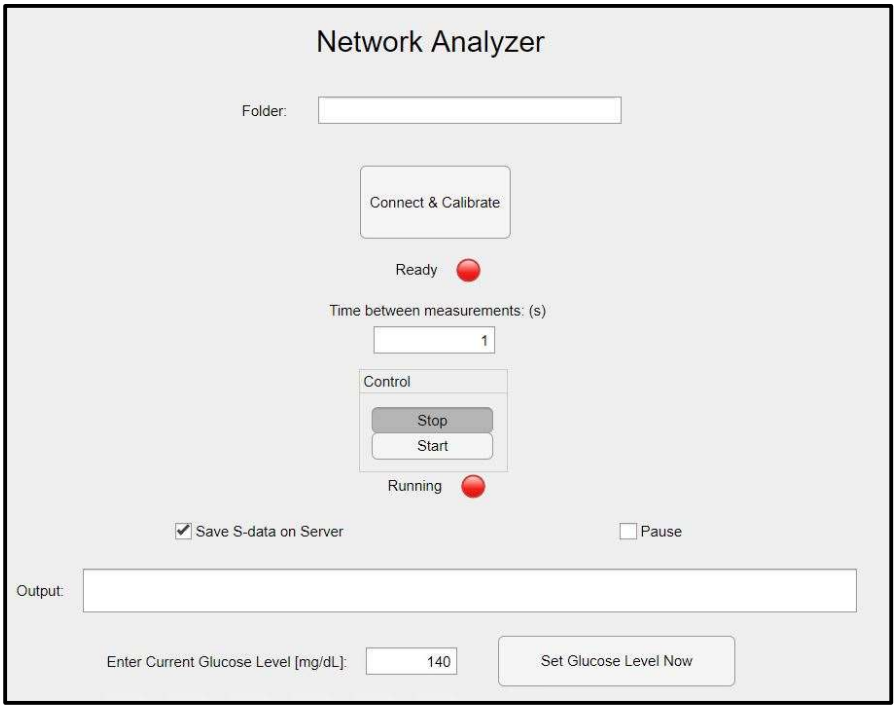

Figure 4.2. MATLAB VNA Application

Due to the product specific software required for the R140, two entirely different versions of the MATLAB VNA app were developed. They will have the same output and have identical functionality, but one is equipped to work with the R140 and the other will connect to the lab bench VNA’s. The MATLAB program for the R140 VNA is based on sample code provided on the Copper Mountain Technologies website. Figure 4.2 shows the interface for the R140 version of the application. The lab bench VNA’s require slightly different code, based on code MATLAB code developed by prior students for other courses. That program was called NAP, for Network Analyzer Program. The NAP program had been and modified to take automated

measurements for this blood glucose level monitoring project but it was further updated and modified in this iteration in order to be compatible with the new modifications such as metadata collection, server integration, an alternative algorithm and a few big fixes to address some existing issues.

For any VNA, the network analyzers should be allowed to run at measurement frequency for a while before calibration. Particularly with the R140, which has an internal temperature sensor utilized by the MATLAB program, the device will heat up to about 105°F over time. If a calibration is done before the VNA reaches this operating temperature, the results can become skewed by the change in temperature. Copper Mountain Technologies recommends letting the VNA run for at least 30 minutes before calibration. For more accurate measurement, this same procedure should be followed with the lab bench VNA's.

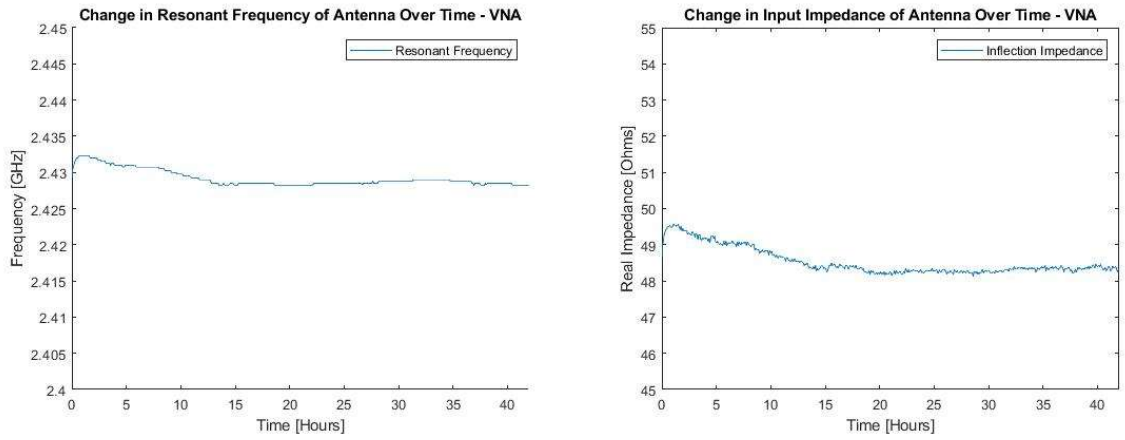

Figure 4.3. Stability Test for Lab VNA Measurements

Extensive testing was done on both types of VNA (R140 and lab bench) where the resonant frequency of an antenna in free space was collected every 5 minutes over a 42-hour period. The resonant frequency found was much more stable when the VNA's were allowed to run for at least an hour prior to calibration. The sensitivity test showed that the 'hot' calibration improved the stability of the measurement significantly. The R-140 was tested with an antenna resonating 2.525 GHz and the measurement held between 2.526 and 2524 GHz over the 42-hour period. The temperature measurement was taken over this period and showed that the R-140 VNA was running at a constant temperature of 105°F for the entire test. The antenna had a sharp resonance

of -20 dB for S11. Likewise, the lab bench VNA was connected to a similar antenna with -40 dB for S11 at 2.432 GHz. For the 42-hour period, the resonant frequency remained between 2.4282 and 2.4322 GHz. Figure 4.3 shows this data. This sensitivity information helped improve the subsequent tests where the resonant frequency was also measured. Allowing the VNA's to have a 'hot' calibration is a necessary step in implementing this process, be it in the lab or in a clinical setting.

Before the VNA is calibrated, the frequency range and number of points must be set. For these applications, a standard of 1601 points were used across the VNA's. The center frequency for majority of the antennas designed is approximately 2.4 GHz when near a MUT, so the ranges used were 2-3 GHz, 2.2-2.6 GHz and 2.3-2.5 GHz depending on the test being done.

The VNA's were calibrated using a standard Short-Open-Load kit of N-type male components. The calibration done was as close to the antenna as possible. The antennas have an SMA female connector, so the calibration with the N-type kit was able to be done within one N-type to SMA adapter to the antenna. Having the reference plane close to the antenna sensor will improve the accuracy of the measurement. The same adapter and cable setup was used across the various lab testing done with the antennas. The calibration kit can be specified in the R-140 software but it does not need to be correct. The calibration itself will correct for any differences when the kit is not specified. The electrical length should still be adjusted if necessary, typically using the short as a reference and moving the response to the left side of the smith chart.

Once the calibration was verified, the VNA needs to be set into 'Polar' format. This will allow the MATLAB applications to capture the real and imaginary components of the S11 measurement. All markers should be cleared as well. For the R140, the RVNA software is able to save the current state, to be recalled by the MATLAB program. With the lab bench VNA's, the MATLAB program can be launched once the VNA is ready, as launching the program will turn remove local control of the VNA. The local control can be reestablished by pressing the 'local' button. In order to pre-load a 'state' with the R140, the state file should be saved in the default location for RVNA state files on the computer hard drive. The MATLAB program calls a Microsoft Excel macro that loads in the state file, so whichever state file being used needs to be referenced by the Excel file in the same directory as the MATLAB program.

The interfaces for both versions of the program are slightly different and the underlying code for connecting to the VNA is specific to the VNA model. Apart from these variations, the actual automation for collecting data is identical. The program will loop until stopped, where each iteration it records the full complex S11 data, calculates input impedance, determines the inflection impedance value, uploads the data and results to the server and then waits the specified delay time before repeating the loop.

In order to access the server, the login and password of the RIT account are hardcoded into the program. The MATLAB code used programs from [24] in order to perform an scp operation. This information is protected in the Web App version of the program and cannot be accessed. Data security is an important consideration and using the secure RIT network provides this protection. The folder location on the server is specified as an input field of the MATLAB program. Each test or usage of the program can use a different folder for simplicity and organization. The server folders and files can be managed by a separate terminal login to the server. The delay between measurements can be adjusted by adding more wait time. The fastest speed is approximately one measurement every 10 seconds but this will change depending on the computer running the program. Each measurement is time-stamped using the MATLAB date and time function and this time stamp is used to display the data in subsequent programs. This is important because the different programs are not synchronized in time, where each one accesses the server independently. In the event that one of the MATLAB programs cannot access the server, a network connection loop is entered where measurements are halted. The program will attempt to reestablish a connection one hundred times, waiting the specified delay time in between each attempt. The user is alerted to this on the output line. When the connection returns the measurements will resume.

Current Hour	Current Minute	Current Second	Inflection Impedance [Ohm]	Frequency [Hz]	S11 [DB]	S11 [ANG DEG]	Zin [RE Ohms]	Zin [IM Ohms]	Error Flag [1==Error]	Glucose Level [mg/dL]
15	25	59	54.2964021	2500000000	-6.558509133	-8.102954391	134.1878472	-22.81830649	0	104
15	25	59	54.2964021	2500125000	-6.577671715	-8.299288515	133.6478762	-23.19310058	0	104
15	25	59	54.2964021	2500250000	-6.566956161	-8.215077866	133.9221774	-23.05096434	0	104
15	25	59	54.2964021	2500375000	-6.600907976	-8.415529527	133.1273672	-23.32637158	0	104
15	25	59	54.2964021	2500500000	-6.570423102	-8.409923748	133.6509415	-23.53131146	0	104
15	25	59	54.2964021	2500625000	-6.592591881	-8.595388304	133.0706209	-23.8466533	0	104
15	25	59	54.2964021	2500750000	-6.634498856	-8.623748255	132.3375905	-23.61478545	0	104
15	25	59	54.2964021	2500875000	-6.626001184	-8.776342924	132.3108584	-24.06112301	0	104

Figure 4.4. Sample Data File

Once the measurement is captured, the magnitude and phase of the S11 measurement are stored by the program. The input impedance is calculated and also stored as a variable. Each iteration of the loop will result in a new data file being written. This file will include the following variables: the current hour, the current minute, the current second, a single value for inflection impedance, a vector of frequency values measured, a vector of S11 magnitude, a vector of S11 angle, a vector for real input impedance, a vector for imaginary input impedance, a single value error flag and a single value of metadata. Typically, the measurement vectors over frequency had 1601 points. The metadata value can be used to record a traditionally measured blood glucose reading. For lab testing purposes with the R140, the metadata value was used to store the current internal temperature of the VNA. The error flag plays a role in the inflection impedance algorithm.

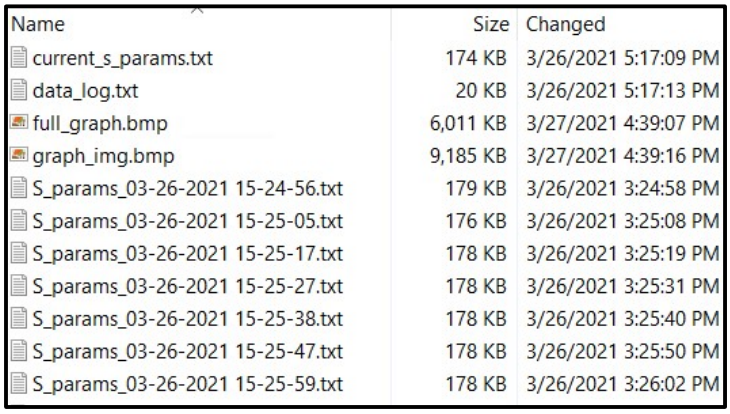

Name	Size	Changed
current_s_params.txt	174 KB	3/26/2021 5:17:09 PM
data_log.txt	20 KB	3/26/2021 5:17:13 PM
full_graph.bmp	6,011 KB	3/27/2021 4:39:07 PM
graph_img.bmp	9,185 KB	3/27/2021 4:39:16 PM
S_params_03-26-2021 15-24-56.txt	179 KB	3/26/2021 3:24:58 PM
S_params_03-26-2021 15-25-05.txt	176 KB	3/26/2021 3:25:08 PM
S_params_03-26-2021 15-25-17.txt	178 KB	3/26/2021 3:25:19 PM
S_params_03-26-2021 15-25-27.txt	178 KB	3/26/2021 3:25:31 PM
S_params_03-26-2021 15-25-38.txt	178 KB	3/26/2021 3:25:40 PM
S_params_03-26-2021 15-25-47.txt	178 KB	3/26/2021 3:25:50 PM
S_params_03-26-2021 15-25-59.txt	178 KB	3/26/2021 3:26:02 PM

Figure 4.5. Server Files

This file is created as an ordinary .txt file from a table variable in MATLAB. Figure 4.4 shows the first few rows of a samples .txt data file. The benefit of using this customized .txt file over a standard .s1p Touchstone file in this case is the addition of the time stamping and metadata. The file was customized to fit the precise needs of this system. Each file is approximately 180 kB which is not an issue for the server space that was allocated, even when frequent measurements are being recorded. Figure 4.5 shows a collection of these files on the server. When each file is uploaded, a copy of it will also overwrite the most recent s-parameter file. This latest data file will change every iteration and it will be referenced by the other programs.

In the case of the R140, the computer running the MATLAB program needs RVNA installed, which is the Copper Mountain Technology software for operating the R140. MATLAB uses the

COM server to communicate with the application and therefore the R140. The lab bench VNA's are also operated using the COM server. In order to access the server, the MATLAB program needs a standard internet connection. A pause button was added to temporarily halt measurements. This button was used for changing the glucose concentration during a test. In addition to network interruption, the program will also stop if the connection to the VNA is lost. This would occur if the VNA malfunctioned or the USB connection was broken.

4.2. Permittivity change algorithm

The antenna response was observed in different environments during testing. For the purposes of this study, most important factor affecting the sensor is the effective dielectric permittivity around the antenna. Ideally, the sensor will operate in such a way that changes in the effective permittivity are driven solely by changes in the glucose concentration of the MUT. It was observed in prior research [3] through both simulation and testing that the resonant frequency of the antenna was the metric of the response that correlated with changes in permittivity. The resonant frequency was defined as the frequency where the magnitude of reflection was a minimum. The changes in the frequency of where the imaginary input impedance is zero have also been considered based on simulation. [25] Based on the testing done with the new antennas, a new metric based on changes in the real input impedance is proposed in this study.

Extensive simulation has been done looking at the reflection and input impedance as the relative permittivity of the material surrounding the antenna changes. For the specific setup used in this study, the changes in the real input impedance were observed to be more consistent when relative permittivity changes analogous to realistic changes in blood glucose levels were taking place, based on prior in-vitro measurements [3]. To be specific, the modified Cole-Cole model had the permittivity of blood change from about 60 to 50 as blood glucose levels were increased from 72mg/dL to 313mg/dL. This range represents expected patient blood glucose levels. A patient having less than 140mg/dL is considered normal. Between 140mg/dL and 200mg/dL is prediabetic. A level greater than 200mg/dL is considered diabetic. The phantom for blood used in this study was distilled water with a relative permittivity close to 80. Glucose was added and subtracted to adjust the permittivity in the range of 66-80 in order to emulate the change in permittivity of blood. The glucose concentrations necessary to change the permittivity by the

same amount were much larger than they would have been for blood. One solution had a glucose concentration of 385g/dL, which was from 400 mL of water and 100 mL of glucose. This solution changed the relative permittivity of the water from 78 to 66 as the solution was added to the water. The basis in-vitro measurements of blood considered were not all from one patient, so there is variance in the data from measurement to measurement due to the differences between the patients themselves. When more reliable in-vitro measurements of blood at different glucose levels are acquired, the permittivity change needed to be modeled can be revisited.

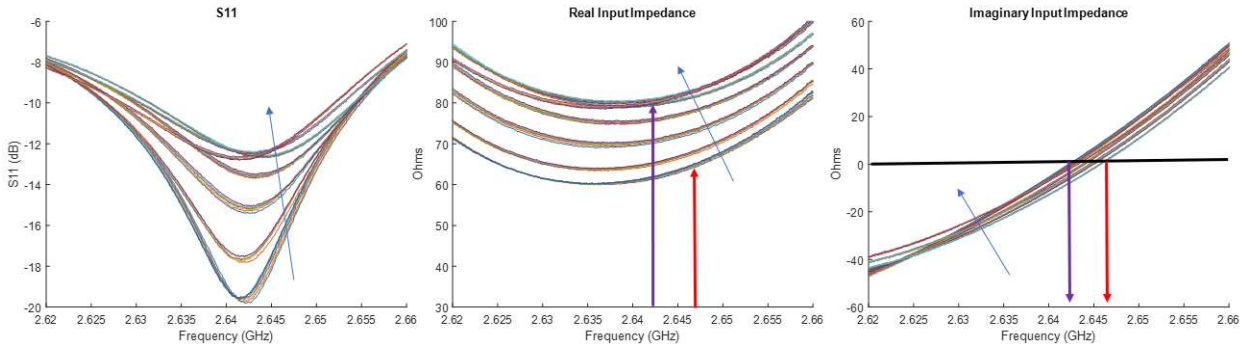

Figure 4.6. Change in Antenna Response with Increasing Glucose

For the current setup, the inflection impedance was defined as the real impedance value of an antenna response at the frequency where the imaginary impedance value is closest to zero and the magnitude of reflection is minimized. Figure 4.6 shows the different metrics of the antenna response as the concentration of glucose is increased. Each band in the real input impedance curve corresponds to a new discrete concentration of glucose. As the glucose level increased, the magnitude of the reflection increased and the frequency of minimum reflection rose slightly. The frequency of the zero crossing of the imaginary input impedance decreased.

Antenna responses similar to the one shown in Figure 4.5 were used in developing the current algorithm based on inflection impedance. The red and purple arrows indicate the range of frequencies corresponding to the zero crossing of the imaginary input impedance. The algorithm was built upon to factor in a ‘zero-crossing’ point of the imaginary input impedance. The measured imaginary input impedance curve is difficult to predict and does not follow the same general shape of the reflection curve with one or more minima. Therefore, additional checks needed to be put in place to account for variations in the shape and behavior of the imaginary

input impedance measurement. The input impedance measurement is run through a data smoothing function that finds the moving average in order to remove the high frequency noise in the measurement.

The algorithm finds every positive inflection point in the absolute value of the imaginary input impedance. This includes zero crossings, relative minima and relative maxima. Out of all of these points, the magnitude of the reflection at each point is compared. The inflection point with the lowest reflection is chosen and the real input impedance is measured to be the inflection impedance at this moment in time. Assuming a strong resonance of the sensor, this measurement gives an almost nearly purely resistive value, when the real input impedance is close to 50 Ohms.

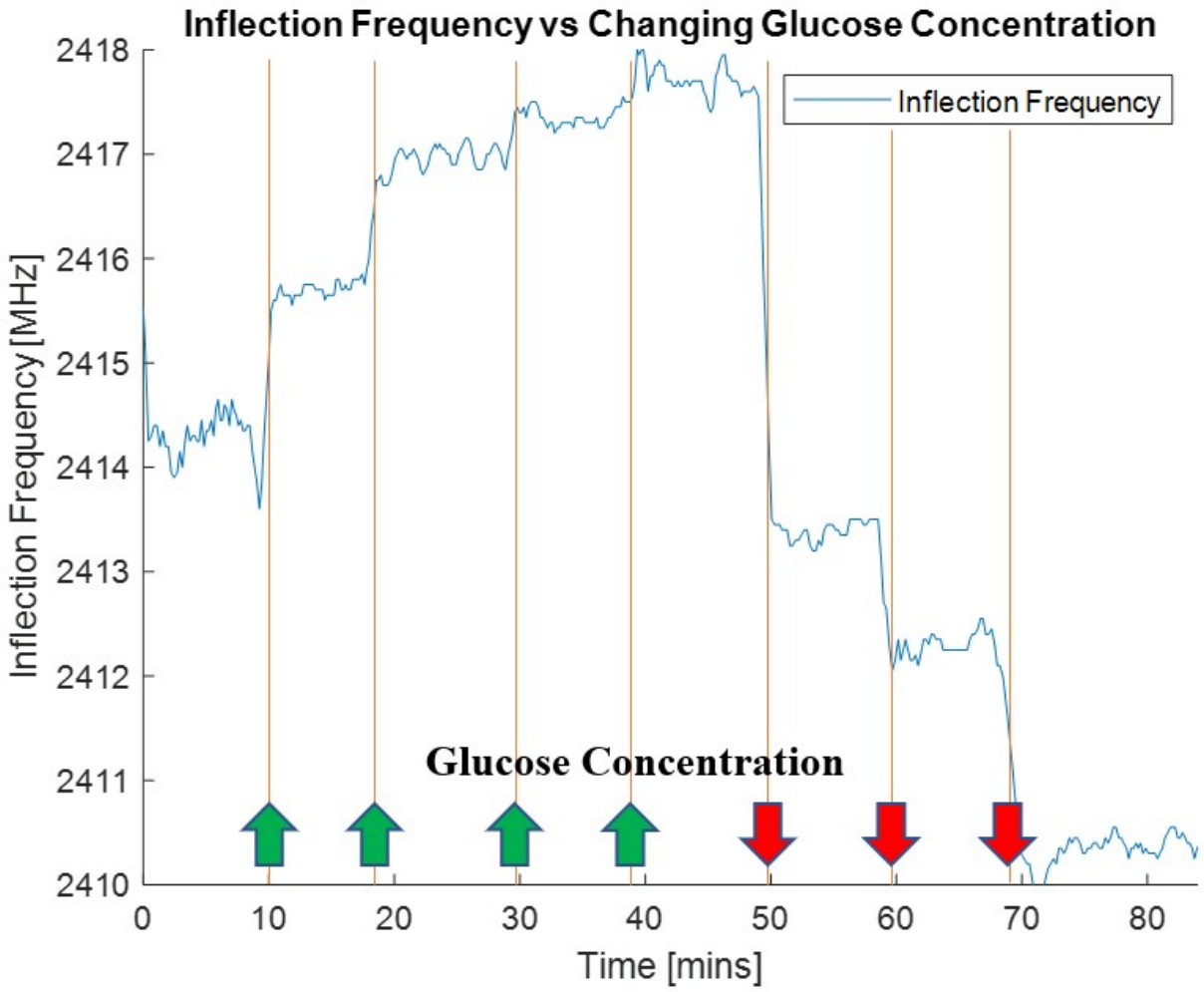

Figure 4.7. Change in Inflection Frequency with Changing Glucose Concentration

When the algorithm is used, the result may tend to also follow the frequency where the imaginary input impedance is zero. In some cases, this means that tracking this frequency is a valid substitute for the algorithm. It was observed during testing with glucose and water that this frequency changes more than the minimum reflection frequency, so that metric was used instead. The primary algorithm was more reliable than the zero-crossing frequency but in many cases either one can be used to demonstrate a change permittivity. Figure 4.7 shows the change in inflection frequency with changes in glucose concentration to the MUT. The test setup used for these results will be shown in chapter 5. These results demonstrate a case where, based on the testing environment, the inflection frequency was a good metric for tracking changes in glucose level.

The inflection impedance value was demonstrated to change inversely with the dielectric permittivity of the MUT and therefore directly with the glucose concentration for the present setup. When working with the different sensors and in different measurement setups, be they phantom models or on patients, the algorithm may need to be tuned or adjusted in order to track the changes in permittivity. Similar to how the algorithm was developed based on repeated testing with the phantom models, the clinical trials may require changes to the metrics currently in place. The phantom testing together with prior work are a strong prediction of how the sensor may behave in the trial but ultimately the performance will be determined by the trial itself.

In order to best adapt the system for different antenna responses, secondary analysis can be employed. The error flag can alert users when such analysis is necessary. One such secondary algorithm for finding a minimum reflection weighted by imaginary input impedance when no adequate inflection points were present was tested. In the case that the imaginary input impedance does not have any valid inflection points, a secondary algorithm is used. Across all the points a sum is calculated by adding the magnitude of the reflection in dB with the absolute value of the real input impedance. The point with the smallest sum is where the resonant frequency is located. This secondary algorithm is empirical and is working to find the minimum reflection with the smallest real input impedance where they are equally weighted. In the case of a strong resonance, the point of minimum reflection will dominate and the smallest sum will be located there. There is an error check at this stage as well. If none of these sums are less than a certain threshold, it is determined that there is no valid response measurement. In this case, the

value from the previous measurement is substituted and an error flag is set. This will maintain continuity in the case of a single measurement that is taken improperly. However, if no valid metric is found over many measurements the process should be stopped by the user. The user is made aware of the poor measurement via the error flag on the separate data monitoring MATLAB application.

4.3. Data upload and monitoring

After the algorithm has determined a measurement and the raw data is uploaded, the measurement value is displayed in the output box. The message will notify the user of the time of upload as well. At the same time, the data measurement program creates and then subsequently updates a data log file for storing each measurement. The updated data log along with the most recent measurement are uploaded to the server each time the loop repeats. The data log file is another .txt file similar to the s-parameter file and an example data log is shown in Figure 4.8.

Hour	Minute	Second	Elapsed Time [s]	Inflection Impedance [Ohm]	Glucose Level [mg/dL]
15	24	56	0	53.9614188	102.2
15	25	5	9	54.286088	104
15	25	17	21	54.21907563	104
15	25	27	31	54.25062764	104
15	25	38	42	54.32746561	104

Figure 4.8. Sample Data Log File

The data log and data files can be accessed on the server manually while the system is running. The server is located on the RIT computer cloud. It can be accessed from anywhere with an approved RIT account login. WinSCP and PuTTY are the two useful programs for accessing the server for viewing data during or after the application has run, but any SSH login should work.

In order to automate the data monitoring process, a sperate MATLAB application was created for viewing the live results. The data monitoring application is setup similarly to the data collection program where the folder on the server is specified. However, this program can be run from anywhere on any computer with MATLAB. No other supporting software or hardware connections are needed.

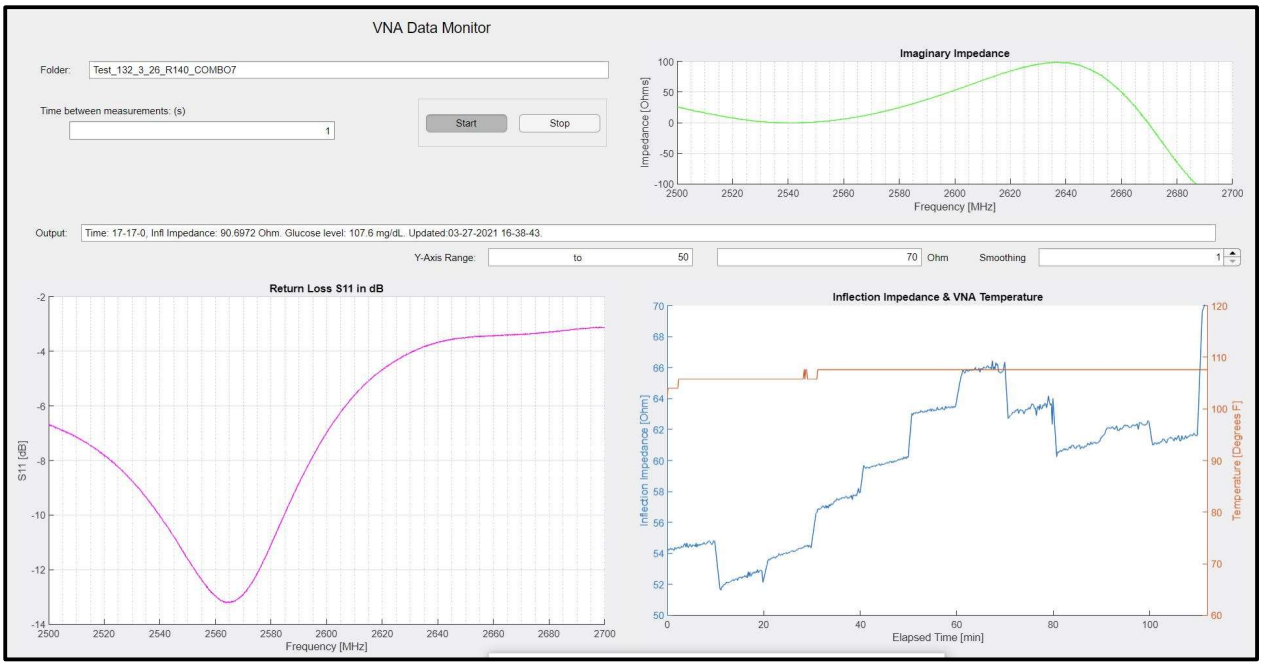

Figure 4.9. MATLAB Monitoring Application

The viewer application will download the latest measurement and data log files from the server automatically in a loop. Graphs of S11 in dB and the imaginary input impedance are displayed over frequency. There is no way for the viewer application to communicate with the measurement collection application, it will only passively display data. Figure 4.9 shows the MATLAB monitoring application running during a test in the lab. The plot of return loss and imaginary impedance show the latest measurement result. The inflection impedance plot over time is a plot of the most recent data log, including all previous measurements.

The viewer application also displays two plots of resonant frequency over time. This plot includes a metadata axis for glucose level measurements or temperature measurements input at the data collection application. One of these plots features an adjustable y-axis and an x-axis that spans all of the time that has passed. The other plot has an automatic y-axis and a shifted x-axis, adjusted to give 45 minutes of headway. The viewer application uploads both of these plots to the server as bitmap images. The application uploads the figures as they appear on screen, so adjusting the size of the figures is not recommended. This is because the smart phone application is setup to load in the figures at the size that they are originally in MATLAB.

The data monitoring application takes longer to update than the data measurement application because it has to generate several figures. Originally, the algorithm and calculations were done on the data monitoring application itself. However, this led to measurements missing being included in the data log. Although the frequency of measurements was higher, the live analysis was slower. For this reason, the calculations and data log updating were moved to the measurement collection application. The two applications run independently and access the server independently. There are no issues with simultaneous SSH sessions from the applications due to the write and then read nature of the programs. The data measurement application is only writing and the data monitoring application is only reading. They each can perform these tasks at a different pace.

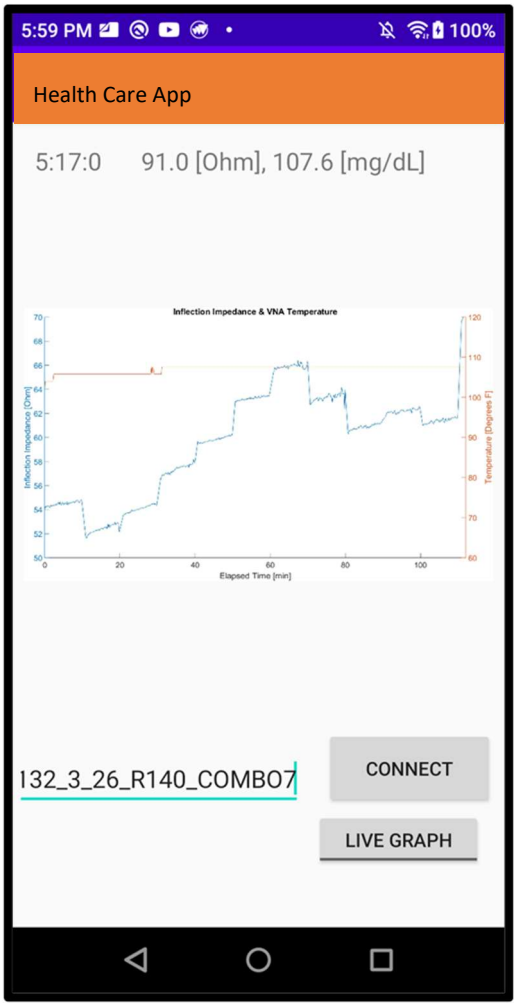

Figure 4.10. Smartphone Application

4.4. Smartphone application

The data monitoring was also made possible on a mobile smartphone device. A simple application developed in Android Studio for Android phones functions similarly to the data monitoring MATLAB application, where given the server folder name it will download the latest data log and the images of the plots. The application can toggle which graph is viewed by the plot and the last row of the data log is downloaded and shown on screen. The latest measurement time, the latest resonant frequency and the latest glucose level will be displayed. The app program is a single function that recursively calls itself repeatedly until stopped. The app will update itself with the latest data from the server every 15 seconds. Figure 4.10 shows a screen capture of the smartphone application during a test of the system.

All of the data is available on the server at any time for analysis. Using WinSCP, the data can be downloaded and accessed with offline MATLAB programs. All of the raw S-parameter data is saved on the server, which means that a different algorithm can be employed after the fact.

MATLAB has the capability to port applications into a Web App format. These applications do not need an instance of MATLAB itself to be running, but merely the MATLAB Web Application Server. It is also not possible for other users to change these web apps or view the code once they are published. This will work for the MATLAB applications discussed in this section and can make them more accessible for new users.

5. Combination of Measurements: Antenna Response and Dielectric Permittivity

The testing procedures from chapter 3 and 4 can be combined to incorporate the same MUT. Changing the glucose concentration of a phantom substance, while measuring both the permittivity and the antenna response in a lab setting is the best approximation of the data that will be available in a clinical trial. The combined test setup was used to relate the antenna response to the change in permittivity of the phantom substance. This relationship will be fundamental to the clinical trial.

5.1. Combination test setup

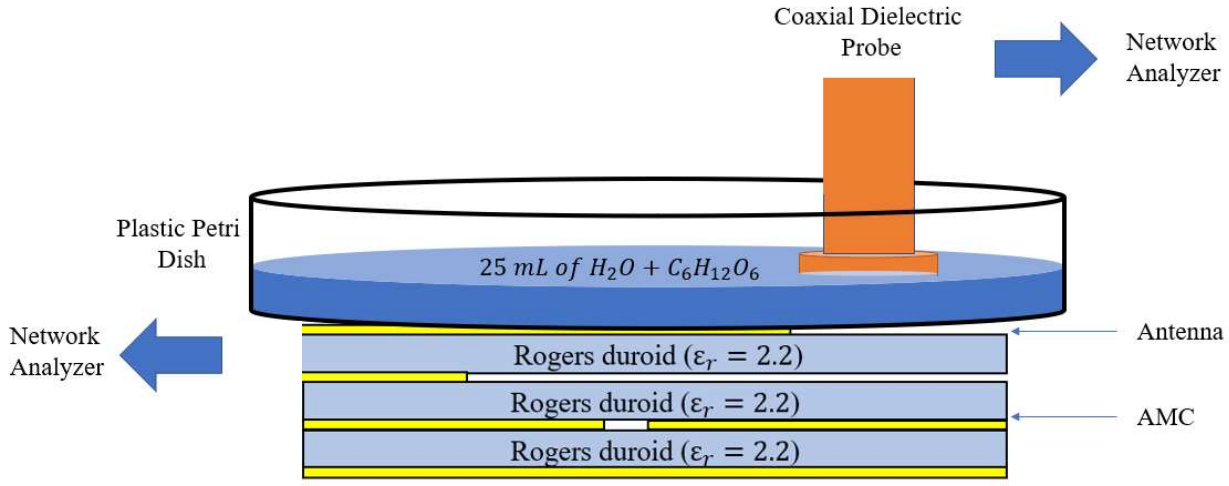

Figure 5.1. Diagram of Combined Test Setup

Several different testing environments were tested in order to combine the two measurement methods. Lab equipment such as beakers, a magnetic mixing plate, pipettes, syringes and petri dishes were used in the process of developing a working testing setup. Overall, the best testing setup found is shown in figure 5.1. Clamps are used in order to suspend both the antenna and the probe in the air, such that the end of the probe sits in the water. The antenna response was very sensitive to the height of the water in the dish and therefore the total amount of water used. In order to increase the concentration of glucose in the dish, water must be removed and then

replaced with water having a higher concentration of glucose. Measurements are paused while the change is taking place, and the same process can be repeated but with distilled water to lower the concentration of glucose. 2.5 mL, 5 mL and 10 mL of water were removed and then added back during testing in order to have both small and large changes in glucose concentration.

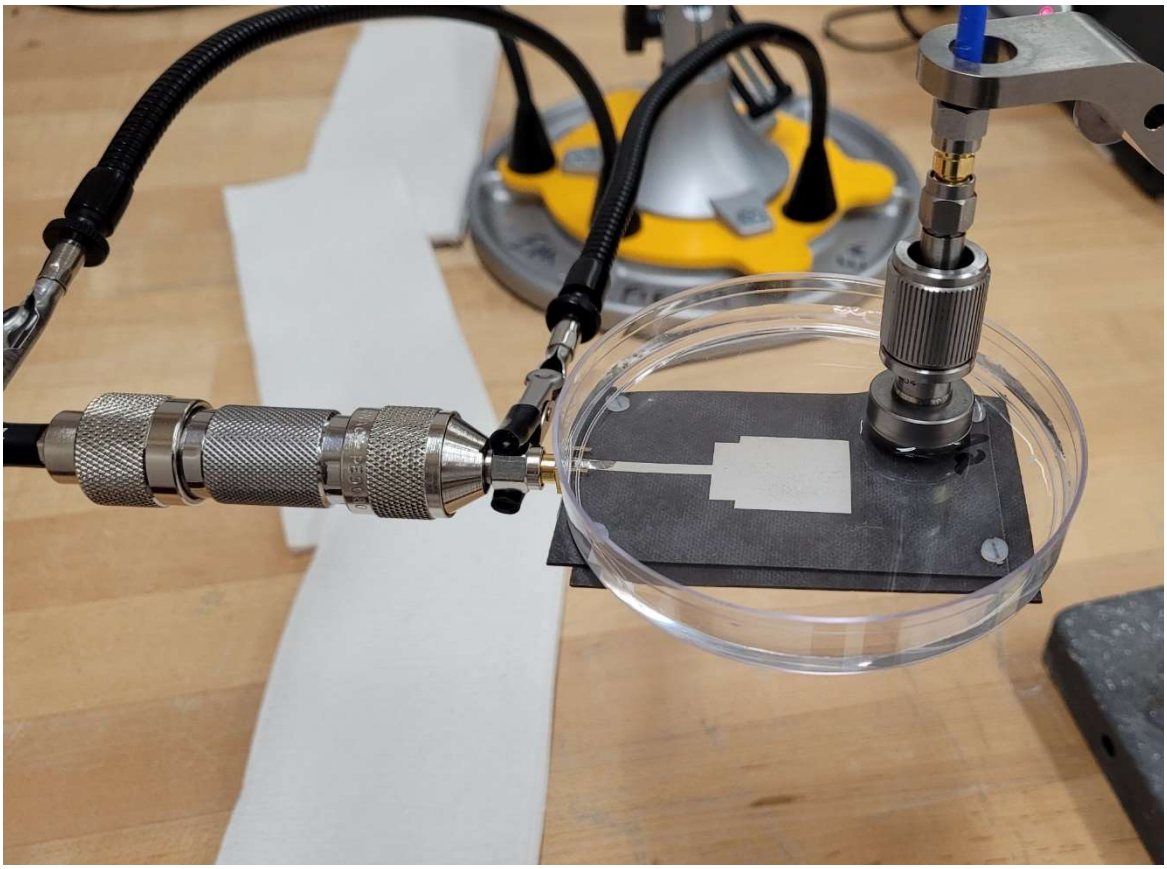

Figure 5.2. Combination Testing Setup

Figure 5.2 shows the combined test setup in the lab. The amount of water in the dish was adjusted so that the sensor would have a strong resonance. It was observed that the best resonance is achieved when there is 25 mL of water in the dish. The setup was verified for consistency, with a test similar to figure 4.3, and was shown to be stable over time with one issue. The resonance was continually degrading as the water in the dish evaporated. The change in the water level due to evaporation could be observed as an increasing slope during the tests. This will be demonstrated in the analysis of the test results. Having the antenna response change with the evaporation of the water made consistency between different tests difficult, as the water

level was always changing. The evaporating water level was proven to be the cause of change in the antenna response when the setup was left running over night and only 22 mL of water remained in the dish. 3 mL of water were added and the antenna response was restored. The evaporation is an issue for long term testing, which the clinical trial will include, but for testing in the short term this change can be ignored. The change due to evaporation demonstrates the high sensitivity of the antenna response to changes in the MUT.

5.2. Sensor sensitivity testing

In order to verify the sensitivity of the antenna sensor within realistic glucose concentrations, small amounts of a weak glucose water solution were added and the change in the response was measured. 4.87 mL of glucose power was added to a beaker of 500 mL of water and mixed to create a solution with a glucose concentration of 1500 mg/dL. Every 5 minutes, 2.5 mL of water were removed from the petri dish and replaced with water from the beaker. The glucose concentrations in the dish were calculated, and the antenna response over time is shown in figure 5.3.

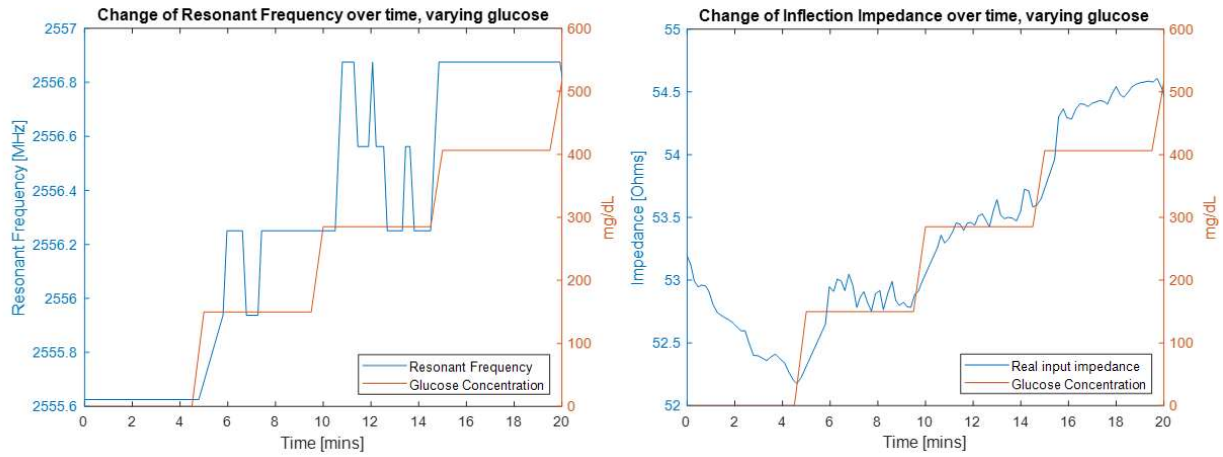

Figure 5.3. Change in Antenna Response Over Time with Increasing Glucose

For the concentrations of glucose used, the best metrics for tracking change in glucose concentration were the resonant frequency, where reflection in a minimum, and the inflection impedance, where the input impedance is purely resistive. The changes over time in real and imaginary impedance are shown in figure 5.4. The real impedance curve is increasing with

increasing glucose level, similar to figure 4.6, but the imaginary impedance curve does not change much. This is why the resonant frequency is preferred over the inflection frequency for tracking glucose in this test.

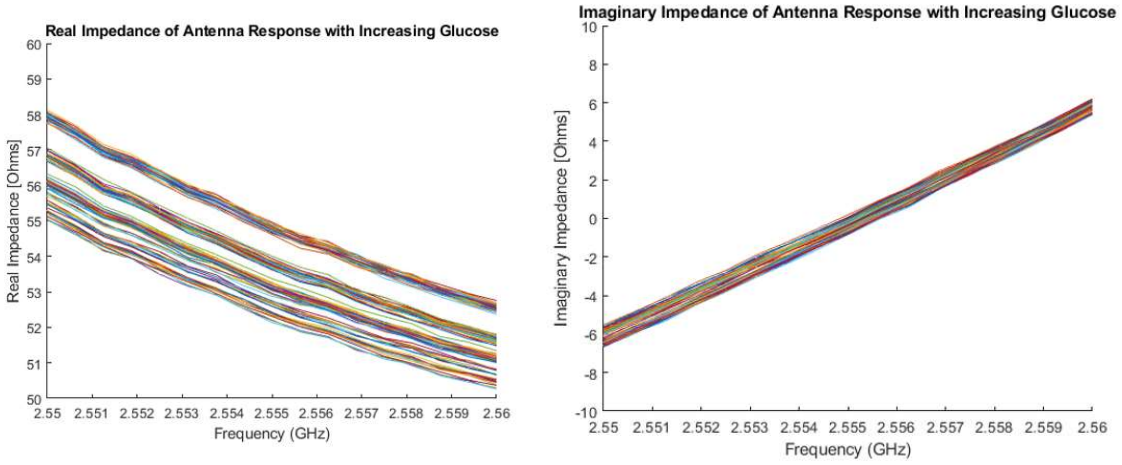

Figure 5.4. Change in Antenna Impedance Over Time with Increasing Glucose

The real impedance clearly increases in discrete jumps at the glucose level increases. This behavior was also observed in the magnitude of the S11 curve, which is shown in figure 5.5.

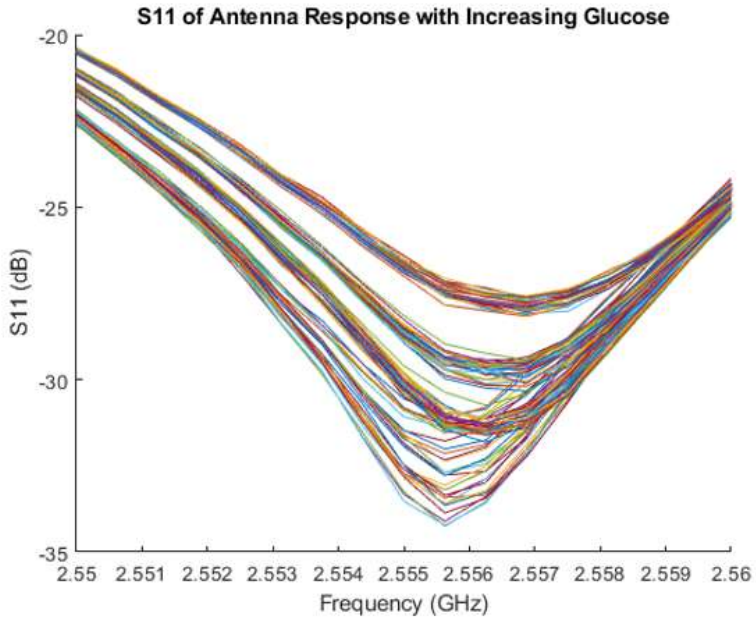

Figure 5.5. Change in Antenna Reflection Over Time with Increasing Glucose

The minimum of the S11 curve shifts to the left and increases in frequency as the concentration of glucose is increased. This is a similar response to what was observed in figure 4.7, but this is different from the response measured in figure 4.6. This inconsistency could be due to a few factors, including the differences in absolute glucose concentrations used and possible variations in the test setup. The change in the response observed during the clinical trial will ultimately reveal the best metrics to be used in the on-body test environment. The test was repeated again, with a smaller resolution in frequency, where the glucose level was both increased and decreased. The results for the inflection impedance are shown in figure 5.6.

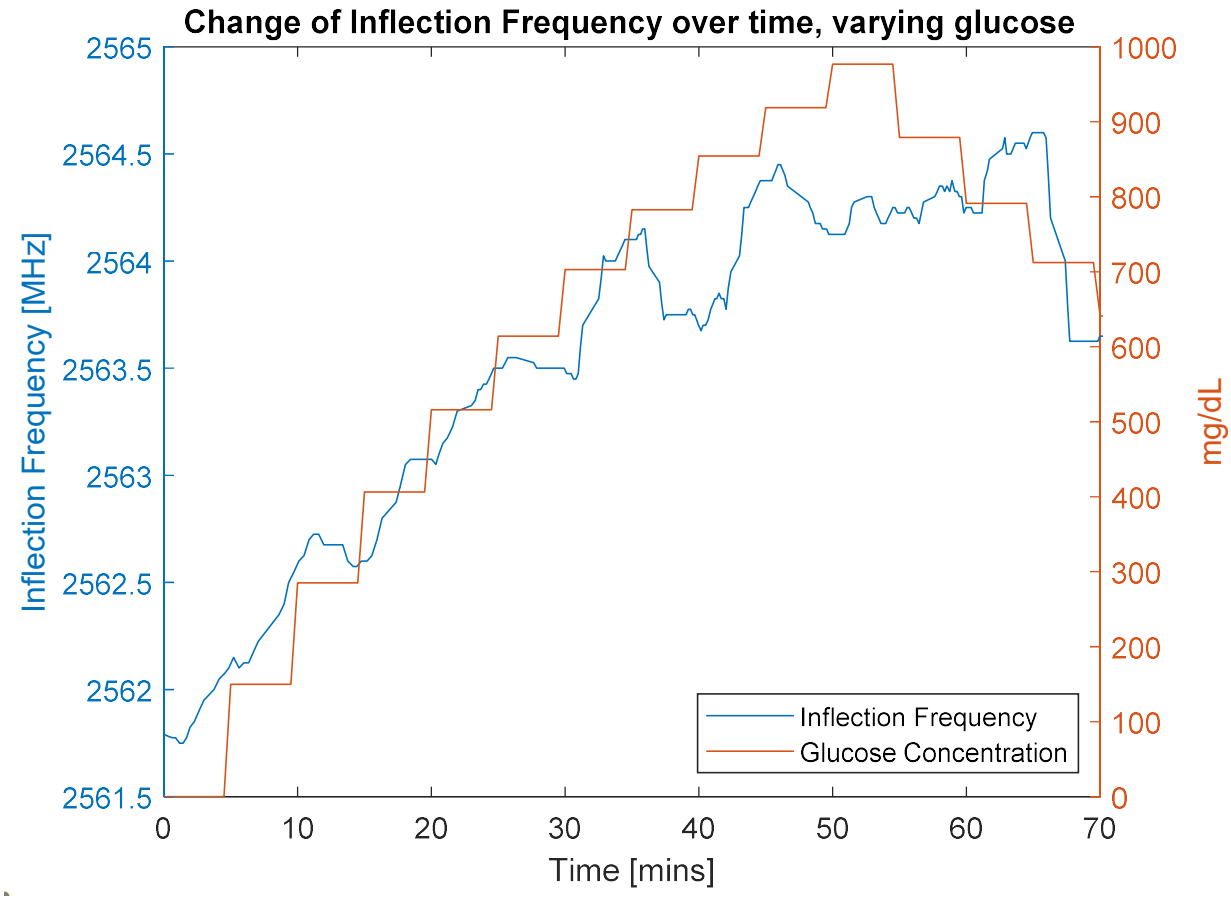

Figure 5.6. Repeated Test, Change in Antenna Response with Changing Glucose Level

The test setup shown in figure 5.2 was used for the results shown in figure 5.6. For this test, the inflection impedance did not track closely with the change in glucose, but the inflection frequency did. This is due to the consistent shift in the zero-crossing point for the imaginary

input impedance. The changes in the imaginary input impedance measurement as glucose is increasing are shown in figure 5.7.

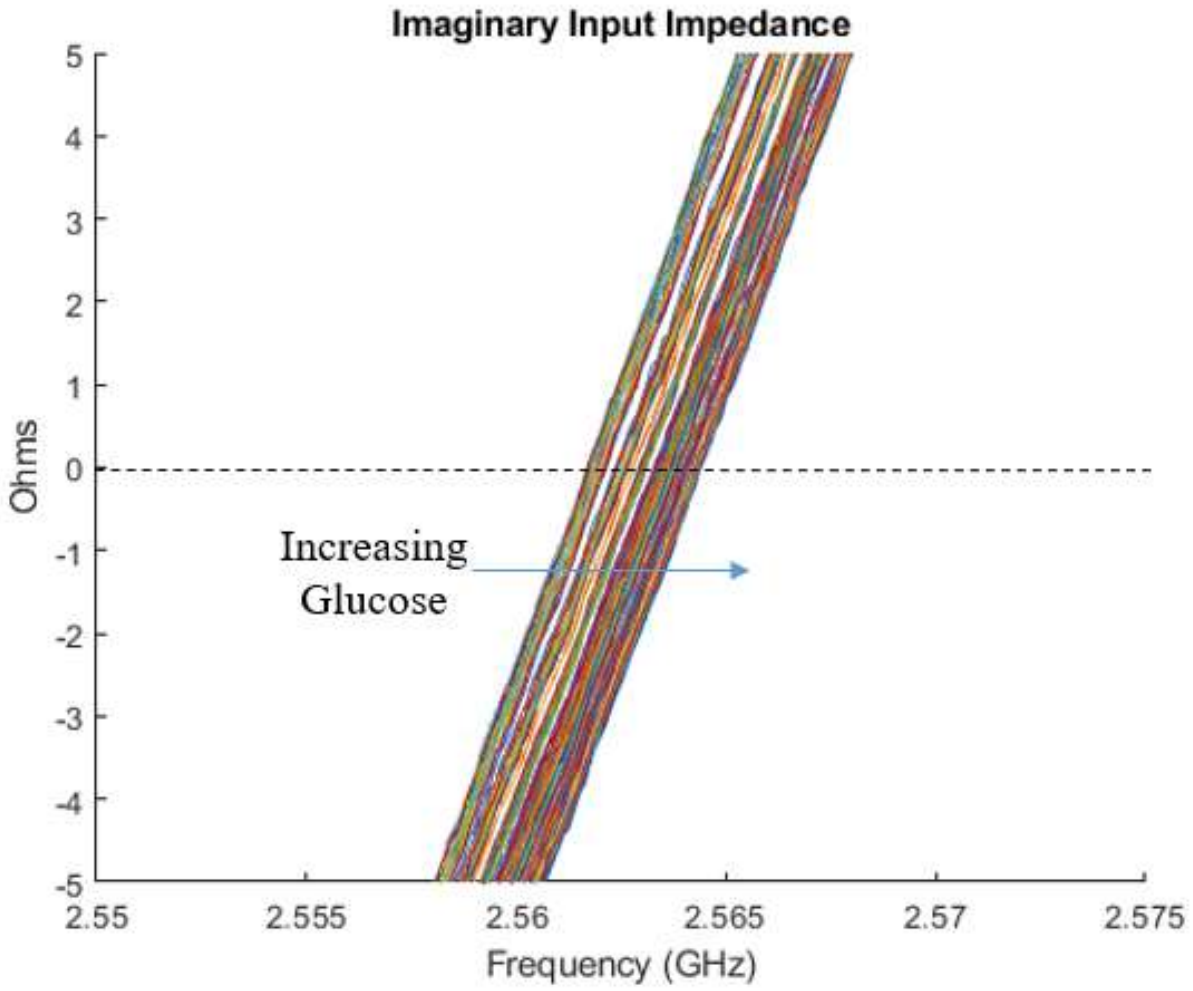

Figure 5.7. Change in Antenna Imaginary Impedance Over Time with Increasing Glucose

For the results shown in both figures 5.4 and 5.7, the change in the frequency of the zero crossing for the imaginary input impedance was sensitive enough to tack the change in glucose concentration. In this case, the minimum S11 resonant frequency also tracked the change. The frequency resolution needs to be small enough in order for the inflection frequency algorithm to have sufficient measurement resolution.

In order to further verify the sensitivity of the antenna sensor, another test was conducted with an alternative setup. This setup had the antenna sensor submerged in 500 mL of water. The glucose

concentration of the water was increased from 0 mg/dL to 300 mg/dL and then decreased to 260 mg/dL during a 90-minute test period. The setup for the test is shown in figure 5.8.

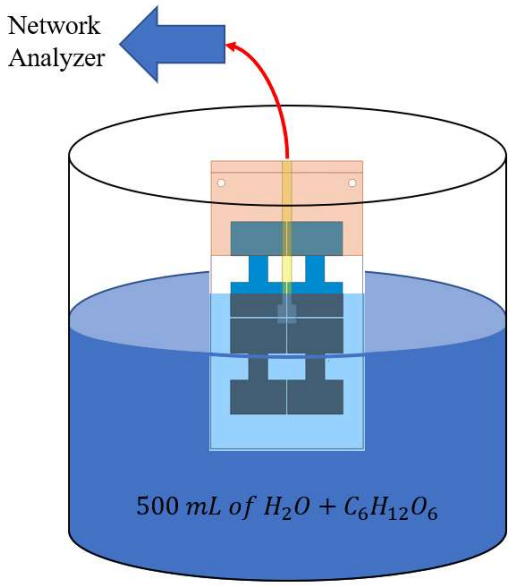

Figure 5.8. Diagram of Alternative Sensitivity Test Setup

The actual setup for this test is shown in figure 5.9.

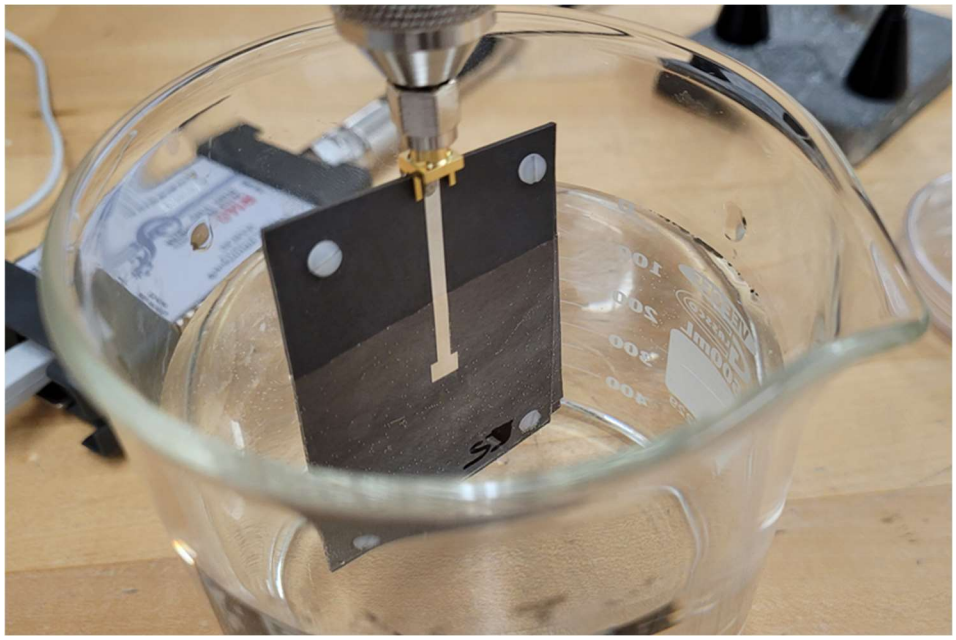

Figure 5.9. Alternative Sensitivity Test Setup

The probe was not used for this alternative test. Due to the antenna's contact with the water, the S11 measurement of the antenna response had significant noise. Theis noise was also present on the imaginary input impedance curve. A plot of the S11 and imaginary input impedance curves as the glucose concentration is increasing is shown in figure 5.10.

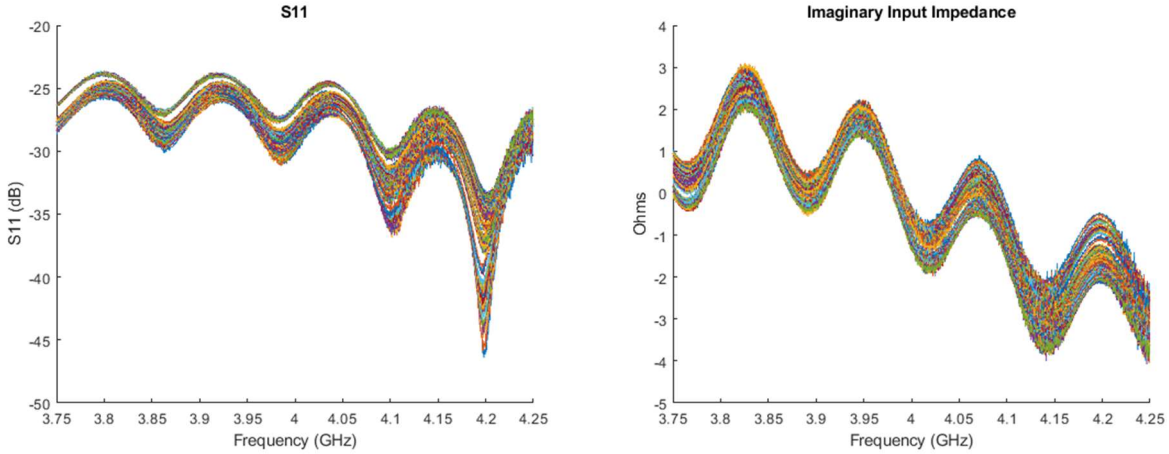

Figure 5.10. S11 and Imaginary Input Impedance in Alternative Test with Increasing Glucose

The resonant frequency of the antenna was about 4200 MHz, which is significantly higher than any other test. The inflection frequency algorithm is looking for the frequency at which the imaginary input impedance curve has a local maxima or minima towards zero and the S11 reflection is minimized. In order to implement this algorithm effectively, a moving average function is applied to the imaginary input impedance curve. The moving average is defined by a smoothing factor which is how many terms contribute to the average. If too few terms are used, then the noise will persist in the result. If too many terms are used, the measurement information will be lost in the smoothing process. After the data was collected, possible smoothing factors were tested based on the change in the glucose concentration. The smoothing factors in the range of 30-60 terms were resulted in a decent tracking of the glucose concentration with the inflection frequency. Figure 5.11. shows the imaginary input impedance in the frequency range of interest when the best smoothing factor of 30 is applied to the curve. Figure 5.12 shows the change in the inflection frequency and the glucose concentration over time. The inflection frequency result itself is smoothed with a factor of 150. This is because the frequency resolution used for this test was based on 1601 points between 3750 MHz and 4250 MHz.

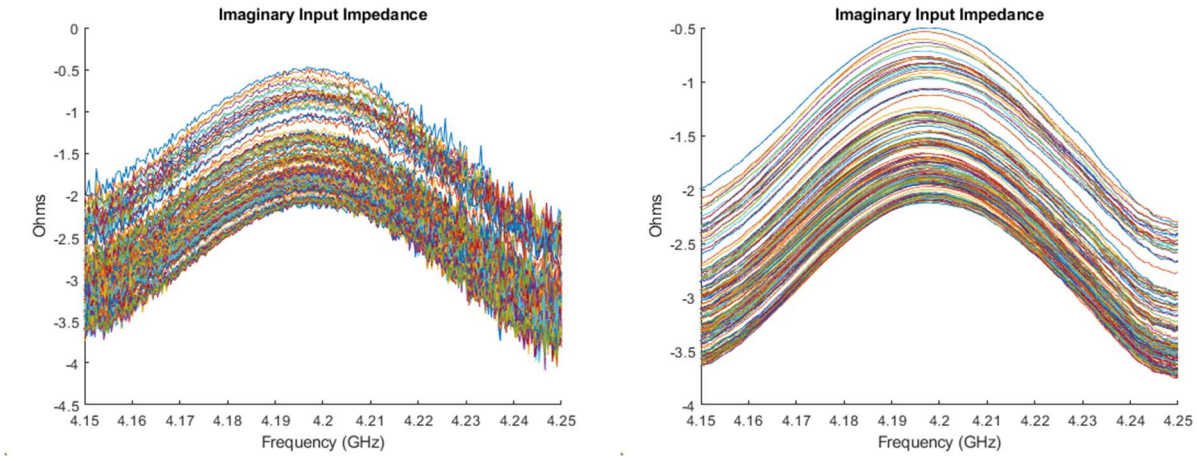

Figure 5.11. Original vs. Smoothed Imaginary Input Impedance in Alternative Test Setup with Increasing Glucose

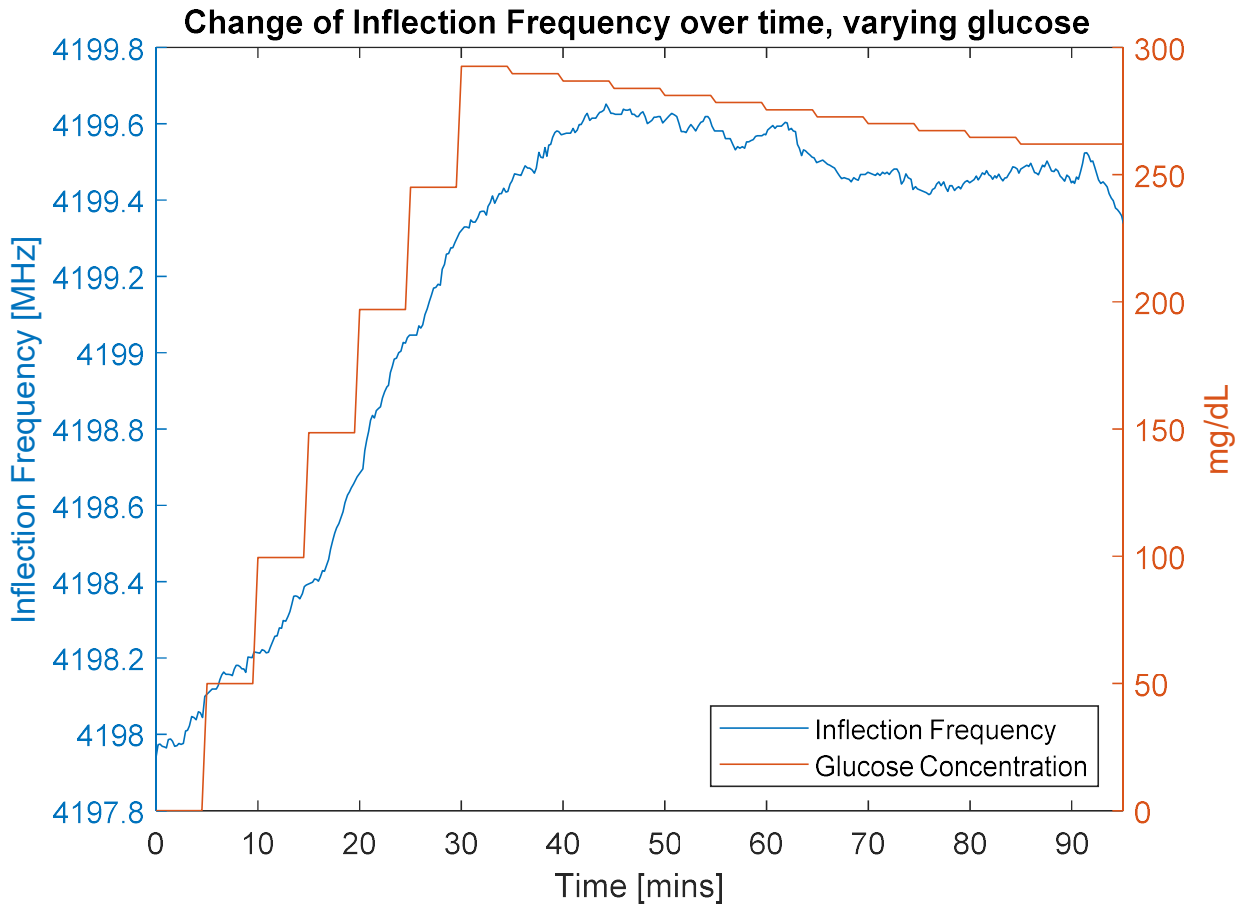

Figure 5.12. Alternative Test, Change in Antenna Response with Changing Glucose Level

The results from the alternative test demonstrate the sensitivity of the inflection impedance algorithm to noise measurements. A good smoothing factor must be determined for each test setup prior to the test based on the noise level in the measurements.

5.3. Combined probe and sensor results

When measuring the antenna response is combined with measuring the permittivity of the MUT, the antenna response is compared directly to the measured permittivity instead of a glucose concentration. The inflection impedance was primarily used as a metric for these tests because larger glucose concentrations, similar to the test in figure 3.6, were used. Figure 5.13 shows the results of a test where the concentration of glucose in the dish was increased over time. The measured permittivity decreased and the inflection impedance increased.

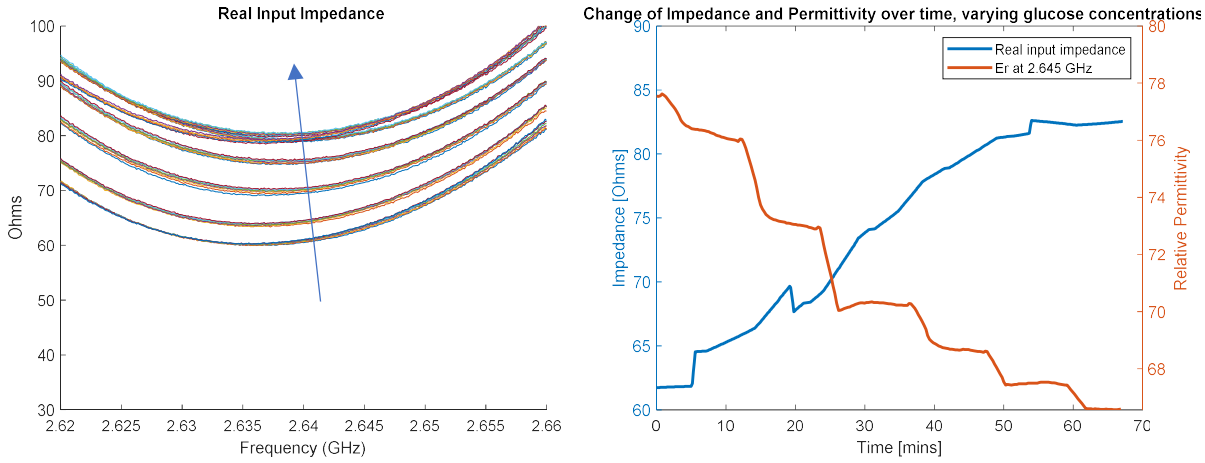

Figure 5.13. Change in Inflection Impedance over Time, Decreasing Permittivity with Glucose

The different levels in the real input impedance curve correspond to different permittivity levels and therefore different glucose concentrations. A large change in concentration was used and the real input impedance increased by about 20 Ohms. This increase brought about less resonance for the antenna, where the minimum S11 magnitude increased from about -20 dB to -12 dB. The change in the S11 curve is problematic because losing resonance will decrease the amount of energy that is radiated into the MUT significantly. Operating within a permittivity range that maintains a strong resonance is a limitation of this sensor.

In order to test both the increase and decrease of permittivity on the antenna's response, two tests were done where the concentration of glucose was increased and then subsequently decreased over time. The results from these tests are shown in figure 5.7.

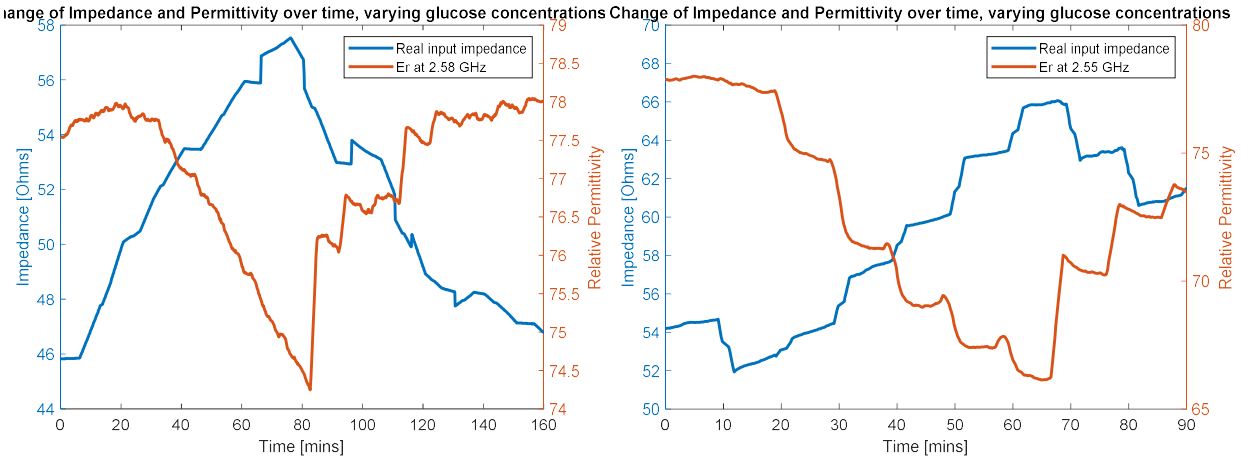

Figure 5.14. Combination Test Results with Increasing and then Decreasing Glucose

For all of the combination tests, the data was monitored remotely as described in chapter 4. These tests can be repeated during the clinical trial in order to further refine the metric for tracking the change in glucose level. During the trail, the probe will be measuring an in-vitro blood sample from a patient who is being monitored by the antenna sensor. The trial setup will attempt to repeat the combined test results from figure 5.14 with the addition of traditional blood glucose measurements for comparison.

5.4. Analytical model

Similar to an analytical modification to the Cole-Cole equation for permittivity to add in a glucose dependence, an equation relating the antenna response to permittivity and therefore glucose concentration was also investigated. Both an analytical model and a machine learning approach require a large amount of consistent training data. This training data will be collected during the clinical trial. In [14], an equivalent circuit model for the antenna sensor was proposed based on the antenna response and a traditionally measured blood glucose level. The circuit components were given glucose dependencies based on the change in input impedance. The circuit is shown in figure 5.15.

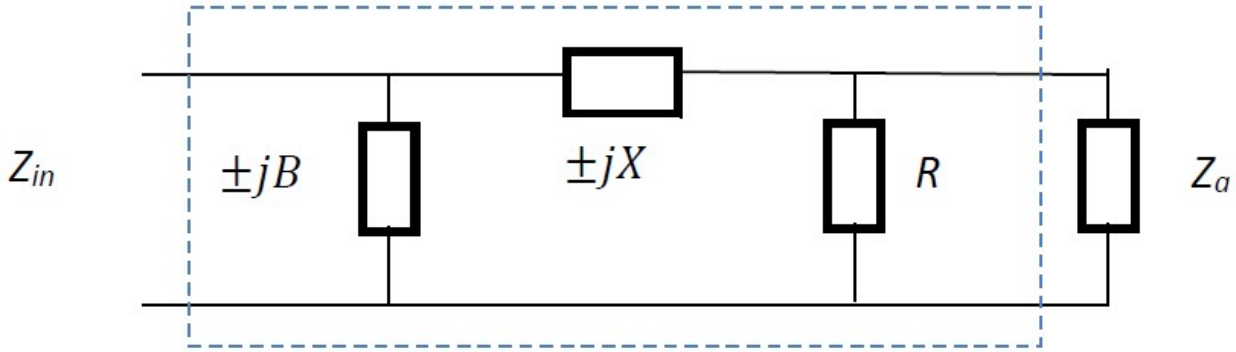

Figure 5.15. Equivalent Circuit Model for Antenna Sensor from [14]

Based on the inflection impedance measurements taken in this work, it may be sufficient to have a simple series resistance that changes with the glucose level. In contrast, the approach in [9] uses machine learning to map the entire antenna response to the correct glucose level. Either way, each approach will be limited in accuracy by the training data that is used. The current system facilitates the collection of such data so that during the clinical trial, a better algorithm can be developed.

6. Clinical Study

The design of the clinical trial will be critical for ensuring that the study is a success. Documentation for designing clinical trials discuss common design flaws and fundamental design issues. In [26], a table is laid out that details the different phases for a clinical study. While not all of the phases listed are necessary for the purposes of this work, it is still useful to map out the clinical trial design in its entirety.

6.1. Alternative Hypothesis

The claim that the study is aiming to prove is that the antenna sensor is accurate and effective at measuring the blood glucose level of a patient. The continuous measurement system will be utilized to collect data and some automated algorithm, that will be developed, will conduct the analysis on the measurement to make the glucose level determination. The effectiveness will be judged based on the consistency of the measurement and the patient and physician experience using the sensor. The baseline for comparison will be blood glucose measurements from in-vitro blood samples. In order to aid in the development of the algorithm and give evidence as to what is occurring, permittivity measurements will also be made from the in-vitro blood samples.

6.2. Intent to Treat

Due to the nature of this trial, the testing will not be randomized. Each eligible volunteer will receive the same treatment. The antenna sensor will be used to make on-body antenna response measurements, the probe will be used to make permittivity measurements of in-vitro blood samples and their traditionally measured blood glucose level will be recorded. Nothing that is part of the trial will be actively done to the patients, sans taking the blood samples, because they are mainly under observation for measurement data.

6.3. Null Hypothesis

It has been shown that the level of glucose in the tissue of a body will have some change on the dielectric permittivity of that tissue. The in-vitro measurements of blood samples will further confirm this specifically for the patients in the trial. The null hypothesis is that the antenna sensors proposed in this study will not be able to track the changes in glucose level from

permittivity changes in the blood and ultimately determine the absolute glucose level through an algorithm.

6.4. Phase I

The first phase of this trial will feature a small number of patients and will focus mostly on consistency. In this phase, the method for securing the antenna sensor to the patients will be investigated. Different places on the body, different straps and coverings as well as different types of monopoles will be tested out in this phase. Between a few patients, the same or similar methods of applying the antenna sensor should be used to demonstrate a similar resonance in the antenna response. The blood glucose levels are not as important in this stage, as it is more for establishing a repeatable procedure for applying the antenna sensor that can be done by healthcare providers to patients admitted to a clinic. The consistency over time will be especially critical, where any environmental changes over time such as patient movement must be observed in order to attribute drifts in the antenna sensor's response. A consistent response across several patients over time will indicate that the antenna sensor will be stable enough to generate useful data.

6.5. Phase II

For the second phase of the trial, more patients can be recruited for measurements. The established procedure will be done for applying the antenna sensor to the patients. The in-vitro blood samples will also be collected for permittivity measurements. For this phase, a correlation between the traditionally measured blood glucose levels, the antenna sensor response and the measured permittivity will be sought after. In order for the sensor to be able to track the changes in blood glucose level, some metric of the response, possibly a metric such as inflection frequency that was investigated in chapter 5, must correlate with both the permittivity and the traditionally measured blood glucose level. This phase will aim to recreate some of the data plots from the combination testing, where these correlations are observable over time. Linking the permittivity change of the in-vitro samples to the change in the antenna sensor response over time is critical in order to claim that the internal change in permittivity is driving the change in the sensor.

6.6. Phase III

The third phase of the trial will focus on collecting training data. Using the established procedure and the observed correlations, more patients can be included to collect large amounts of data over time. The antenna sensor's response will function as an input vector and be mapped by either an analytical equation of a machine learning algorithm to the traditionally measured blood glucose measurement. The in-vitro permittivity measurements can guide the development of the algorithm.

6.7. Phase IV

The fourth phase of the trial will consist of collecting test data to test the accuracy of the measurement system. Once the algorithm for relating the antenna sensor response to the blood glucose level is developed, it will be used make measurements that will be compared against the traditionally measured blood glucose levels. The antenna sensor system should be able to make accurate measurements of the patient's blood glucose level based on the current and prior antenna response. The continuous measurements and their accuracy will be available to the healthcare professional in order to assist in treatment of the patient.

At this point, multiple extensions to this project could be suggested. A machine learning approach to predict the onset of diabetes partially based on blood glucose levels is suggested in [27] and [28]. Such a system could be integrated with the blood glucose measurements collected in phase four.

6.8. Power and Error Types

The null hypothesis cannot be rejected if phase one does not result in a consistent procedure for having the antenna sensor generate a consistent baseline reading. If this occurs then the architecture of the antenna sensor itself needs to be investigated. It may be possible to move forward with a sensor that appears to be inconsistent if machine learning is applied in phase three but it will be impossible to derive an analytical equation without a sufficient baseline. In the absence of a consistent baseline, a false negative may be observed in the subsequent phases of the trial. In order to avoid a type two error, the setup must ensure that each measurement setup is

immune from disturbances and variations. A similar progression as demonstrated in [9] needs to be followed.

After sensor stability is achieved the null hypothesis could still not be rejected if there is no observed correlation in the glucose level and the antenna sensor response. This would mean that either the sensor is not sensitive enough or that it the permittivity of the tissue is not changing solely with the glucose level. In order to determine the failure mode, the in-vitro measurements of blood permittivity will also be correlated. If the antenna sensor response does correlate well with the glucose level and the in-vitro permittivity measurements of blood do not then there may be an actual correlation between the antenna sensor and the blood glucose level. This would result in a false positivity where the null hypothesis should still not be rejected and this would be considered a type I error.

Once the correlation is observed and phase two is complete it is reasonable to reject at least part of the null hypothesis. The ability for the sensor to track the changes in glucose level lies within the correlation between the antenna sensor response and the blood glucose level. The determination of the absolute glucose level will be a result of training data in the form of supervised learning.

6.9. Key Outcomes

The goal of the trial is to improve the system from chapter 5 for on-body measurements. The clinical trial in [9] showed very little variation across some general demographics of possible patients. The outcome of phase one will be a procedure for applying the antenna sensor to patients consistently. The outcome of phase two will be the proven correlation between the antenna response and the blood glucose level as a result of the blood changing the permittivity of the tissue within the body. The outcomes of phases three and four will be the development and testing of an algorithm for making absolute blood glucose measurements using the antenna sensor.

Depending on the application, an antenna sensor only capable of showing whether or not the blood glucose level in increasing or decreasing may be sufficient. In this case the results from phase two, once the correlation is proven to be consistent, will determine that the antenna sensor

proposed in this work is suited for this purpose. The emphasis would be placed on the antenna sensor measuring a decrease in the blood glucose level, as is commonly desired with diabetic patients. The algorithm presented in chapter 4 could be modified to, based on the slope of the previous readings, classify the current measurement as increasing or decreasing which could prove to be a useful extension of the system.

6.10 Challenges

The most significant obstacle to overcome during the trial is in phase one. Achieving a consistent response with a single patient over time needs to allow for a small amount of variation created by interferences. Determining how much these variations effect the antenna sensor response will help instruct the trial to further remove these interferences. If it is determined that there are too many to remove or overcome, the sensor architecture will need to be improved. It may occur that the current sensor requires an unrealistic level of stillness from a patient. In order to address this issue in [9], multiple sensors and machine learning were instituted. A similar approach could be tested in this trial where two or more of the proposed antenna sensors are used on the same patient. This would require two network analyzers for collecting data, but the server-based MATLAB system can be extended to incorporate multiple sources of data for analysis.

7. Conclusion and Future Work

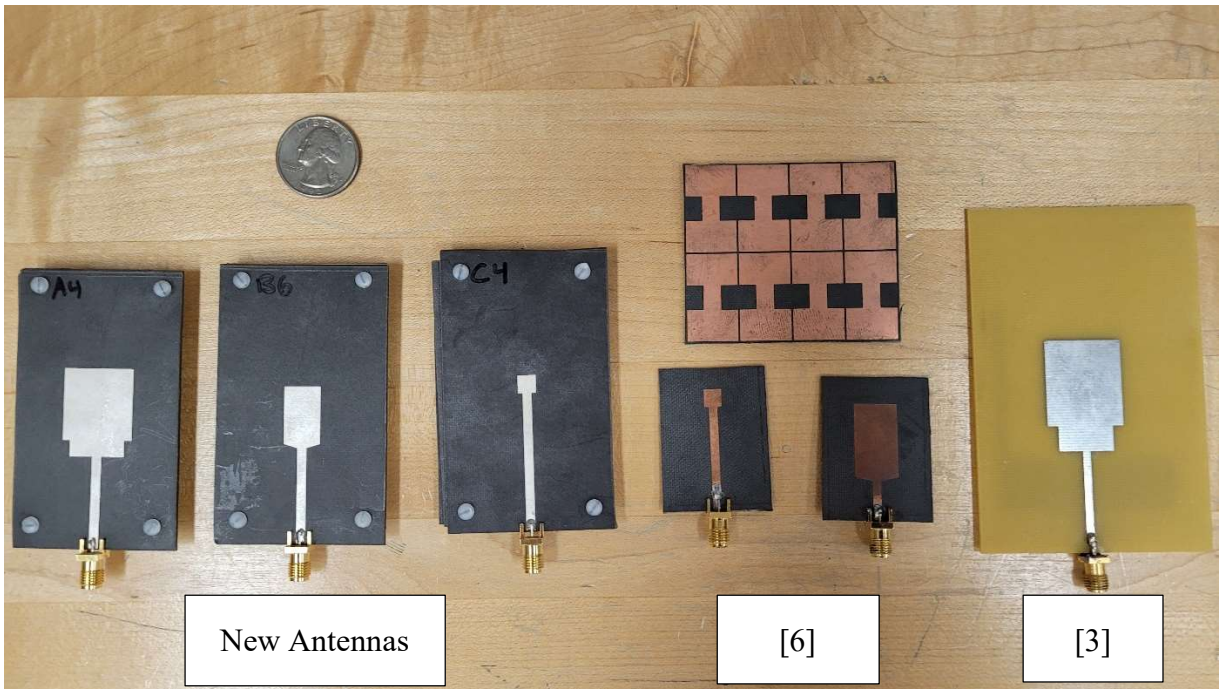

Figure 7.1. Comparison of new antennas with previously fabricated versions

The proposed antenna sensor system is an improvement on the prior work done in the ETA lab at RIT. The utilization of AMC designs and the integration into an automated system has made a powerful tool for use in the clinical trial. The small, compact and robust sensor has the potential to be a stable and consistent measurement device for non-invasive continuous blood glucose measurements. Figure 7.1 shows a comparison of the new antenna sensor prototypes with previous versions. The clinical trial provides an opportunity to further improve on the fabricated design, support prior research by showing a correlation in measurements and collect useful data for building an analysis algorithm.

Overall, the most challenging contribution of this research was the development of a consistent testing setup for use in the lab with the antenna sensor. Many different setups were tested that resulted in inconsistent results. Specifically, the combination setup with the dish on the antenna took several iterations before it could be used reliably. The ability to capture the results with this test was also the most rewarding aspect of this work. The simultaneous linkage of the antenna

sensor results and the permittivity measurements had not been done before in the ETA lab at RIT. This kind of test yields a powerful example to be followed during the clinical trials.

7.1. Future work

- Cooperate with health care professionals for input on the system, the clinical trial and the use cases. Gathering as much feedback as possible from the medical perspective on this project will be instrumental in continuing to make improvements. Physicians that are involved with this project should have a full working knowledge of the limitations and challenges that still exist.
- Investigate possible RF interference with the sensor during the clinical trial. There is a probability that any other transmitting devices at the frequency of interest may impact the measurement results.
- Conducting the clinical trial will be the most expedient way to locate any problems with the system. There are several obstacles discussed in [8] that cannot be fully explored without the advent of real blood and actual on-body measurements.
- Investigate the long term usage effects of this antenna sensor, on the order of 36-48 hours of continuously applied measurements
- Following the model of [9], further investigation can be done into using multiple sensors. A brief study was conducted in this report regarding a transmit and receive system, but other avenues exist, such as a filter.
- The software used in this project to facilitate the automated collection of data could be further optimized, depending on how exactly it is used in the clinical trial.
- The determination of analytical equations, both to modify the Cole-Cole equation and to measure blood glucose levels with the antenna sensor will rely on data from the clinical trial. An investigation into the feasibility of a machine learning approach for both metrics may also be necessary.

References

[1] B. Freer and J. Venkataraman, "Feasibility study for non-invasive blood glucose monitoring," in *2010 IEEE Antennas and Propagation Society International Symposium*, 2010, pp. 1-4.

[2] J. Venkataraman and B. Freer, "Feasibility of non-invasive blood glucose monitoring: In-vitro measurements and phantom models," in *2011 IEEE International Symposium on Antennas and Propagation (APSURSI)*, 2011, pp. 603-606.

[3] B. Freer, "Feasibility of a non-invasive wireless blood glucose monitor," M.S., Rochester Institute of Technology, Ann Arbor, 2011.

[4] D. Inc, "Dexcom, Inc., "Dexcom Continuous Glucose Monitoring," 2020. [Online]. Available: https://www.dexcom.com/.", ed, 2021.

[5] M. Vettoretti, S. D. Favero, G. Sparacino, and A. Facchinetti, "Modeling the error of factory-calibrated continuous glucose monitoring sensors: application to Dexcom G6 sensor data," in *2019 41st Annual International Conference of the IEEE Engineering in Medicine and Biology Society (EMBC)*, 2019, pp. 750-753.

[6] M. Tschaikner*, et al.*, "Development of a Single-Site Device for Conjoined Glucose Sensing and Insulin Delivery in Type-1 Diabetes Patients," *IEEE Transactions on Biomedical Engineering,* vol. 67, pp. 312-322, 2020.

[7] T. Yilmaz, R. Foster, and Y. Hao, "Radio-Frequency and Microwave Techniques for Non-Invasive Measurement of Blood Glucose Levels," *Diagnostics (Basel, Switzerland),* vol. 9, p. 6, 2019.

[8] V. Turgul and I. Kale, "RF/Microwave Non-invasive Blood Glucose Monitoring: An Overview of the Limitations, Challenges & State-of-the-Art," in *2019 E-Health and Bioengineering Conference (EHB)*, 2019, pp. 1-4.

[9] J. Hanna*, et al.*, "Noninvasive, wearable, and tunable electromagnetic multisensing system for continuous glucose monitoring, mimicking vasculature anatomy," *Science Advances,* vol. 6, p. eaba5320, 2020.

[10] M. Iyer, "Compact Antenna with Artificial Magnetic Conductor for Noninvasive Continuous Blood Glucose Monitoring," M.E., Rochester Institute of Technology, Ann Arbor, 2018.

[11] S. Gabriel, R. W. Lau, and C. Gabriel, "The dielectric properties of biological tissues: III. Parametric models for the dielectric spectrum of tissues," *Physics in medicine & biology,* vol. 41, p. 2271, 1996.

[12] T. Karacolak, E. C. Moreland, and E. Topsakal, "Cole–cole model for glucose-dependent dielectric properties of blood plasma for continuous glucose monitoring," *Microwave and Optical Technology Letters,* vol. 55, pp. 1160-1164, 2013/05/01 2013.

[13] V. Turgul and I. Kale, "Characterization of the complex permittivity of glucose/water solutions for noninvasive RF/Microwave blood glucose sensing," in *2016 IEEE*

International Instrumentation and Measurement Technology Conference Proceedings, 2016, pp. 1-5.

[14] M. Sidley, "Calibration for real-time non-invasive blood glucose monitoring," Rochester Institute of Technology, Ann Arbor, 2013.

[15] S. Jacobson, "Wearable Antennas Backed by Artificial Magnetic Conductor for Enhanced Gain and Reduced Back Radiation," M.S., Rochester Institute of Technology, Ann Arbor, 2020.

[16] E. R. Adair and R. C. Petersen, "Biological effects of radiofrequency/microwave radiation," *IEEE Transactions on Microwave Theory and Techniques,* vol. 50, pp. 953-962, 2002.

[17] D. R. Smith, S. Schultz, P. Markoš, and C. M. Soukoulis, "Determination of effective permittivity and permeability of metamaterials from reflection and transmission coefficients," *Physical Review B,* vol. 65, p. 195104, 04/19/ 2002.

[18] R. F. C. Jr., "Compliance with FCC Exposure Guidelines for RadiofrequencyElectromagnetic Fields," ed, 2004.

[19] D. Cazacu, S. Constantin, and D. Constantin, "On the computation of the SAR for a 3D human head model using Ansys HFSS," in *2015 7th International Conference on Electronics, Computers and Artificial Intelligence (ECAI)*, 2015, pp. P-81-P-84.

[20] C. M. Technologies, "1-Port VNA Series," C. M. Technologies, Ed., 202002 ed. Indianapolis: Copper Mountain Technologies, 2021.

[21] J. Henry, "Optimize your WLANs for phones & Tablets (and Welcome Other Mobile Devices too)," in *Cisco Live*, Barcelona, 2018.

[22] "Results of Tests on Cell Phone RF Exposure Compliance," F. C. Commission, Ed., ed. Columbia, MD: Federal Communication Commission, 2019.

[23] K. Beam and J. Venkataraman, "Phantom models for in-vitro measurements of blood glucose," in *2011 IEEE International Symposium on Antennas and Propagation (APSURSI)*, 2011, pp. 1860-1862.

[24] D. Freedman, "matlab-ssh2," ed, 2014, pp. A new Matlab interface for using the Ganymed-SS2 Java library.

[25] A. Adhyapak, M. Sidley, and J. Venkataraman, "Analytical model for real time, noninvasive estimation of blood glucose level," in *2014 36th Annual International Conference of the IEEE Engineering in Medicine and Biology Society*, 2014, pp. 5020-5023.

[26] S. R. Evans, "Fundamentals of clinical trial design," *Journal of experimental stroke & translational medicine,* vol. 3, pp. 19-27, 2010.

[27] Z. Tafa, N. Pervetica, and B. Karahoda, "An intelligent system for diabetes prediction," in *2015 4th Mediterranean Conference on Embedded Computing (MECO)*, 2015, pp. 378-382.

[28] P. Sonar and K. JayaMalini, "Diabetes Prediction Using Different Machine Learning Approaches," in *2019 3rd International Conference on Computing Methodologies and Communication (ICCMC)*, 2019, pp. 367-371.